SANDIA REPORT

SAND2009-6444
Unlimited Release
Printed October 2009

Tracking of Nuclear Production using Indigenous Species: Final LDRD Report

Todd M. Alam, M. Kathleen Alam, Sarah K. McIntyre, David Volk§, Muniasamy Neerathilingam§, and Bruce A. Luxon§, G.A. Shakeel Ansari§

Prepared by
Sandia National Laboratories
Albuquerque, New Mexico 87185

Sandia is a multiprogram laboratory operated by Sandia Corporation,
a Lockheed Martin Company, for the United States Department of Energy's
National Nuclear Security Administration under Contract DE-AC04-94AL85000.

§ University of Texas Medical Branch, Galveston, TX 77555

Issued by Sandia National Laboratories, operated for the United States Department of Energy by Sandia Corporation.

Available to DOE and DOE contractors from
U.S. Department of Energy
Office of Scientific and Technical Information
P.O. Box 62
Oak Ridge, TN 37831

Telephone: (865) 576-8401
Facsimile: (865) 576-5728
E-Mail: reports@adonis.osti.gov
Online ordering: http://www.osti.gov/bridge

Available to the public from
U.S. Department of Commerce
National Technical Information Service
5285 Port Royal Rd.
Springfield, VA 22161

Telephone: (800) 553-6847
Facsimile: (703) 605-6900
E-Mail: orders@ntis.fedworld.gov
Online order: http://www.ntis.gov/help/ordermethods.asp?loc=7-4-0#online

SAND2009-6444
Unlimited Release
Printed October 2009

Tracking of Nuclear Production using Indigenous Species: Final LDRD Report

Todd M. Alam[*1], M. Kathleen Alam[*2], Sara K. McIntyre[1], David Volk[3], Muniasamy Neerathilingam[3], and Bruce A. Luxon[3], G.A. Shakeel Ansari[3]

[1]Department of Electronic & Nanostructured Materials
[2]Energetics Characterization Department
Sandia National Laboratories
P.O. Box 5800
Albuquerque, New Mexico 87185

[3]University of Texas, Medical Branch
Galveston, TX 77555

Abstract

Our LDRD research project sought to develop an analytical method for detection of chemicals used in nuclear materials processing. Our approach is distinctly different than current research involving hardware based sensors. By utilizing the response of indigenous species of plants and/or animals surrounding (or within) a nuclear processing facility, we propose tracking 'suspicious molecules'[1] relevant to nuclear materials processing. As proof of concept, we have examined TBP, tributylphosphate, used in uranium enrichment as well as plutonium extraction from spent nuclear fuels. We will compare TBP to the TPP (triphenylphosphate) analog to determine the uniqueness of the metabonomic response. We show that there is a unique metabonomic response within our animal model to TBP. The TBP signature can further be delineated from that of TPP. We have also developed unique methods of instrumental transfer for metabonomic data sets.

* Authors to whom correspondence should be addressed: tmalam@sandia.gov and mkalam@sandia.gov

Acknowledgements

The authors would like to acknowledge Sarah K. McIntyre for assistance in the NMR instrumental transfer experiments, along with efforts maintain the NMR laboratories. We thank the Synthetic Organic Chemistry Core of the UTMB NIEHS Center for Environmental Toxicology as well as support from the NIEHS Center (Grant ES#06676) for synthesizing TBP metabolites. Sandia is a multiprogram laboratory operated by Sandia Corporation, a Lockheed Martin Company, for the United States Department of Energy's National Nuclear Security Administration under Contract DE-AC04-94AL85000. This work was funded entirely by the Sandia Laboratory Directed Research Development (LDRD) program.

TABLE OF CONTENTS

LIST OF FIGURES

TABLES

NOMENCLATURE

DOE	Department of Energy
SNL	Sandia National Laboratories
NMR	Nuclear Magnetic Resonance
DA	Discriminate Analysis
PLSDA	Partial Least Squares Discriminate Analysis
O-PLSDA	Orthogonal-PLSDA
OSC	Orthogonal Signal Correction

Executive Summary

The use of metabolic signatures as a method to detect nuclear production was explored. By tracking of indigenous flora and fauna and their metabolic response (metabonomics) to environmental release of chemicals associated with nuclear materials processing, one may be able to address the counter/non proliferation puzzle of when and where nuclear production is occurring. In this project nuclear magnetic resonance (NMR)-based metabonomic studies were directed towards identifying the response of animals to both acute and chronic chemical exposure. Spague-Dawley Rats were used as the mammalian model in this study to determine the efficacy of biological systems as indigenous sensors. We have shown that the metabolic response of our mammalian model is indeed altered by exposure to both acute and chronic levels of TBP (tributyl phosphate), an extractant used in nuclear fuel rod reprocessing. The signature found was to be distinct, not only from the background, but from a homolog chemical, TPP (triphenyl phosphate), used in industrial processing. Further, in anticipation of field application of our sensor, we explored and developed methods for NMR instrumental model transfer, needed for general application of the sensor. These results demonstrate that metabonomic studies can indeed identify past exposure to specific nuclear processing chemicals.

Page Left Intentionally Blank

Chapter 1

Tracking Nuclear Production using Indigenous Species

1.1. Introduction to Tracking Nuclear Production

Tracking and proving proliferation of nuclear materials production, in particular uranium enrichment and/or plutonium production can be a difficult task, as evidenced by the scrutiny of Iran's and North Korea's uranium enrichment programs. Through tracking of indigenous flora and fauna and their metabolic response (metabonomics) to environmental release of chemicals associated with nuclear materials processing, one may be able to address the counter/non proliferation puzzle of when and where production is occurring. By determining the unique metabonomic signatures that are produced to specific chemicals by different plants and animals (birds, mammals, fish, trees, algae, etc) due to low level exposure it may be possible to provide evidence for nuclear materials processing. This indigenous species sensing will identify facilities that should be targeted for other sensor deployment. A schematic representation of this concept is shown in Figure 1.1. In this LDRD project, we stepped toward the development of a metabonomic toolbox for the identification of nuclear processing sites. As a proof of principle we have demonstrated the response on rats (a mammalian model) to two different industrial chemicals, one being pervasive in its use as a nuclear processing chemical. We have also developed chemometric tools needed for the analysis of these complex, multidimensional data sets. One can envision extensions of this work to the metabolic response of other organisms, such as plants, reptiles and birds, to provide a highly multiplexed response not currently available.

Our work has focused on proof of principle experiments using TBP (tributyl phosphate) and TPP (triphenyl phosphate) within a murine model, specifically the Sprague-Dawley rat. Our 'sensor', in this instance, is the biochemical response of the animal to its environment. This approach is an application within the relatively new field

of metabonomics, which focuses on a systems approach to studying metabolic responses to external stimuli. Note that metabonomics is indeed distinct from the field of metabolomics which seeks to catalog and quantify low level metabolites produced by cells.[2-4]

Biological cells, in order to maintain homeostasis, respond to external stimuli, such a toxins or drugs, by altering their physiology. This results in the production of a unique signature of biochemical changes (i.e., metabolic response) that can be used as indicators for exposure. Metabolites are typically monitored using NMR since hundreds of metabolites can be monitored simultaneously. Rather than detecting and associating a particular metabolite with a disease or induced toxicity, a pattern of metabolites is developed, thus creating a unique signature associated with the biochemical response. Metabonomic response has been used to a large extent, for drug toxicity studies. More studies have been appearing showing the potential of metabonomics for environmental toxicology.[5-8]

For the purposes of this LDRD, our goal has been to determine if chemicals used in nuclear processing provide a unique and detectable metabolomic response. We have chosen to compare the response of TBP to that of TPP using ^{1}H nuclear magnetic resonance (NMR) spectroscopy. TBP is an extractant used to separate the P^{239} and U^{238} from the rest of the materials in spent nuclear fuel rods in a process known as PUREX or Plutonium and Uranium Recovery by Extraction. Spent fuel is dissolved into nitric acid and filtered. A solvent composed of 30% TBP and 70% kerosene extract uranium and plutonium into the organic phase. At present, PUREX is the most common reprocessing method. Other methods for extraction that could see more widespread use in the future are UREX (uranium extraction), TRUEX (TransUranic Extraction), SANEX (Selective ActinNide Extraction), UNEX (Universal Extraction) and DIAMEX (Diamide Extraction).[9, 10]

Chapter 2 presents the initial investigations into using ^{1}H NMR-base metabonomics to track TBP exposure, and identifies some of the metabolites that are impacted by the toxic response to acute TBP exposure. Given that the goal is to distinguish a signature of TBP from other environmental disturbances, we will also compare the metabonomic response of TBP to tri-phenyl phosphate (TPP), a high-volume

industrial-use chemical expected to have similar breakdown products to that of TBP. For these expanded studies simple inspection of the NMR spectra are not sufficient for classification purposes. Chemometric techniques must be employed for the discrimination of the different chemical exposures. **Chapter 3** details our efforts to develop Chemometric techniques, particularly orthogonal partial least squares discriminate analysis (O-PLSDA) for the identification and separation of TBP and TPP exposure. **Chapter 4** extends these studies to investigate the response to chronic (low dose) exposure to TBP and TPP over a 15 week period.

Concern over the ability to transfer these Chemometric models to multiple analysis sites, in particular between different NMR laboratories, also prompted the investigation of model transfer as a part of this LDRD project. **Chapter 5** describes efforts towards the development of instrumental transfer methods designed for NMR spectroscopy. **Chapter 6** details one of the issues with existing instrumental transfer methods and introduces a variance filtered-instrumental transfer method developed in this laboratory to address these issues.

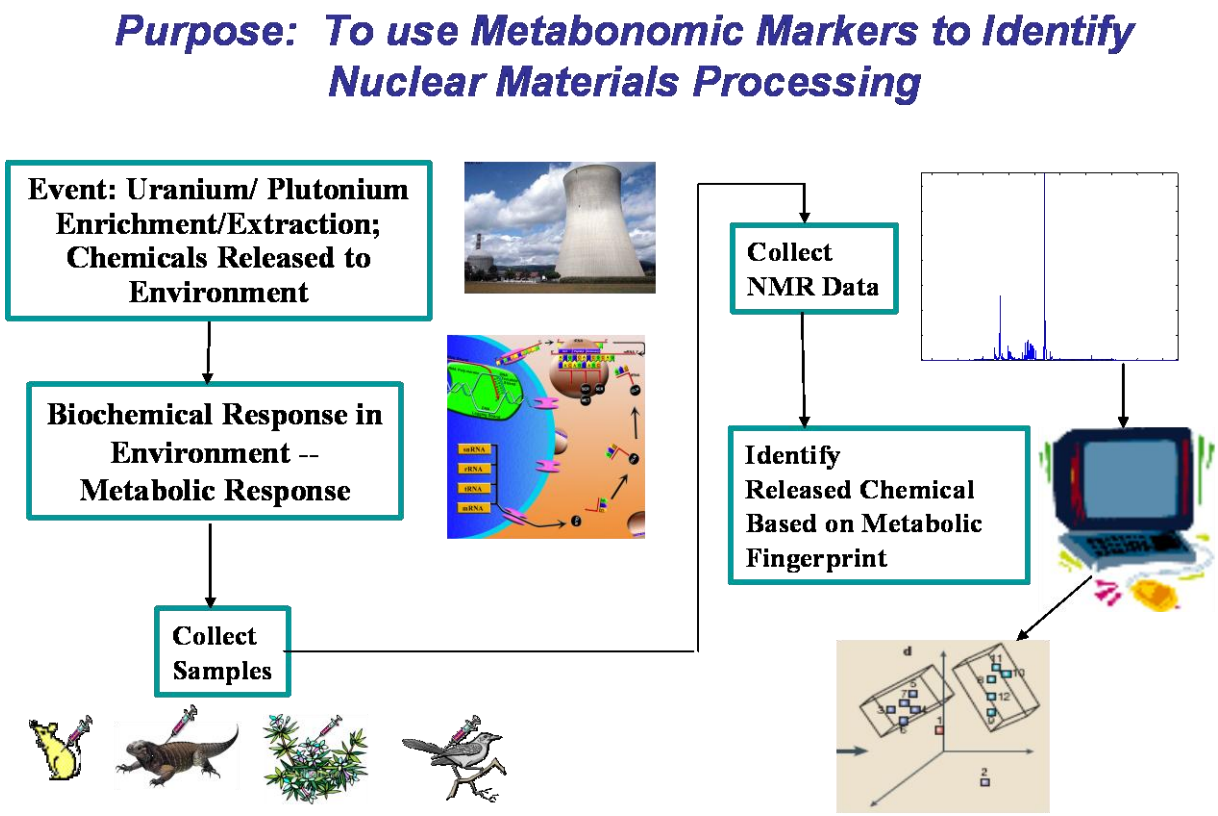

Figure 1.1: Schematic showing the use of metabonomics on indigenous species to identify and track the use of unique chemicals used in nuclear materials processing.

Chapter 2

^{1}H NMR-Based Metabonomic Investigation of Tributyl Phosphate Exposure in Rats

2.1. Introduction to Acute TBP Studies

Tributyl phosphate (TBP) is a toxic organophosphorous compound widely used in nuclear processing,[11-13] chemical industries [14] and the formulation of fire-resistant aircraft hydraulic fluids.[14] As a consequence, environmental pollution and occupational exposure involving TBP is a major public health concern due to delayed cholinergic toxicity and neurotoxicity effects.[14, 15] Workers exposed to TBP concentrations of 15 mg/m^3 in air have complained of nausea and headache,[16] while direct administration of TBP to rats produce urinary bladder hyperplasia, papillomas and transitional cell carcinomas at high doses.[17] TBP also presents an acute toxicity hazard to freshwater living organisms, even at low concentrations.[18-21]

Metabonomics is a multi-parametric approach that allows detection of the metabolic response due to chemical exposure,[22, 23] and has previously been used for environmental,[24] pharmaceutical,[25] biomarker discovery,[26] and toxicology investigations.[27] Metabonomics can combine multivariate pattern recognition techniques with the metabolic profiling capabilities of a wide range of technologies, including gas chromatography-mass spectrometry (GC-MS), liquid chromatography-mass spectrometry (LC-MS), and nuclear magnetic resonance (NMR) spectroscopy. NMR can be used as a universal survey technique for small molecule metabolites including the ability to monitor physiological changes induced by toxic insult of chemical (or mixture of chemicals). Under the ideal conditions, ^{1}H-NMR peaks intensities are directly proportional to metabolite concentration and thus are useful for a prediction and biomarker discovery.[28] NMR is relatively insensitive in comparison with MS-based techniques, but does not rely on prior separation of analytes and allows possible sample recovery for further analyses.

In this chapter we explore the use of high resolution ^{1}H NMR-based metabonomics to identify the metabolic variations associated with TBP exposure, including the identification of direct TBP metabolites in urine samples.

2.2. Methods for Acute TBP Studies

2.2.1. Animal Experiments

Male Sprague-Dawley rats weighing 200 - 220g (Harlan Sprague–Dawley Inc., Indianapolis, IN, USA) were acclimatized for two weeks at a controlled humidity and temperature in the animal care facility at the University of Texas Medical Branch (UTMB) Galveston, prior to the start of the experiment. All animal experiments were performed in the Animal Resource Center (ARC) at UTMB using a protocol approved by the Institutional Animal Care and Use (IACUC) program. Seven rats were randomly divided into a treated group (4 rats) and a control (3 rats) group. Tributyl phosphate (TBP- 98.0% purity, Sigma Aldrich, USA) was dissolved in 1 ml corn oil and was administered by gavage to the treated rats using a 15 mg/kg body weight dose (~3.3 mg/rat), while the control rats received 1 ml of corn oil only. Suzuki *et al*. used a similar dosage for studying the metabolism in rats.[29] Following dosing, the rats were transferred into individual metabolic cages. Urine was collected over a 24 hr period, filtered, and subsequently stored at -80 °C until further analysis. The collected urine volumes ranged between 4.25 and 6.25 ml, with no group bias. TBP administration did not affect survival of rats during these chronic exposure experiments. The urine from one of the TBP-treated rats was discolored red, similar to previously reported observation involving TBP exposure by Auletta *et al.*. [30]

2.2.2. NMR Sample Preparation.

A 100 µl aliquot of rat urine was diluted with 650 µl of buffer, for a final buffer concentration of 250 mM phosphate, pH = 6.0, 10% D_2O (99.9%), containing 500 µM of sodium 4,4-dimethyl-4-silapentane-1-suphonate (DSS) as an internal chemical shift reference. Proton (^{1}H) NMR data of the urine samples were obtained on a Varian Unity Plus 600 MHz spectrometer. The one-dimensional (1D) spectra were collected at 25 ºC with a tnnoesy pulse sequence, using a 1 s pre-saturation delay, a 100 ms mixing time, 4 s

acquisition time, a signal averaging of 256 transients, 4 dummy scans, a 6 μs π/2 pulse, a 7.2 kHz sweep width, 25K complex points, zero filled to 64K. Similar acquisition conditions were used for collecting NMR spectra of urine samples spiked with dibutyl phosphate (DBP, Sigma Aldrich, USA), and for overlay experiments spectra individually collected for N-acetyl-(S-3- hydroxobutyl)-L-cysteine and N-acetyl-(S-3- oxobutyl)-L-cysteine. The two cysteine compounds were synthesized at the Synthetic Organic Chemistry Core of the UTMB NIEHS Center for Environmental Toxicology (UTMB, Galveston, TX) following literature procedure. [29, 31]

2.2.3. Metabolite Identification and Statistical Analysis

The NMR data were Fourier-transformed, phased, referenced and baseline-corrected in the Chenomx NMR Suite 5.1 (Edmonton, Canada). The methyl singlet of DSS (500 μM) served as an internal standard for both chemical shifts and quantification. Spectral identification and quantification of clearly identifiable metabolites was carried out using the database in the Chenomx NMR Suite. The spectral chemical shifts and quantification procedure used was previously demonstrated to provide absolute concentration accuracies in excess of 90%.[32] Two NMR spectral regions, $\delta = 0.18$ to 4.6 and $\delta = 5.0$ to 9.4 ppm (which excluded water) were binned into 0.01 ppm wide regions, providing 882 integrated regions for analysis. The z-score determination, hierarchical clustering, and principal component analysis (PCA) were performed using the Spotfire DecisionSite 9.0 software (TIBCO Spotfire, U.S Somerville, MA). For the hierarchical clustering and principal component analysis, normalized z-scores were used. The z-score (or standard score) at each spectra frequency or bin region (ν) is defined by

$$z = I(\nu) - \bar{I}(\nu) / \sigma(\nu) \tag{2.1}$$

where $I(\nu)$ and $\bar{I}(\nu)$ are the spectral intensity and mean intensity, respectively, for that spectral region, and $\sigma(\nu)$ is the standard deviation of measured spectral intensities for that spectral region.

The chemical shifts that were determined by clustering methods as being significantly different between dosed and control animals were used for the identification

and quantification of the metabolites using the Chenomx NMR Suite. Metabolite identifications were achieved by matching the spectral positions, intensities, and coupling patterns of each metabolite proton with those available in the metabolite library of the Chenomx NMR suite.

2.3. Results and Discussion for TBP Acute Studies

Distinct spectral differences were readily observed (Figure 2.1) between the ^{1}H NMR spectra of the urine samples collected from control rats versus TBP-treated rats. This separation based on metabolite NMR differences between the TBP-dosed and control groups is also seen in the PCA analysis (Figure 2.2) in which 158 binned spectral regions, previously determined by a t-test to be significantly different between the two groups with a probability of $p < 0.05$, were used. To identify the specific metabolites that are contributing to this group classification, hierarchical clustering of these 158 identified binned spectral regions was performed and the result is shown as a heat map (Figure 2.3). Two distinct clusters corresponding to TBP-dosed and control animals were identified. In this figure the red color indicates increased relative concentration of the metabolites within the treated animals, while green indicates a decreased relative concentration (or absence) of metabolites. The elevation of metabolite concentrations in the TBP-treated rats was initially used to identify regions corresponding to catabolic products of TBP along with identification of endogenous metabolites impacted by TBP exposure, as described below.

2.3.1. Identification of Metabolites and Intermediates of TBP

The discriminating regions of the ^{1}H NMR urine spectra are shown in Figures 2.4a-c for the control and TBP-treated animals. Those chemical shifts that provide discrimination between the TBP-treated and control animals are noted in the figure and are also shown in Table 2.1.

We first focused on identifying the metabolized products of TBP via the pathways originally described by Suzuki *et al.*,[29, 31] where the dominant breakdown species include dibutyl phosphate (DBP) and the butyl dihydroxyphosphate. Suzuki and co-workers demonstrated that these dealkylation products do not appear to result from

simple hydrolysis of the TBP phosphate atom, but instead involve metabolic intermediates with hydroxylation of the butyl moieties.[29, 31] In a latter study they demonstrated that the butyl elimination is partly due to the action of glutathione-S-transferase, which can result in the formation of the S-containing metabolites N-acetyl-(S-3-oxobutyl)-L-cysteine and N-acetyl-(S-3- hydroxobutyl)-L-cysteine.[29, 31] To identify these metabolized products, DBP spiking experiments were monitored using ^{1}H NMR (Figure 2.5). Resonances that showed increased intensities following spiking were observed at δ = 0.91-0.92 ppm, 1.37-1.38 ppm and 1.60-1.61 ppm and correspond closely with the spectral regions identified in Figure 2.4a that allowed for identification of TBP-treated and control animals (see also Table 2.1), suggesting that DBP production is responsible for this separation. Figure 2.6 shows the overlap of the ^{1}H NMR spectra of the N-acetyl-(S-3- hydroxobutyl)-L-cysteine intermediate. The N-acetyl-(S-3- oxobutyl)-L-cysteine were not identified in our study (data not shown), due to overlapping peaks with other excreted metabolites. Other proposed metabolites of TBP might not be expected to be detectable by ^{1}H NMR at this dose amount, since these compounds are predicted to exist in only trace amounts.[29, 31] The minimum detectable limit for intermediates was estimated from the DBP-spiking experiments to be on the order of 25 μM. Thus, at this TBP dose (15 mg/kg) it is possible to detect TBP degradation metabolites by NMR. DBP is a major excreting intermediate of TBP as previously reported.[29, 31] Detection of other intermediates at low concentration may be possible by increasing the TBP dose or by use of NMR spectrometers or probes with a higher sensitivity.

2.3.2. The Metabonomic Response to TBP Exposure

The other endogenous metabolites corresponding to TBP exposure were also determined. The chemical shifts of metabolite species showing significant concentration differences between the TBP-treated and control groups are listed in Table 1, and were identified using the clustering method (heat map Figure 2.3). The reported metabolite concentrations were normalized with creatinine concentration for all of the samples. The creatinine concentrations ranged between 1.07 – 3.57 mM with no apparent group bias and no observed significant differences in between groups. It was also validated by

comparing the raw intensities of the creatinine chemical shift bins, which were not selected as being significant ($p < 0.05$), thus indicating that creatinine was showing no dissimilarity in excretion among the groups.

The major endogenous metabolites responsible for dosed/control separation were identified using the Chenomx NMR suite metabolite library, and included: citrate, cis-aconitate, 2-oxoglutarate, succinate, fumarate, benzoate, urea, and trigonelline. The concentration of these metabolites for the TBP-dosed and control animals is shown in Figure 2.7. Citrate, cis-aconitate, succinate, fumarate, and 2-oxoglutarate are the key intermediates of the Kreb's cycle.

Decreased levels of Kreb's cycle intermediates in the urinary excretion indicate increased cellular energy metabolism,[23] although the changes in the intermediates did not indicate any specific mechanism of toxicity. A decrease of the Kreb's cycle intermediate in the urine has been observed in heavy metal or chemical- induced nephrotoxicity, and has been attributed to toxin-induced alternation in tubular acid-base status or the effects on the key enzymes in the Kreb's cycle.[33, 34] The observation of a similar decrease in Kreb's cycle intermediates in our studies suggests a similar effect for TBP or corresponding breakdown intermediates. Variations in the concentration of the other identified metabolites (benzoate, urea, and trigonelline) implies that TBP or its intermediate also impact different metabolic pathways. Further investigations are needed to fully identify these pathways. The low urea concentrations observed in the TBP-treated rats may reflect changes in the kidney urea transporters [35] or a reduction in the cellular protein break-down process, because urea excretion levels increase as a result of protein degradation.[36] Benzoate is a urine metabolite used as a detoxification marker with high benzoate concentrations indicating poor detoxification.[37] The observation of decreased benzoate concentration in TBP-dosed rats versus control animals suggests an increased detoxification process. The remaining affected metabolite, trigonelline, is a product of the metabolism of niacin (vitamin B3) which is excreted in the urine. The decreased amount of endogenous trigonelline might be a defective mechanism in the niacin metabolism either caused directly or indirectly by TBP in the biofluids of physiological system.

2.4. Conclusions

The ^{1}H NMR-based metabonomic results provide a method for an early detection of a metabonomic response to acute exposure to TBP, even at low doses. These studies demonstrate the metabolic intermediates of TBP could be used as signatures for the exposure to TBP. In particular, the chemical shifts leading to classification between TBP-dose and control animals were attributed to dibutylhydroxy phosphate (DBP) and N-acetyl-(S-3- hydroxobutyl)-L-cysteine. It was also shown that metabolite intermediates involved in the Kreb's cycle were impacted by TBP-exposure, along with other endogenous metabolites (benzoate, urea and trigolline). These metabolite variations provide a powerful signature to TBP exposure in animals, and may provide a method to monitor exposure for diverse applications ranging from water surety, nuclear processing and environmental monitoring. Additional metabonomic studies involving chronic low-dose exposure to TBP in animals are in progress.

Table 2.1: ^{1}H NMR Chemical Shifts of TBP Intermediates and Other Metabolites

Metabolite	**Chemical shifts**[a]
2-Oxoglutarate	2.43, 2.99
Benzoate	7.54, 7.62, 7.82
Citrate	2.54, 2.68
Creatinine	3.03, 4.05
Fumarate	6.60
Cis-aconitate	5.9, 3.1
Urea	5.77
Succinate	2.41
Trigonelline	9.11, 8.88, 8.07, 4.43
Dibutyl phosphate	0.91, 1.12, 1.37-1.39, 1.60, 1.61, 3.43, 3.44, 3.52-3.55, 3.84 - 3.89
N-acetyl-(3-hydroxybutyl)-S-L-cysteine	1.12, 1.73, 2.05, 2.86, 3.04, 3.91,4.35, 8.03

[a] Chemical shifts were identified and measured with recognized pattern using the Chenomx 5.1 database.

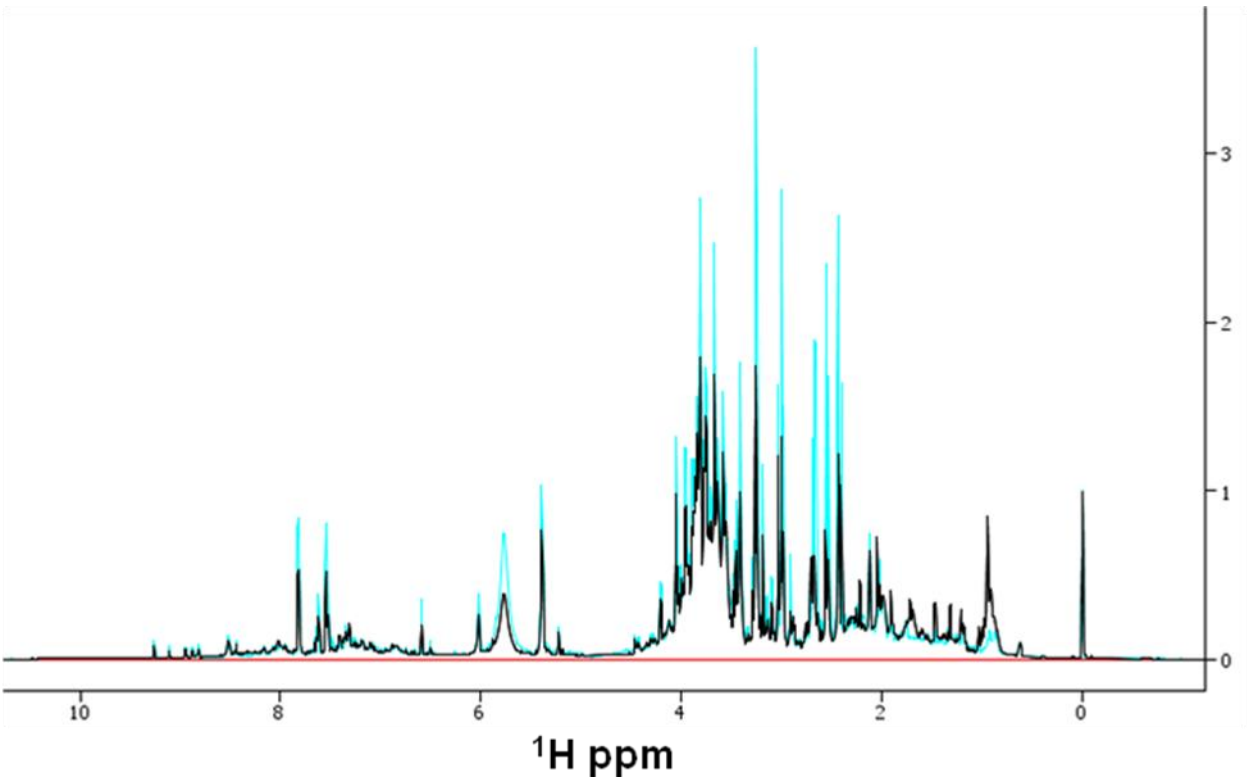

Figure 2.1: One-dimensional ^{1}H NMR spectra (unbinned) showing the difference in observed metabolites for the excreted urine of TBP-treated (black) versus control (cyan) rats. The chemical shifts were referenced to internal DSS (500 µM), δ = 0.0 ppm.

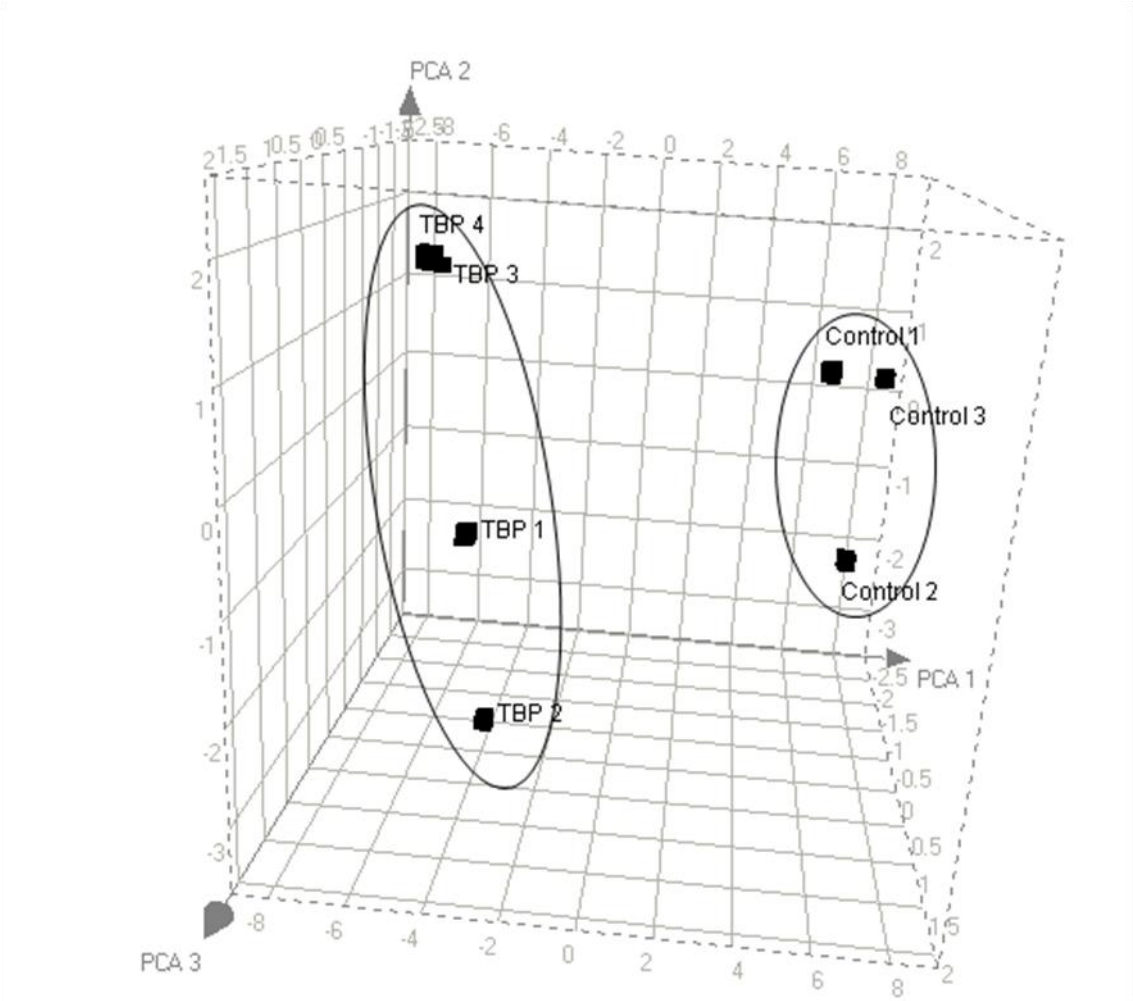

Figure 2.2: PCA analysis of the ^{1}H NMR spectra of urine showing separation between the TBP-treated and control groups based on the z-scores of the binned spectra using 158 spectral regions having confidence levels of $p < 0.05$.

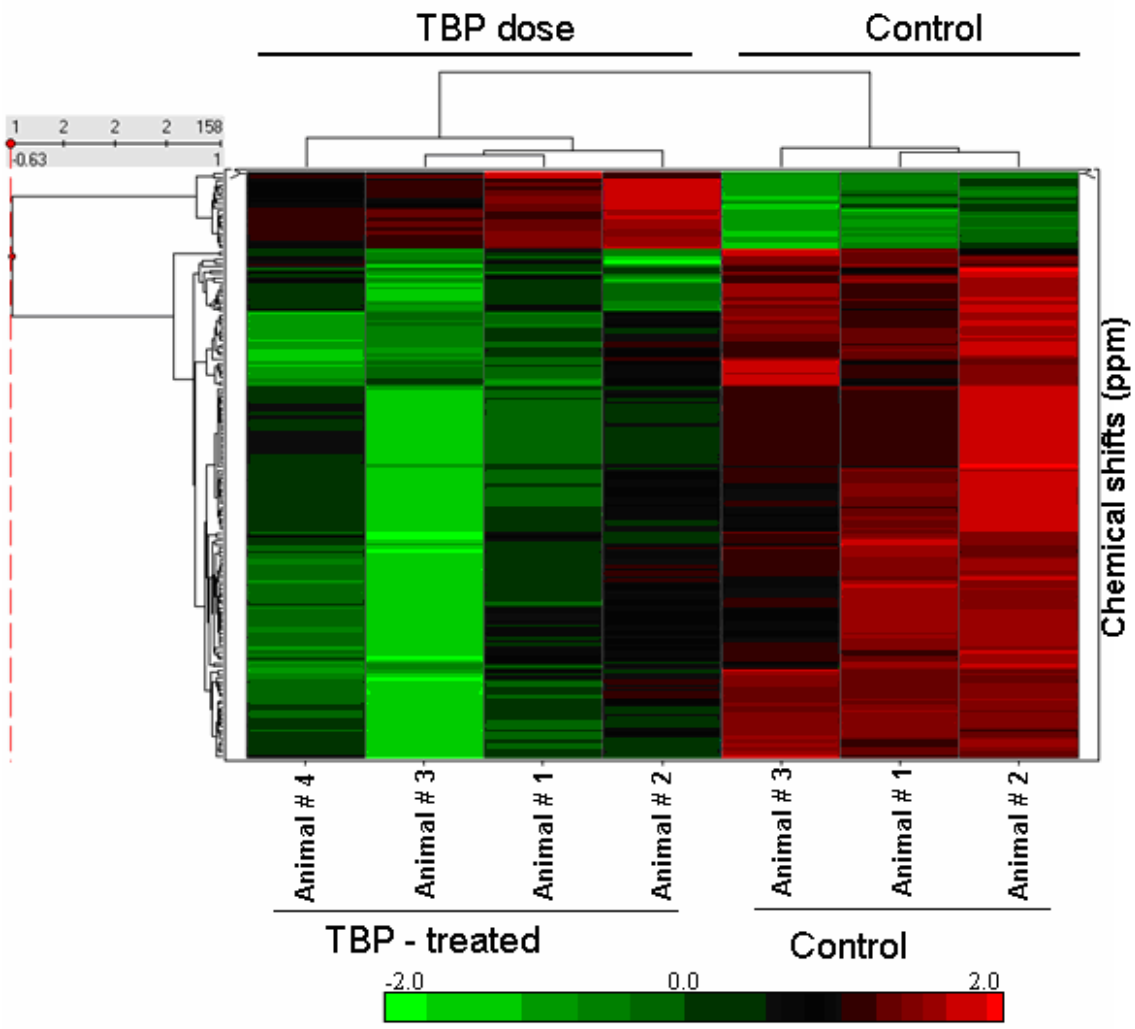

Figure 2.3: Heat map generated by hierarchical clustering based on calculated z-scores from the ^{1}H NMR spectral bins of rat urine showing the clustering of TBP-treated and control groups utilizing 158 binned regions (having confidence of $p<0.05$). Red blocks indicate increased z-scores (scaled relative concentration) whereas green indicates decreased z-scores according to the scale shown.

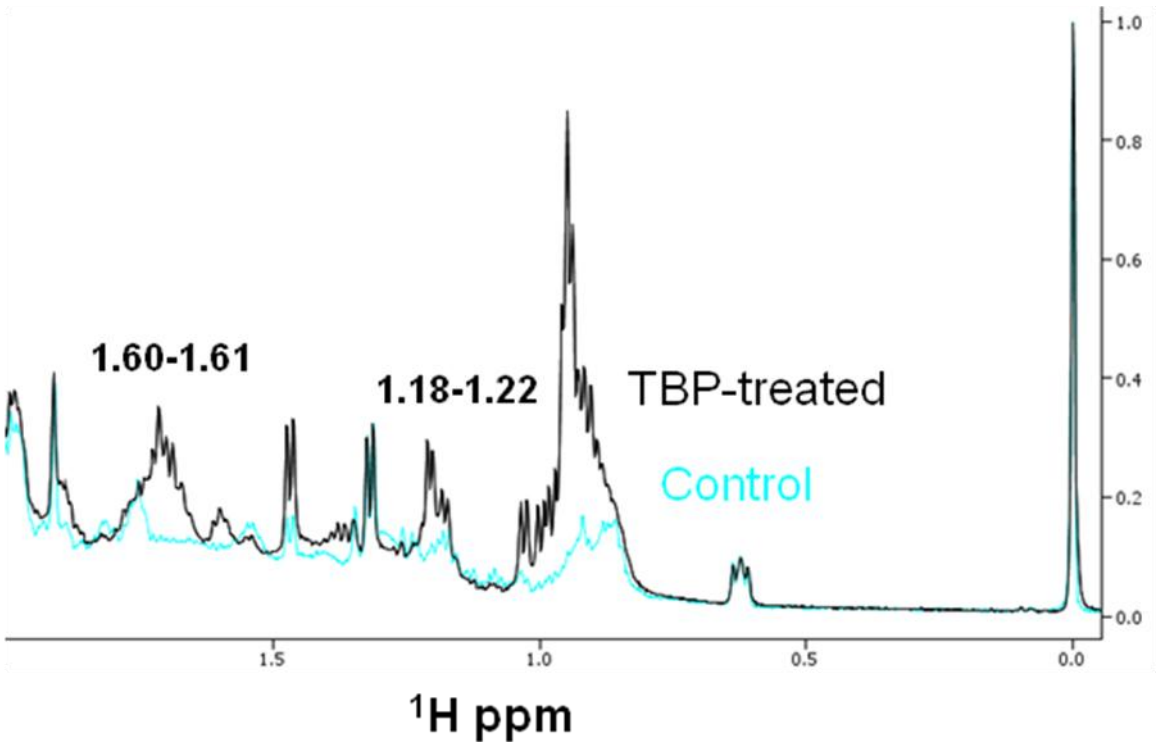

Figure 2.4. Overlay of the 1D-^{1}H NMR urine spectra of the TBP-treated (black, animal number 2) and control (cyan, animal number 7) animals showing the spectral difference in the (a) aliphatic region (δ = 0 to +2 ppm), b) the δ = 1.98 to 3 ppm region and for the c) δ = 7.75 to 8.2 ppm spectral region. The chemical shifts showing significant difference between the dosed and untreated groups is shown in box (see also Table 1) and were identified using hierarchal clustering analysis. For the aliphatic region the discriminating chemical shifts correspond to the metabolic degradation products of TBP, such as DBP and N-acetyl-(S-3- hydroxobutyl)-L-cysteine**,** while in the aromatic region the N-acetyl-(S-3- hydroxobutyl)-L-cysteine intermediate (δ = 8.03 – 8.04 ppm) is realized.

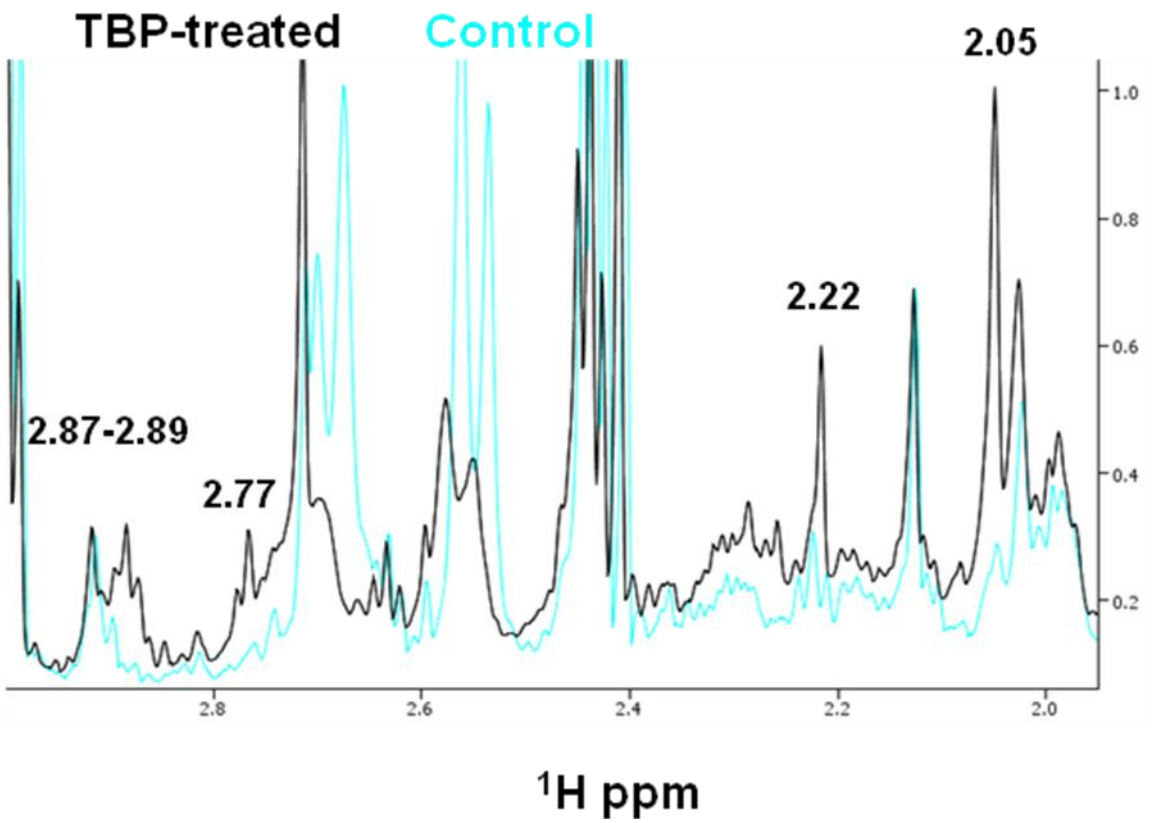
TBP-treated
Control
2.05
2.22
2.87-2.89
2.77
1.0
0.8
0.6
0.4
0.2
2.8
2.6
2.4
2.2
2.0
¹H ppm

Figure 2.4b

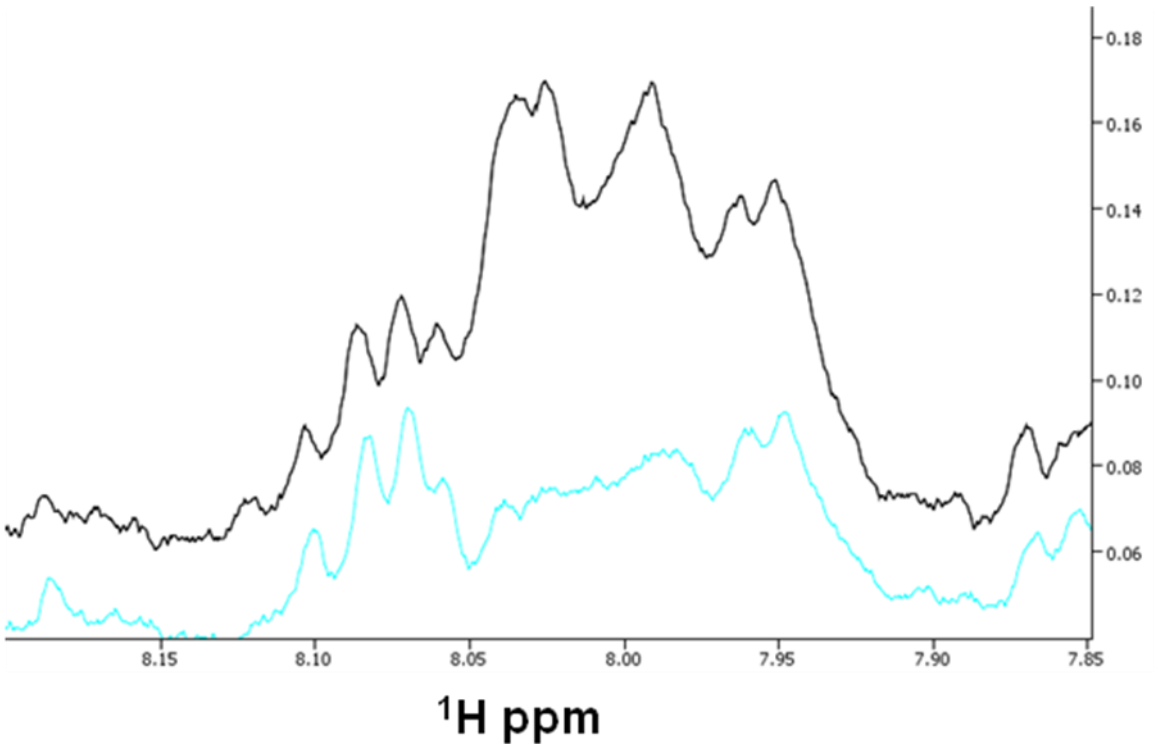

Figure 2.4c

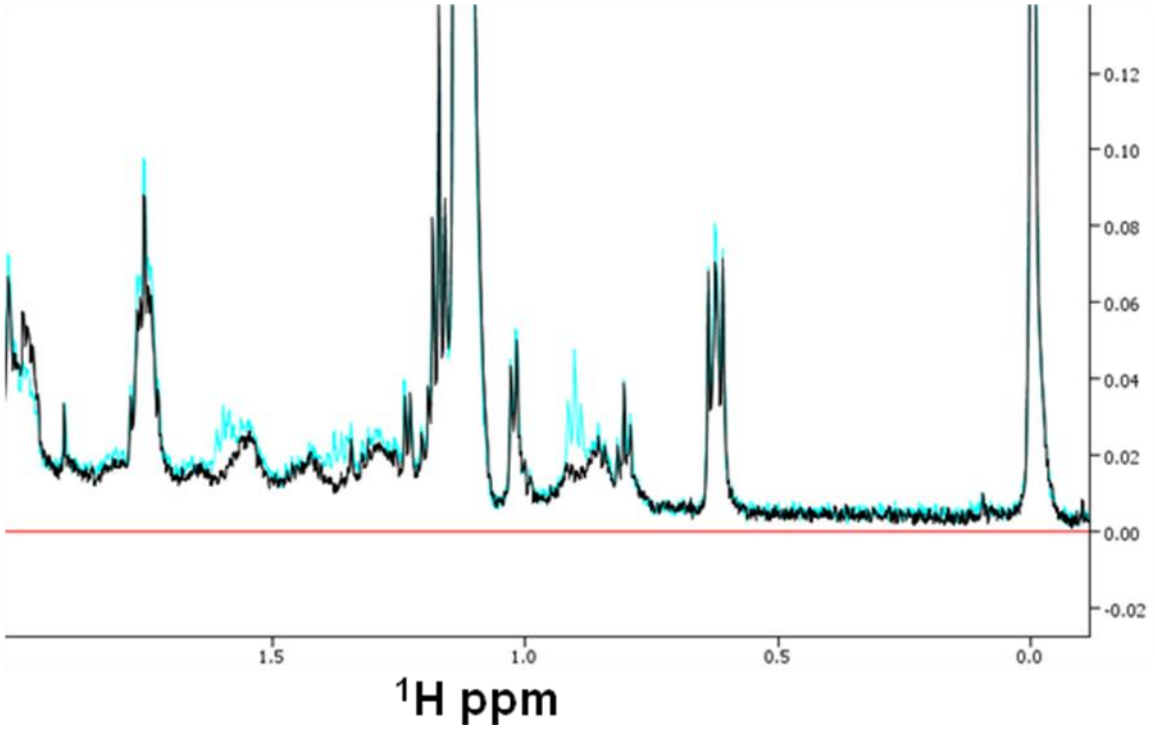

Figure 2.5. Overlay of 1D-^{1}H NMR spectral region (0.0 - 2.0ppm) of control (black) and DBP-spiked urine (cyan) at a 25µM concentration allowing for identification of the DBP chemical shifts at δ = 0.91, 0.92, 1.37, 1.38, 1.60 and 1.61 ppm.

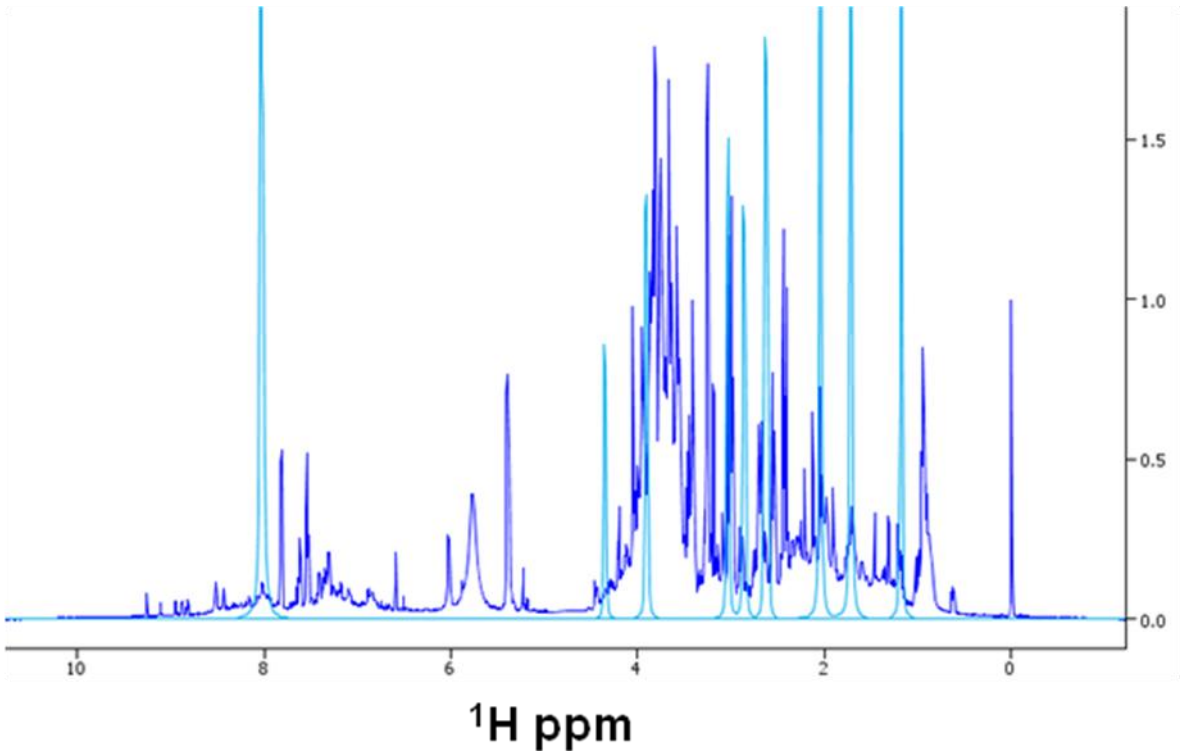

Figure 2.6. Overlay of 1D-^{1}H NMR spectra of urine from TBP treated animals (blue) and the chemically synthesized TBP intermediates N-acetyl-(S-3- hydroxobutyl)-L-cysteine (cyan blue). The elevated peaks chemical shifts (δ = 1.18-1.22, 2.05, 2.87-2.89, 8.03 and 8.04) observed in the TBP-treated which pattern matches with the N-acetyl-(S-3- hydroxobutyl)-L-cysteine. The chemical shifts δ = 1.7, 2.6, 3.0 and 4.4 ppm were not resolvable in the urine sample, because of the overlapping peaks of other metabolites.

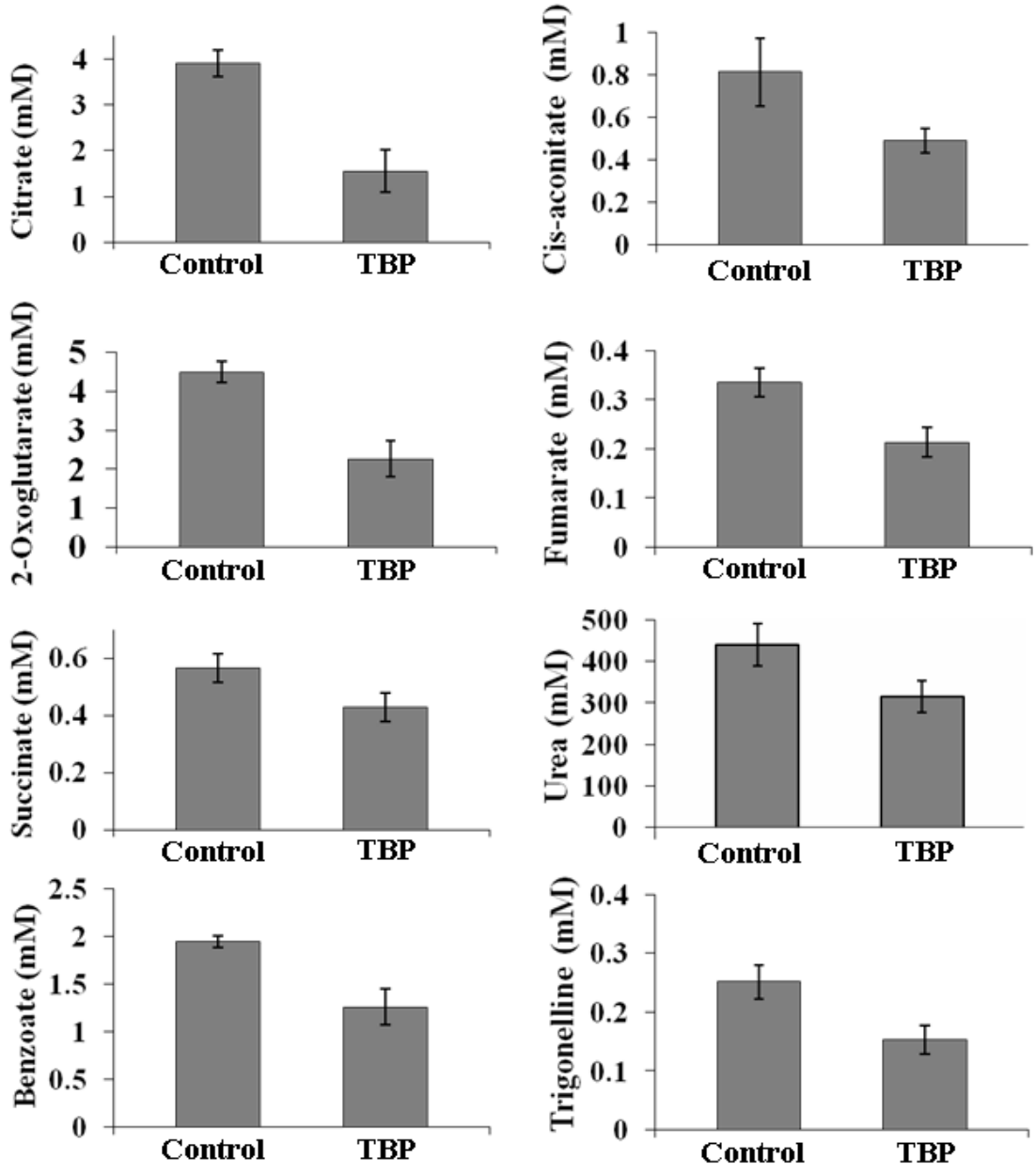

Figure 2.7. Average metabolite concentrations (± standard deviation) for TBP-treated (n = 4) control (n = 3) animals (metabolites normalized with creatinine concentration). The internal DSS signal is utilized as the concentration reference (500 µM).

Page Left Intentionally Blank

Chapter 3

^{1}H NMR Metabonomic Study of Rat Response to Acute Tri-Phenyl Phosphate and Tri-Butyl Phosphate Exposure

3.1. Introduction to Acute TBP and TPP Exposure Studies

Tributyl phosphate (TBP) and triphenyl phosphate (TPP) have numerous industrial applications including use as a flame retardant in plastics and resins, a non-flammable plasticizer in acetate, polyester and polyurethane films, as well as being a component of hydraulic fluids and lubricant oils [38]. TBP is also used during solvent extraction of nuclear waste and reprocessing of nuclear material based on the PUREX (Plutonium-Uranium Reduction EXtraction) process [39, 40]. Environmental exposure to these phosphates results mainly from hydraulic oil leakage or from the leaching or combustion and volatilization of plastics.

The acute oral toxicity of TBP is considered relatively low, with an LD_{50} (oral) in rats reported between 2000 and 3000 mg/kg, [41] or 1000 mg/kg following intraperitoneal injections. Short term toxicity studies include studies of variation in organ morphology,[42-46] serum activity,[47] the role in neurotoxicity, [48] oncogenicity [17, 30] and the production of teratogenic effects [49]. Similarly the acute oral LD_{50} of TPP is reported between 5000 and 20,000 mg/kg with studies in rats addressing the immunotoxicity, and teratogenicity of TPP [50-52].

Investigations into the metabolism of TBP and TPP have been more limited. Studies in rats using ^{14}C-labeled TBP revealed up to 11 different phosphate containing metabolites originating from TBP, with the mono- and di-butyl phosphate being the dominant metabolite species observed [29]. It was argued that these metabolites were not the result of simple hydrolysis of the TBP, but were produced almost exclusively from the early formation of a dibutyl 3-hydrobutyl phosphate intermediate. This argument was also supported by the majority of the ^{14}C-labeled metabolites observed being hydroxylated on the butyl C-3 position. Later studies also indentified several S-containing metabolites following TBP dose demonstrating that glutathione-S-transferase is involved in the metabolism of TBP [31]. In a similar study, the

metabolism of tris(2-choloethyl) phosphate in rats was shown to produce the bis(2-chloroethyl) hydrogen phosphate and the bis(2-choloehtyl) carboxymethyl phosphate along with the glucuronide of the bis(2-cholorethyl) 2-hydroxyethyl phosphate [53]. To the best of our knowledge, only a initial report into the metabolic biomarkers of indicative of TBP or TPP exposure has been reported [54].

Nuclear magnetic resonance (NMR) metabolomics/metabonomics has proven to be an innovative and promising approach to study the response of organisms to chemical exposure [55-60]. Metabonomics couples advanced spectroscopic techniques with multivariate or chemometric analysis to identify metabolic signatures correlated with some external stimulus (toxic exposure). In this paper we report the ^{1}H NMR metabonomic urine studies of rats exposed to a single acute dose of TBP or TPP, and identify the spectral regions and metabolites responsible for exposure classification.

3.2. Methods

3.2.1. Animal Studies

The studies were performed on male Sprague-Dawley rats weighing 200-220 g (Harlan Sprague–Dawley Inc., Indianapolis, IN, USA) which were acclimatized for two weeks prior to the first dose in the animal care facility at the University of Texas Medical Branch (UTMB) Galveston. All animal experiments were performed in the Animal Resource Center (ARC) at UTMB using a protocol approved by the Institutional Animal Care and Use (IACUC) program. For this study 23 rats were divided into a group (4 rats) treated with tributyl phosphate (TBP) rats), a group (6 rats) receiving a high dose triphenyl phosphate (TPP), a group (6 rats) receiving a low dose of TPP and a control group (3 rats for the TBP experiment and 5 rats for the TPP experiment). The TBP and TPP exposure experiments were performed at different periods several months apart, but the final NMR data of the collected urine was combined into a single data set for analysis. TBP (CAS # 126-73-8, 98.0% purity, Sigma Alridch, USA) was dissolved in 1 ml corn oil and was administered to the TBP-treated rats by gavage (force feeding) using a single 15 mg/kg body weight dose (~3.3 mg/rat), while the control rats received 1 ml of corn oil only. TPP (CAS # 115-86-6, > 99%, Sigma-Aldrich) was dissolved in 1 ml corn oil for either a single low dose of 2.025 mg/kg (0.405 mg/rat) or a single high dose high dose of 20.25 mg/kg (4.05 mg/rat) and then administered by gavage to the TPP-treated rats. Again the control rats received 1 ml of corn oil by gavage. In addition, one rat did not receiving any corn oil or gavage

and was designated as the normal in these studies. Suzuki *et al*., used a similar dosage for studying the metabolism in rats [29]. Following dosing, the rats were transferred into individual metabolic cages, with the urine being collected for a 24 hr period, filtered, and subsequently stored at -80 °C until further analysis. The urine volumes collected ranged between 4.25 and 6.25 ml, with no group bias. Neither the acute TBP nor TPP administration affected the rat survival rate during these experiments.

3.2.2. NMR Spectroscopy and Analysis

The NMR samples were prepared by mixing 100 µl of urine with 650 µl of phosphate buffer giving a final concentration of 250 mM phosphate (pH = 6.0), 10% D_2O, containing 500 µM DSS (2,2-dimethyl-2-silapentane-5-sulfonic acid) as a chemical shift indicator. The ^1H NMR spectra were obtained using a Varian Unity Plus 600 with a HCN 5mm probe at 25 ^oC. A standard 1D NOESY pulse sequence, with a 1s recycle delay, a 1s water pre-saturation, 4 dummy scans, 256 scan averages, a 6 µs $\pi/2$ pulse width and a 100 ms mixing time (τ_m) was employed. A spectral width of 20 ppm, with 28K complex points, zero-filled to 64K points prior to Fourier transformation using a 0.5 Hz line broadening was used for all data collection. The NMR spectra were transformed, phased, chemical shift referenced (DSS δ = 0 ppm), baseline corrected using CHENOMX NMR 5.1 Suite (Edmonton, Canada). In addition, line shape deconvolution [61] and removal of the water region 4.6 to 4.9 ppm were performed in the CHENOMX Suite.

The processed NMR spectra were transferred at full resolution (no binning) for analysis in MATLAB2007b (The Mathworks) using PLS Toolbox 4.1 (Eigenvector Research, Inc.). The data sets were normalized using the Probabilistic Quotient Normalization (PQN) method [62] followed by mean centering. The PQN normalized data gave a small improvement in the observed cross-validation errors in comparison to integral normalization or constant sum normalization,[63] and was used for all the analysis presented here. Three classes were chosen for principal least squares discriminate analysis (PLS-DA) and were designated as TBP-treated (class 1), TPP-treated (class 2) and control (class 3). A separation of the TPP-treated animals into a low and high dose (4 total classes) was also explored. Orthogonal signal correction (OSC) was

applied to remove non0correlating spectral variations (2 components) that were not contributing to classification. This O-PLSDA method has been previously described [64-67]. Cross validation was performed using a leave-one-out process, with the cross validation standard error being reported. The uniqueness of the O-PLS-DA model was addressed by a random permutation of the classification labels for all the samples in the data set, followed by cross-validation as previously described [68]. The variable importance in projection (VIP) scores [69] were obtained from the O-PLSDA analysis and mapped onto the original NMR spectra. VIP coefficients reflect the importance of each spectral frequency to each variable in the PLS model. The VIP coefficient for the *k*th parameter (frequency) is the sum over all PLS dimensions (*a*) of the contribution VIN (variable influence)

$$\mathrm{VIP}_k = \sum_a \mathrm{VIN}_{ak}^2 \qquad (3.1)$$

Where VIN_{ak}^2 is equal to the squared PLS weight of that parameters multiplied by the percent explained sum of squares for that PLS dimension. Identification of the metabolites responsible for the spectral features giving rise to the high VIP scores was obtained by manual comparison to the metabolite spectral library available in the CHEMONX NMR 5.1 Suite.

3.3. Results and Discussion

3.3.1. NMR for TBP and TPP Exposure

The non-normalized ^{1}H NMR spectra of urine samples from TBP-treated (4 animals), TPP-treated (11 animals) and control rats (8 animals) is shown in Figure 3.1. These spectra reveal numerous resonances for many different metabolites, along with subtle changes in the metabolite profiles between the three exposure classes. An initial ^{1}H NMR study following TBP-exposure [54] was able to identify several spectral regions and metabolites that differed between TBP-exposed and control animals. Unfortunately, the differences in the relative urine concentration, combined with inter-animal variations and a high complexity of the NMR spectra, makes such visual comparisons between TBP-treated and TPP-treated results increasingly difficult prompting the use of Chemometric analysis as described below.

3.3.2. O-PLSDA of TBP and TPP Exposure

The O-PLSDA classification/prediction plots for the identification of TBP-treated, TPP-treated and control animals based on the ^{1}H NMR data are shown in Figure 3.2. The original model (Figure 3.2a) was developed using the full spectra (9100 frequencies) with 6 latent variables describing 86% of the variance. The separation between the three different exposure classes was very good, with all 23 samples being correctly classified (i.e. classification error was zero). Similar prediction models were developed for the simpler 2-class separation of TBP-treated versus control animals or TPP-treated versus control animals (data not shown). Only results from the combined 3 class analysis of NMR data are discussed here.

The predicted classification following a leave-one-out cross validation analysis is shown in Figure 3.2b. In this figure the class designation represents the average over all the cross-validation trials. There is clearly an increased scatter in the class designation, with the cross validation error increasing to 0.19 for control, 0.00 for TBP and 0.04 for TPP predictions. Even under cross validation the prediction of the TBP-exposed animals is excellent with all samples being correctly identified. Figure 3.2b shows that the TPP-treated and control samples are occasionally misclassified with each other (samples 5 -23), with the error of misclassification being slightly higher for samples #8-13 which corresponds to the high dose of TPP. These cross validation results suggest that it is possible to develop a PLSDA model using the entire NMR

spectra to separate TBP-treated, TPP-treated and control samples, but that it will require a significant number of latent variable to maintain correct classification.

To this point in the analysis no specific spectral regions have been specifically identified or removed during the development of the PLSDA model. In previous studies it is common to select and only include spectral regions that improve the separation between classes. For the investigation it was found that these cross validation results could be slightly improved by only including specific spectral regions known to high VIP coefficients (using Equation 3.1) during the model development. If the NMR data set if filtered to retain only those spectral frequencies that have a VIP coefficient > 3 for all three classes in the PLSDA then the number of spectral frequencies is reduced from 9100 points (full spectra) to 338 points. Subsequent PLSDA on this VIP-filtered data set again provides excellent classification (zero classification errors) in the original model with 6 latent variables capturing 90% of the variance. Cross validation on this VIP-filtered data set resulted in classification errors of 0.06 for control, 0.00 for TBB-treated and 0.04 for TPP-treated animals. Surprisingly this filtering only provided a significant improvement in the classification of the control animals. For the remainder of the discussion we will utilize models developed with the entire spectral data set (9100 frequencies).

Attempts to separate the high and low dose TPP-treated samples from the control and TBP-treated samples using O-PLSDA are shown in Figure 3.S1 in the supplemental section. Even for models incorporating 8 latent variables (87% of the spectral variation captured by the model) there was a classification error of 0.029 for the high dose TPP-treated samples. The control, low dose TPP-treated and TBP treated samples were all correctly identified in the original model. Under cross-validation this classification error increased dramatically to 0.45 (control), 0.71 (TPP-treated, high dose), 0.08 (TPP-treated, low dose) and 0.00 (TBP-treated). These cross validation errors are much higher than the errors observed for the 3-class model described above. Again, all of the TBP-treated samples were correctly identified for this model under cross-validation. It is also possible to develop models looking at only the high and low dose TPP-treated versus the control animals. These results are shown in Figure 3.S2 (supplemental section), and as expected the cross validation errors are smaller than either the 3-class or 4-class models. These results show that models for the separation of high and low-dose TPP-treated animals from TBP-treated and control animals are not very robust, and were not pursued further.

3.3.3. Evaluation of Model Uniqueness

Given the complexity of the developed PLSDA model there is a concern whether the data is simply being over fitted. To address this issue the distribution of the cross validation error of prediction for the O-PLSDA model (3 –class) assuming random permutation of the class labels is shown in Figure 3.3. This analysis was performed to assess the uniqueness of the discriminate analysis for the identification of TBP-treated, TPP-treated and control animals (same model as shown in Figure 3.2). The distributions were obtained by simulation of 1000 random permutations of the sample classification labels, followed by calculation of the resulting cross-validation error for that new random model. For all three classes (TBP-treated, TPP-treated and control) the distributions show a maximum near a cross validation error of ~ 0.5. The distribution for the TBP-treated classification is skewed slightly to higher errors. The red line denotes the cross-validation error determined for the original data set prior to any label permutations, and allows the determination of a measure of probability (ρ). In the case of control classification with a cross validation error of 0.19, ρ < 0.018 meaning that ~18 out of 1000 random data sets would have similar control classification under this model. For the TBP-treated and TPP-treated classification this drops to ρ < 0.002 and 0.001, respectively, meaning that less than 1 or 2 random sample sets out of 1000 would produce a similar or lower cross validation error. These results support the argument that the PLSDA model developed for the TBP-treated and TPP-treated classification is unique.

3.3.4. VIP Identification of Important Metabolites

For this study, we have elected to maintain all the spectral regions in the development of the classification model and then use these results to identify the spectral regions and corresponding metabolites that are responsible for the TBP-treated, TPP-treated and control classification. The VIP coefficients were evaluated for each component in the PLS model using Equation 1, and then were mapped onto the ^{1}H NMR spectra as shown in Figure 3.4. These spectra are color-coded based on their corresponding scaled VIP scores. In this example the mapped VIP scores have been scaled to the highest VIP score for that individual PLS component so that the results for the different classes can be directly compared. The VIP-mapped spectra

corresponding to the TBP-treated component of the PLSDA classification is shown in Figure 3.4a and c, while mapping of the TPP-treated component is shown in Figure 3.4b and d. While there are many similarities in the VIP scores inspection of these figures clearly shows that different spectral regions are responsible for the classification of TBP-treated and TPP-treated animals.

The spectral regions for the top 10 VIP coefficients that were responsible for the prediction of each class are summarized in Table 3.1. Identification of the metabolites responsible for these spectral regions was accomplished by visual fitting to the metabolite spectral library in the CHEMONX NMR Suite. In many instances it was possible to confirm the metabolite identification by comparison of the VIP scores for different the spectral regions associated with a given metabolite. The argument was if a target metabolite is responsible for the high VIP coefficient during classification, then all the spectral lines associated with that metabolite should have similar VIP coefficients. As example, the resonance at δ = 2.43 ppm was tentatively assigned to 2-oxoglutarate, requiring that the corresponding spectral signature of 2-oxoglutarate at δ = 3.0 ppm should have a similar VIP score as was observed experimentally. Similarly the ^{1}H NMR resonances at δ = 7.54, 7.67 and 7.82 ppm were assigned to either the metabolite benzoate or hippurate. The hippurate molecule has an additional methylene resonance at ~ 4 ppm which should have a similar VIP score to the aromatic resonances. Experimentally there were no corresponding VIP scores in this region arguing against hippurate and supporting the assignment of benzoate. There are also spectral regions with very high VIP coefficients that were not assigned to particular metabolites due to the inability to uniquely identify or resolve spectral features in this highly overlapped region.

For the classification of TPP-treated and control animals the top 2 spectral regions of interest based on VIP scores were δ = 3.42 and 3.27 ppm. Presently these resonances were unassigned. The remaining top 5 spectral regions for classification of TPP-treatment correspond to the metabolite 2-oxoglutarate and citrate, while beatine was identified as an important metabolite for the classification of the control animals.

The top 2 spectral regions for classification of TBP-treatment were at δ = 2.54, 2.55, 2.68 and 2.71 ppm which have been assigned to citrate, while the remaining top 5 spectral regions correspond to 2-oxoglutarate and creatine. Citrate and 2-oxoglutarate had previously been identified as an important metabolite for TBP-exposure [54]. In that study they also identified

succinate, benzoate, cis-aconitate, fumarate, urea and trigonelline as important classification metabolites. The VIP coefficients in Table 3.1 show that some of these metabolites are involved in the classification, but have a smaller contribution. For example succinate is involved in the classification of TBP-treated and TPP–treated animals with a VIP score about 20% of the dominant spectral region (unidentified metabolite), while benzoate has more importance in the TBP-treated classification than in the TPP, but has a VIP score that is < 10% of the spectral region with the highest VIP coefficient. Fumarate (δ = 6.6 ppm) had a VIP coefficient that was < 10% of the dominant spectral region. The VIP coefficient for cis-aconitate (δ = 5.9, 3.1 ppm), and trigonelline were small and did not contribute to the classification. Citrtate, succinate, fumarate and 2-oxoglutarate are primarily involved in the citrate (TCA) cycle and are a indicator of changes in the cellular energy metabolism, but do not indicate any specific mechanism of toxicity.

3.4. Concluding Remarks on Acute Studies

In conclusion, this work demonstrates that acute exposure to tributyl phosphate and triphenyl phosphate in rats can be identified and separated based on variations in the urinary metabolites. It was possible to clearly identify TBP-treated versus TPP-treated animals in this study. Separation of high and low dose TPP-treatment did not provide a unique model. Exposure classification was obtained primarily through the variation of common metabolites and is not the result of direct observation metabolic breakdown species of the original phosphates. These results show that metabonomic studies may provide a method to identify environmental exposure to aryl and alkyl phosphates.

Table 3.1: Identification of important spectra regions and metabolites based on the VIP coefficients for O-PLSDA classification.

Resonance (ppm)	**Metabolite**	**Scaled VIP Coefficients**		
		Control	**TBP**	**TPP**
0.91	Dibutyl phosphate	<0.001	0.03	0.02
2.05		0.05	0.13	0.09
2.40	--	0.19	0.17	0.22
2.41	Succinate	<0.10	0.18	0.25
2.43	2-Oxoglutarate	0.37 (5)	0.73 (3)	0.52 (4)
2.54, 2.56	Citrate	0.28	1.00 (1)	0.45
2.68, 2.71	Citrate	0.23	0.80 (2)	0.51 (5)
3.00	2-Oxoglutarate	0.40 (4)	0.63 (4)	0.60 (3)
3.04	Creatine	0.19	0.28 (5)	0.25
3.25	Beatine	0.42 (3)	0.17	0.50
3.27	--	0.82 (2)	0.14	0.84 (2)
3.41	--	0.33	<0.1	0.34
3.42	--	1.00 (1)	<0.1	1.00 (1)
3.43	--	0.25	<0.1	0.25
3.67	--	0.13	0.16	0.17
3.81	--	0.13	0.19	0.17
4.06	Creatine	0.20	0.12	0.22
5.78	Urea	0.03	0.01	0.03
6.60	Fumarate	0.06	0.03	0.07
7.54	Benzoate	0.01	0.09	0.04
7.67	Benzoate	0.01	0.09	0.03
7.82, 7.83	Benzoate	0.01	0.10	0.04

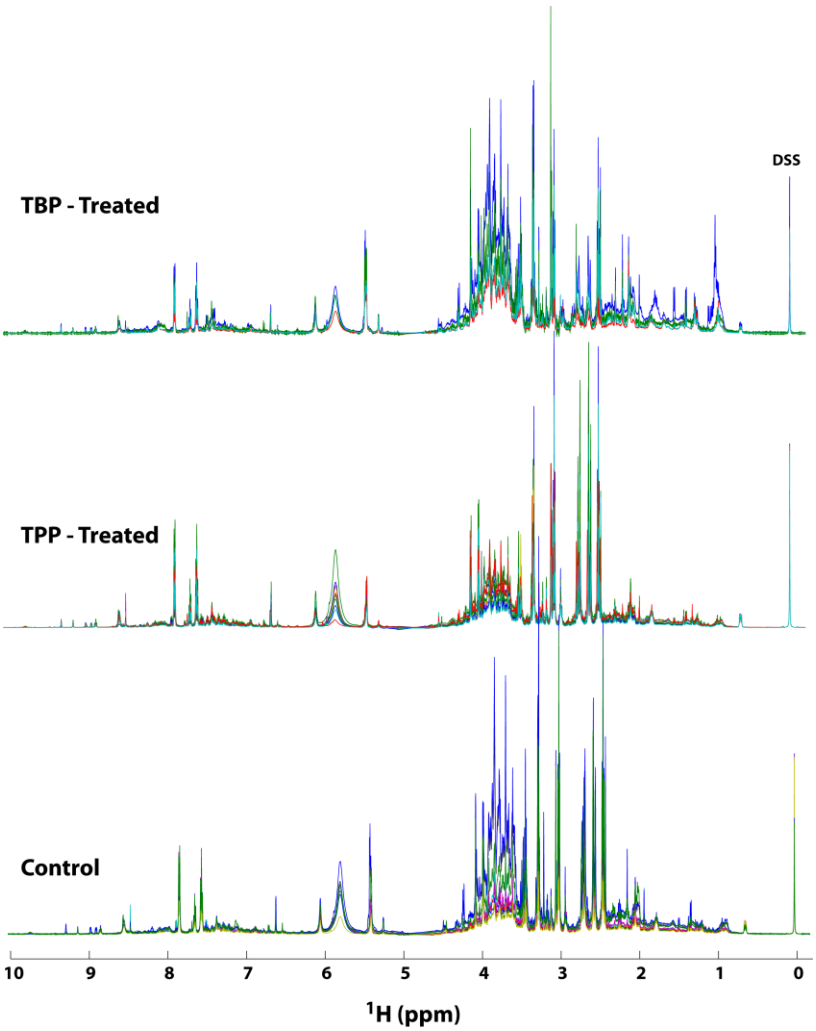

Figure 3.1 600 MHz ^{1}H NMR spectra of rat urine collected from TBP-exposed, TPP-exposed and control animals.

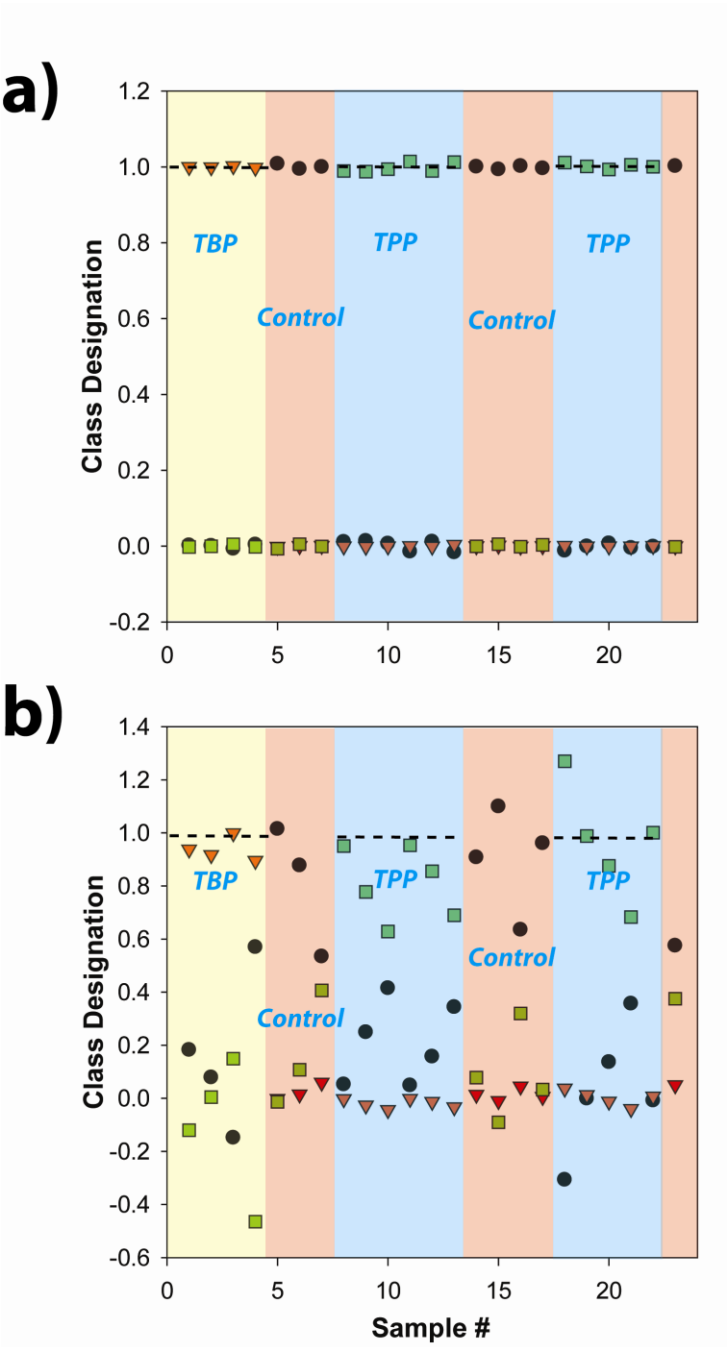

Figure 3.2 Class designation results following O-PLSDA for the 23 urine sample based on classification into TBP-treated, TPP-treated and control animals. The results from the a) original model and b) the average results following leave-one-out cross validation. The predicted results for a TBP-treated (▼), a TPP-treated (■), or a control (●) animal are shown.

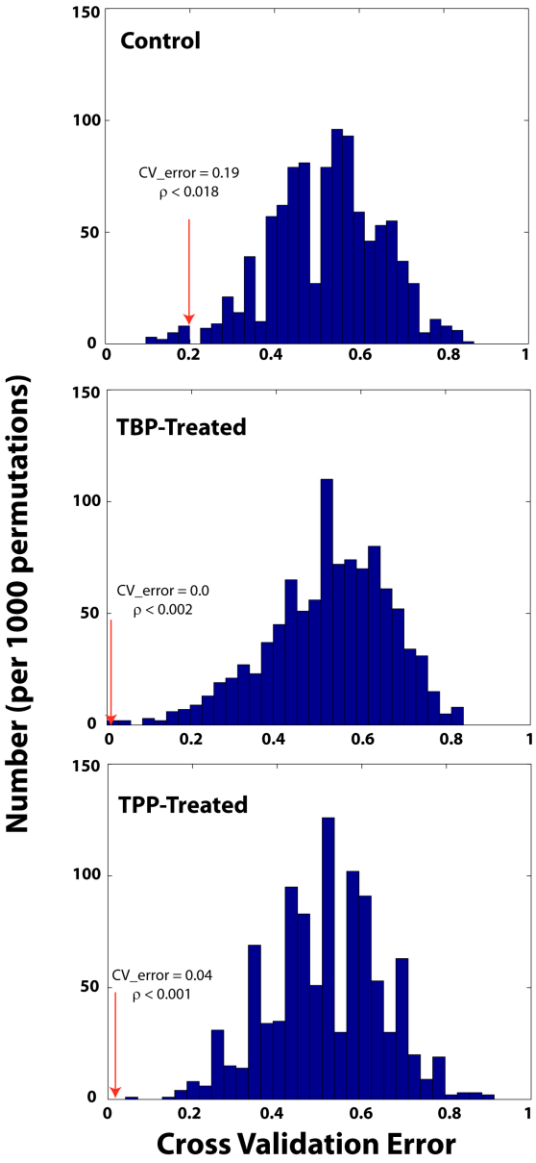

Figure 3.3 Plots of the O-PLSDA cross-validation classification error distributions following random permutations of the classification labels. The results are shown for the control, TBP-treated and TPP-treated classification. The red arrow denotes the cross validation error for the original O-PLSDA model. The probability measure (ρ) was determined from the number of random models that had the same or lower cross validation error as the original model.

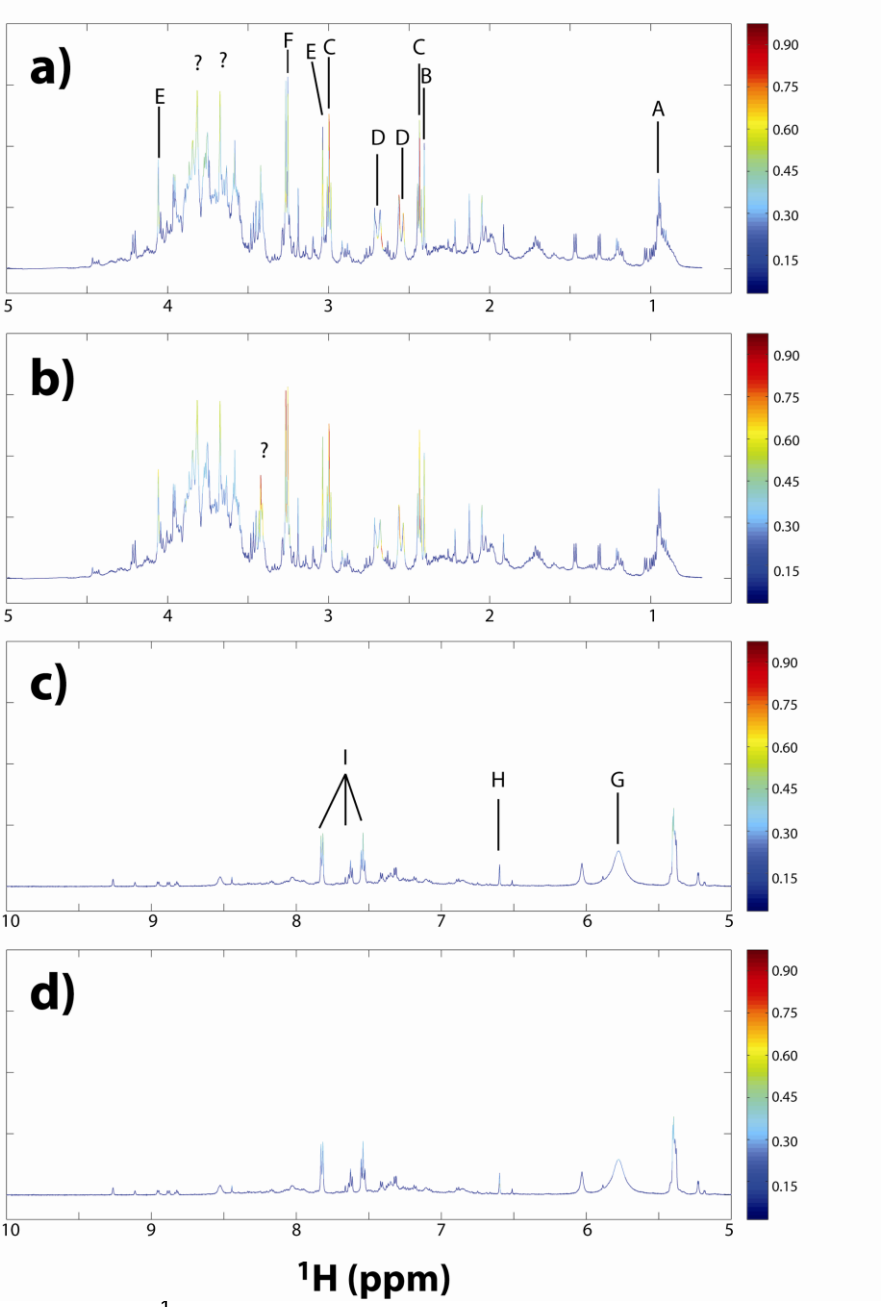

Figure 3.4 Representative ^{1}H NMR spectra with color mapping of the corresponding relative O-PLSDA VIP coefficients for identification of important resonances contributing to the classification. Expansion of different spectral regions color coded using the TBP-treatment VIP coefficients (a and c) and the TPP-treatment VIP coefficients (b and d). The color bar is for VIP coefficients scaled to the maximum VIP observed for that class. Representative metabolites are identified: **A**:Dibutyl phosphate, **B**:Succinate, **C**:2-Oxoglutarate, **D**:Citrate, **E**:Creatine, **F**:Beatine, **G**:Urea, **H**:Fumarate, **I**:Benzoate

3.5. Supplemental for Chapter 3

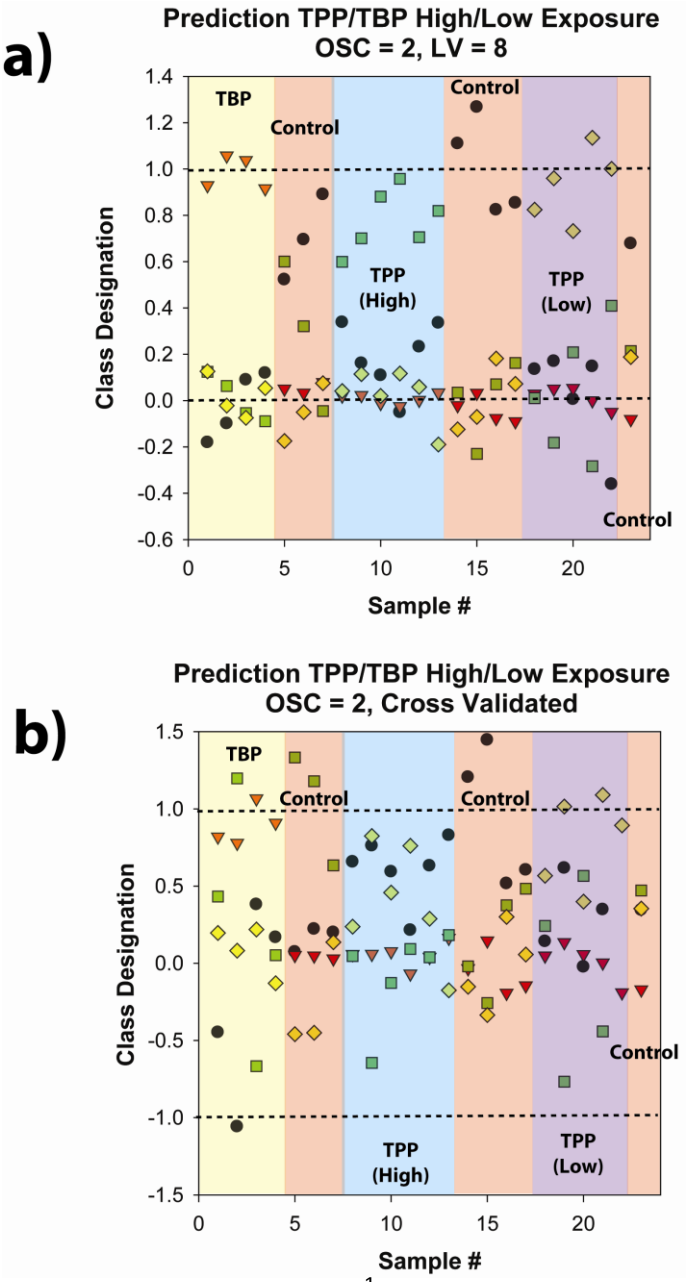

Figure 3S.1. The O-PLSDA prediction from ^{1}H NMR urine spectra based on 4 classes (TBP-treated, high dose TPP-treated, low dose TPP treated and control) of exposure in the rats. The prediction from: a) the original PLSDA model and b) the average prediction following cross validation. It is clear that the model performance for prediction involving 4 classes is significantly poorer than the prediction observed for the 3 class model (Figure 3.2).

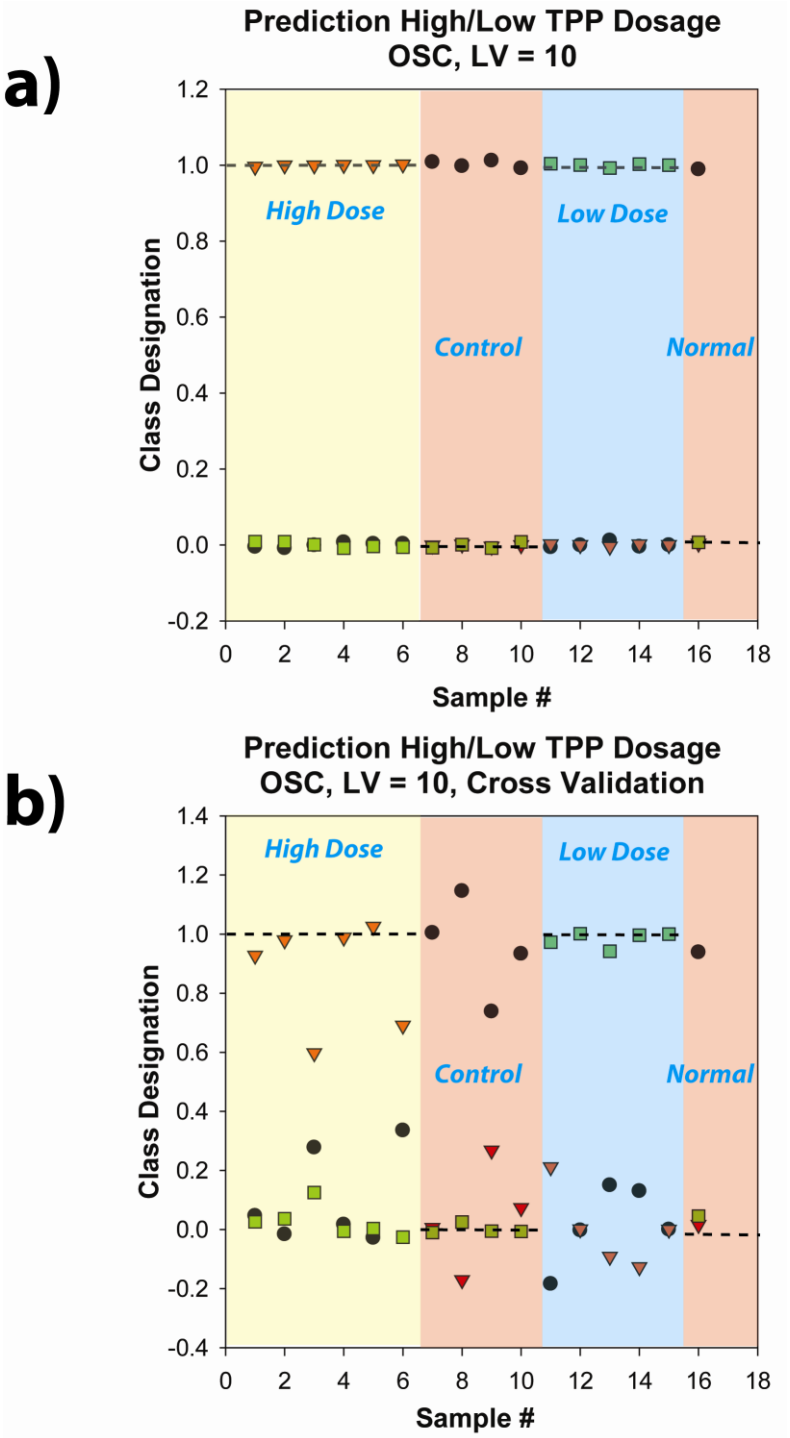

Figure 3.S2. The O-PLSDA prediction from ^{1}H NMR urine spectra for identification of high and low dose of TPP-exposure in rats. The prediction from: a) the original PLSDA model and b) the average prediction following cross validation. The high dose samples showed a slightly higher misclassification than the low-dose TPP-treated samples.

Chapter 4

^{1}H NMR Metabonomic Studies of Chronic TBP and TPP Exposure

4.1. Introduction to Chronic Exposure

Chronic exposure differs from acute exposure not only in the time duration of exposure (months to years), but in typically in the amount of chemical to which the subject is exposed. Because of the smaller amounts and longer durations, the biological response can be distinctly different from that seen with acute exposure. Chronic effects are perhaps more likely to be encountered when exploring environmental exposure to chemicals due to increased distances of the sample from the source, and the expected low concentration release of chemicals under study. Chronic exposure of our murine model was explored to determine the specificity and sensitivity of our methods. Good models were developed for TBP from data collected during chronic exposure that were not influenced by the presence of TPP.

4.2. Experimental for Chronic Exposure

Sixteen (16) rats were randomly divided into three groups for control (6 rats), TBP-exposure (5 rats) and TPP-exposure (5 rats). Tributyl phosphate (TBP- 98.0% purity, Sigma Aldrich, USA) was dissolved in 1 ml corn oil and was administered by gavage to the rats using a 1.5 mg/kg body weight dose, while the TPP (98.0% purity, Sigma Aldridh, USA) was administrated 2.025 mg/kg body weight dose, and the control rats receiving 1 ml of corn oil only. Repeated doses were administered to the animals for 15 weeks (daily dosing Monday through Friday). On each Friday the rats were transferred to metabolic cages for urine collection (~20-22 hours), with the urine stored at -80°C until NMR analysis. Rats were returned to their normal cage every Saturday. Proton (^{1}H) NMR data of the urine samples was obtained for samples of weeks 1, 2, 4, 8, 12, 14 and 15. The NMR sample preparation was detailed in Chapters 2 and 3. The manipulation of the NMR data and analysis using O-PLSDA is described in detail of Chapter 3 and will not be reproduced here.

4.3. Results and Discussion for Chronic Exposure

The classification results for the ^{1}H NMR metabonomic data for chronic exposure to TBP and TPP is shown in Figure 4.1. O-PLSDA is able to separate these results into 3 classes for each week over a period of 15 weeks using 8 latent variables. This high number of latent variables suggests a complex response to TBP and TPP involving multiple metabolites. Similar to the discussion in Chapter 3 this separation is requires the use of OSC to remove spectral variation that is orthogonal to the classification. The prediction error is strongly dependent on the binning size utilized, with the full resolution NMR data showing the highest classification error. This observation suggests that there are subtle line shape variations due to pH and concentration changes over these extended time studies. Optimization of the binning size to reduce these classification errors could be explored during the model development. In addition, it may be possible to utilize a host of different alignment algorithms to reduce these changes. Unfortunately, while such efforts can reduce these overall classification errors, the robustness of the developed model can be compromised. It can also be seen in Figure 4.1 that the scatter in the classification increases in the 13 through 15th week. This is most noticeable in the TPP classification. Additional analysis of the data as a function of exposure time is warranted to identify time-dependent variations in the metabonomic response.

The performance of the O-PLSDA model under cross validation is shown in Figure 4.2. In this figure the classification values represent an average over all the leave-one-out cross validation analysis. The performance of this model is still very good all of the samples being classified correctly.

4.4. Conclusions

The results shown in this chapter demonstrate that ^{1}H NMR metabonomics is able to identify and separate both chronic TBP and TPP exposure over a 15 week period. Through O-PLSDA the classification is distinct, even though the cross validation performance begins to degrade during the later portions of this experiment. Unlike the acute studies (Chapter 3) the performance of O-PLSDA is strongly controlled by the binning size suggesting that this parameter will need to be optimized during subsequent model development.

These are promising results suggesting that ^{1}H NMR metabonomics may be able to identify environmental exposure to organophosphate at very low levels in animal species, if there is a continued chronic exposure. Additional work on the persistence and minimum exposure levels to these chemicals required for these metabonomic signatures is still required, and will be the focus of future work.

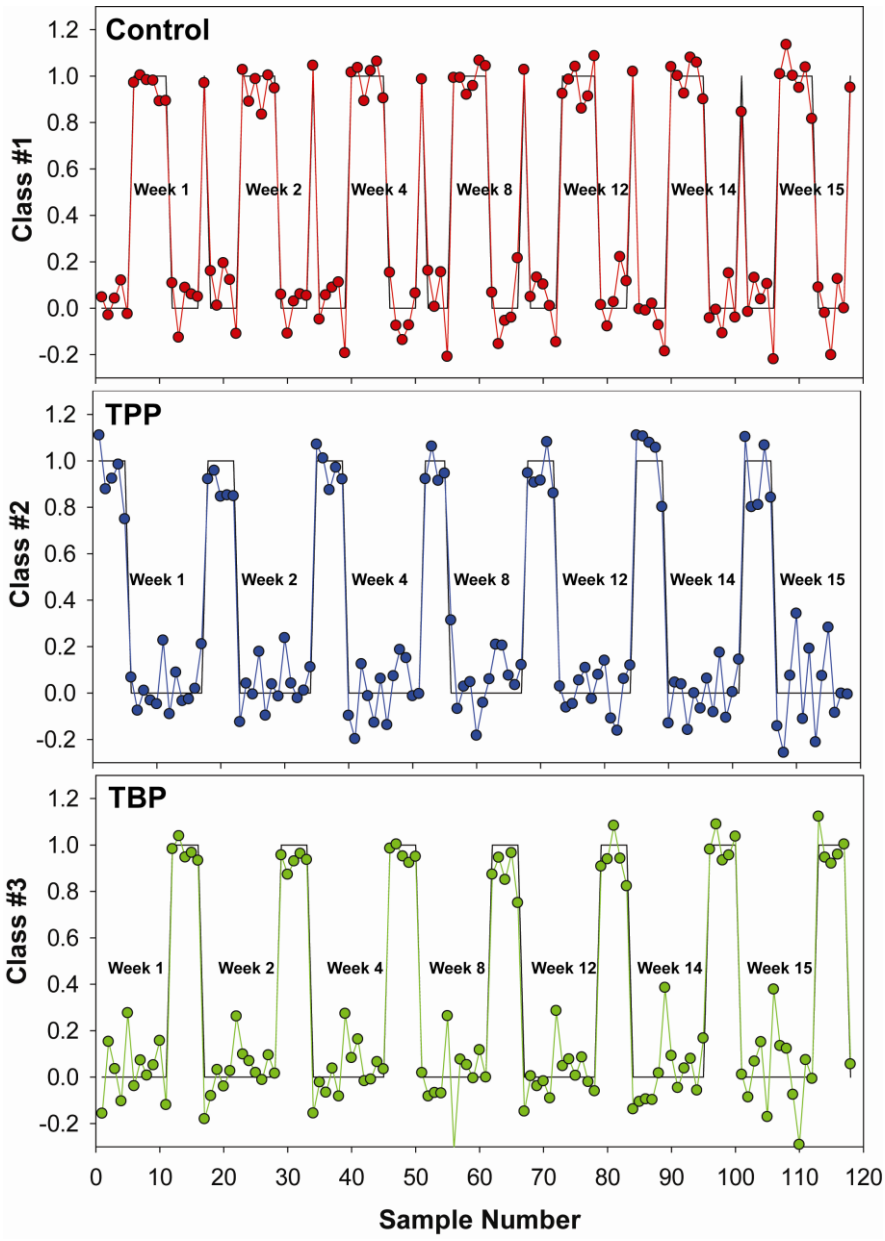

Figure 4.1: O-PLSDA analysis of the ^{1}H NMR spectra for chronic TBP and TPP exposure over a 15 week exposure period.

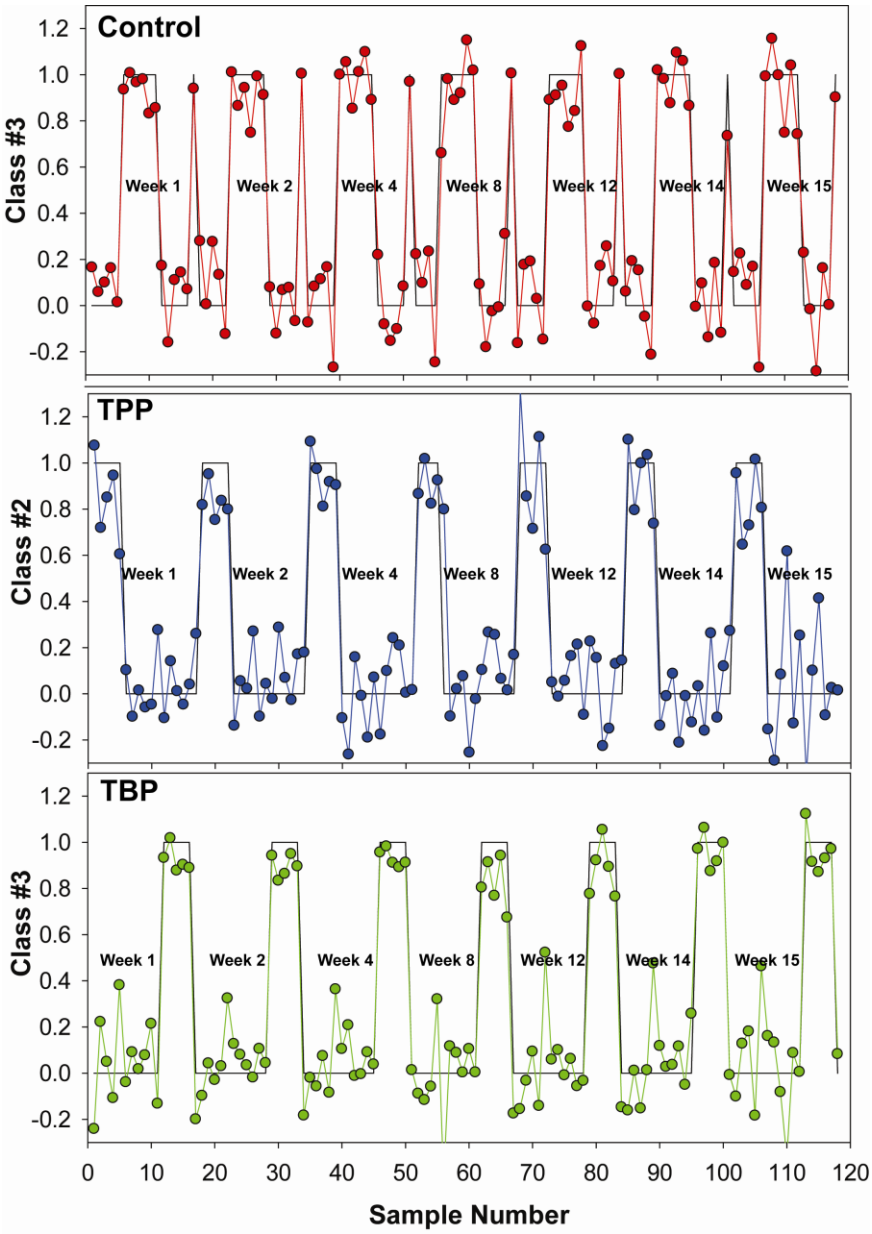

Figure 4.2 O-PLSDA analysis of ^{1}H NMR metabonomic urine data under leave-one out cross validation.

Page Left Intentionally Blank

Chapter 5

Investigation of Chemometric Instrumental Transfer Methods for High-Resolution NMR

5.1. Introduction to Instrumental Transfer

High-resolution nuclear magnetic resonance (NMR) spectroscopy is a powerful technique for the investigation of complex mixtures, and has found application in metabonomic, environmental and pharmaceutical research. The complexity and size of NMR data sets in these fields has resulted in multivariate or chemometric analysis becoming routine within the NMR community.[70-72] It is also becoming increasingly more common to combine NMR spectral data from different sources into large databases prior to chemometric analysis. These sources may include 1) NMR data from different laboratories, 2) data within the same laboratory but obtained on different NMR instruments (including different fields), 3) data from the same NMR instrument over extended time periods, or 4) data obtained using different pulse sequences and solvent suppression techniques. The impact and magnitude of spectral variations related to different instrumental sources within combined data sets is poorly understood. For example, changes in the high resolution ^{1}H NMR spectra associated with the use of different NMR instruments have been explored by Potts and co-workers,[73] who found that instrumental variations can competed with the physiological spectral changes occurring during metabonomic studies. Non-reproducible baselines associated with water solvent suppression were found to introduce significant error. Chemical shift variations, including magnetic field dependent shifts in strongly J-coupled multiple systems were also shown to contribute to the instrument-to-instrument spectral differences. These chemical shift variations were reduced by binning or integral averaging over the citrate region.[73] Similar NMR instrumental variations were also observed for principal component analysis (PCA) of ^{1}H NMR rat plasma metabonomic studies.[74] Saude and co-workers[32] demonstrated that spectral variations in quantitative ^{1}H NMR of synthetic urine samples were introduced by a variety of factors, including pulse sequence employed, water suppression method, differences in the spin-lattice T_1 relaxation rates of the metabolites, along with NMR hardware issues including the type of low-pass filters

employed in the instrumental configuration. Spin-lattice relaxation effects and variation in signal amplitude due to J-coupling evolution during the CPMG (Carr-Purcell-Meiboom-Gill) pulse sequence used for protein background signal suppression have also been reported.[75] In contrast, Keun and company[76] demonstrated that the PCA analysis of ^{1}H NMR spectral data of rat urine samples following hydrazine dosage at two different NMR frequencies were very reproducible, with observed instrument-correlated changes being smaller than the physiological spectral variations. Similarly, the analysis of samples produced from different collaborative centers have shown consistent classification when obtained on the same instrument under the same operating conditions.[77]

Variation of the spectral response between different NMR instruments and/or probes makes comparison of combined data sets challenging. In addition, changes in a given NMR instrument's response over extended time periods may also make classification and quantification of different chemical species difficult. The increased pooling of NMR spectral databases and collaboration of different laboratories with their own NMR instrumentation suggest that a standard operating procedure for NMR data acquisition, calibration and instrumental response corrections is needed. The transfer of calibration models between different NMR instruments or configurations is explored in this paper.

There are several approaches to correct for different spectral responses between instruments commonly referred to as instrumental transfer or standardization. One of the most basic approaches is to use line shape deconvolution to correct for spectral distortions resulting from magnetic field inhomogeneities. These inhomogeneities can arise from imperfect shimming, static magnetic field instabilities, homogeneity variation across the sample detection volume, pulse phase and amplitude variations, magnetic susceptibility discontinuities due to sample configuration, probe design and condition, and field homogeneity modulation due to spinning. In general, these inhomogeneity distortions affect all NMR resonances equally and can be removed or reduced using reference deconvolution. This correction method deconvolutes the experimental spectra with the references signal's line shape and then reconvolutes the spectra with the ideal reference signal line shape. Deconvolution can be considered a simplistic method of instrumental transfer, but it does not address frequency-dependent variations between different instruments. Details and examples of reference deconvolution for high resolution NMR spectra have been described extensively.[61, 78-87]

Another method of instrumental transfer is to add calibration spectra from a secondary instrument to the original calibration set and then recalculate the predictive model. This type of multi-instrument calibration model development is commonly referred to as hybrid calibration (HC).[88] The HC method can be extended to collecting spectra on multiple instrumental configurations and then attempting to build a calibration model that simultaneously performs well for each configuration. A variation of this is to use combined data sets from multiple instruments, then identify and remove spectral differences between the different configurations that do not contribute to either sample classification or the model calibration. Orthogonal signal correction (OSC) is an example of this, and has been used to improve the performance of near infrared (NIR) instrumental transfer.[89] OSC has been applied to ^{1}H NMR metabonomic data to eliminate spectral components due to instrumental variations (on a single instrumental configuration) or physiological changes not associated with classification,[74] but has not been directly applied to NMR instrumental transfer. In the OSC studies of Beckwith-Hall the initial PCA model showed classification based on the NMR instrument identity. Removing two orthogonal components via OSC removed NMR instrument identity clustering in the PCA. This same study demonstrated that OSC can remove time-dependent experimental and physiological spectral changes. Instrumental transfer involving the mapping of one instrumental response onto other instrumental configurations using a finite impulse response (FIR) filtering of the spectra has also been described,[90] but has not been demonstrated for NMR

A limitation of HC and OSC methods is that the addition of more instruments (or instrumental configurations) requires that multivariate models be recalculated. In the case of OSC, the orthogonal components that do not describe the classification or calibration are removed from all the configurations, and the resulting OSC-filtered data is used in the subsequent model development. If an additional instrument configuration is added at a later time, all the data is combined, followed by subsequent OSC analysis and filtering. Unfortunately, this filtering invalidates any previously developed calibration or identification models, and might prove costly or time consuming if new calibration models must be evaluated for each new instrumental configuration. Because of the multiple NMR instrument configurations analyzed in this manuscript, the use of OSC filtering is not presented but will be discussed in a later communication.

The most common instrumental transfer methods involve the direct transfer of experimental spectra from a new (secondary) instrumental configuration to the original master (primary or target) instrument using either direct standardization (DS) or piece-wise direct standardization (PDS) with additive background correction.[91-97] The DS and PDS instrumental transfer methods have been extended to include double-window piece-wise direct standardization (DWPDS).[98] The use of DS and PDS methods have been demonstrated for low-resolution (20 MHz) process NMR spectroscopic data sets.[99] By using the ^{1}H free induction decay (FID) to develop a PLS model for prediction of high load melt index values, the impact of probe ring-down, pulse widths and temperature offsets was addressed. For these time-domain NMR studies, the PDS method was found to be the most successful instrumental transfer method.. These initial low-resolution results demonstrate that instrumental transfer techniques can be applied to NMR spectroscopy and provide the impetus to extend the techniques to high-resolution NMR spectral data sets.

In this chapter, the performance of DS, PDS and DWPDS methods for the transfer of a partial least squares (PLS) calibration model of metabolite concentrations in model mixtures is explored. The optimization of the instrumental transfer methods with respect to the number of transfer calibration standards and filter window size is addressed. In addition, the impacts of phasing, binning and spectral deconvolution on the observed prediction errors between different NMR instrument configurations are evaluated.

5.2. Methods for Instrumental Transfer

5.2.1. NMR Data Sets

A set of 15 standard samples composed of a simple mixture (0 – 50 mM) containing the metabolites citrate, glucose, and glycine in D_2O (pH = 7.0, 10 mM phosphate buffer) with 5 mM 3-trimethylsilylpropionate (TSP) were prepared, sealed in matched tubes and used for all experiments described. The mixture concentrations are provided in the supplemental material. No experimental design was used in preparing these samples. NMR data were collected on 2 different NMR instruments, a Bruker Avance 600 and a Varian Unity Plus 600, using either a 5 mm broadband (BB) X{^{1}H} observe probe (Bruker), a ^{1}H{X} inverse (INV) probe (Bruker), or 2 vintages of a HCN probe (Varian). For each instrument and probe, NMR data using both a single pulse 1D direct and a 1D NOESY (100 ms) sequence was obtained to give data sets for 8 different configurations. These instrumental, configurations will be designated as 1D BB Bruker, NOESY BB Bruker, 1D INV Bruker, NOESY INV Bruker, 1D HCN(a) Varian, NOESY HCN(a) Varian, 1D HCN(b) Varian, and NOESY HCN(b) Varian. A combined data set composed of 120 different ^{1}H NMR spectra (15 samples x 8 configurations) was obtained. Experimental conditions between the different NMR instruments were matched as closely as possible using a spectral width of 7183 Hz, 32K spectral points, zero filling to 64K, 9 μs $\pi/2$ pulse, 1s recycle delay, 64 scan averages, with no water pre-saturation employed. To assure similar data treatment between the different instrument platforms, the NMR data sets were all transformed, phased, referenced and baseline corrected in the CHENOMX NMR Suite 5.0 (Edmonton, Canada). The chemical shifts were referenced to internal TSP, δ = -0.016 ppm. The shift of TSP is pH dependent as incorporated into CHENOMX NMR Suite 5.0. In addition, spectral binning and line shape deconvolution[61] were performed in the CHENOMX Suite. To study the impact of phasing on the model transfer, a single instrumental configuration data set was phased using the automatic baseline routines ABS and ABSD in the Bruker TOPSPIN software, and manually by two different operators to give a total of four different data sets for analysis of phasing effects. The data sets were integral normalized to the total spectral intensity and then mean-centered. Of the 15 standard mixtures, three represent pure component spectra and were removed during model development to reduce extensive biasing and leveraging. This reduction means that 12 samples were used in the development of the calibration model development for a total of 96 different NMR spectra in the data set (12 samples x 8

configurations). A PLS calibration model (using the SIMPLS algorithm) was developed for the relative metabolite concentration on the target instrument (1D BB Bruker) using the 12 calibration samples with three factors on mean-centered data. This model was then used to predict the metabolite concentrations on the remaining seven instrumental configurations for the same calibration samples both before and after instrumental transfer. In order to reduce possible variations between the calibration samples an independent calibration sample set was not utilized on the secondary instruments to evaluate the PLS model.

5.2.2. Instrumental Transfer Computational Details

The analysis of the data and development of the calibration models were performed in MATLAB 2007b (The Mathworks, Inc.), while the different instrumental transfer algorithms employed were implemented using the PLS Toolbox 4.1 (Eigenvector Research). The root-mean-square errors of calibration ($RMSEC_1$) on the primary instrument and the root-mean-square errors of prediction ($RMSEP_j$) of the *j*th secondary instrumental configuration are defined by

$$\text{RMSEP}_j \text{ [or RMSEC}_1\text{]} = \sqrt{\frac{\sum_{p=1}^{n} \hat{y}_p(j) - y_p^{\ 2}}{n}} \tag{5.1}$$

where *n* is the number of calibration samples, $\hat{y}_p(j)$ are the predicted concentration values for the *p*th standard sample on the *j*th instrumental configuration, and y_p is the true concentration. The improvement in prediction for a given instrumental transfer *method* on the *j*th instrumental configuration summing over the *m* different components is given by

$$\%\,\text{improvement}(method, j) = \frac{1}{ncomp} \sum_{m=1}^{ncomp} \frac{\text{RMSEP}_{method,j,m} - \text{RMSEP}_{\text{Raw},j,m}}{\text{RMSEC}_{\text{Raw},1,m}} \times 100 \tag{5.2}$$

where $\text{RMSEP}_{\text{Raw},j,m}$ is the error for the *m*th component, on the *j*th instrument using the *raw* unmodified data with no binning and prior to instrumental transfer.

5.2.3. Direct Standardization

Throughout this chapter scalars are represented by italic lowercase letters, column vectors by boldface lowercase letters, and matrices by boldface capital letters. Mean-centered vectors and matrices are denoted by a bar over the letter. Instrumental transfer using the direct standardization (DS) method correlates the spectra (or FIDs) between different NMR instruments by modeling the responses as:[91-93, 96]

$$\mathbf{S_1} = \mathbf{S}_j\mathbf{F_b} + \mathbf{1b}_{js}^{\mathbf{T}} \tag{5.3}$$

Where the matrix $\mathbf{S_1}$ is the response of the target NMR instrument on which the calibration model was developed, and $\mathbf{S}_j$ is the response matrix of instrumental configuration *j*, $\mathbf{F_b}$ is the $\nu \times \nu$ transformation matrix and $\mathbf{b}_{js}^{\mathbf{T}}$ is the background correction vector (1 x υ) for the *j*th configuration. The response matrix $\mathbf{S}$ ($n \times \nu$) is composed of *n* samples and ν frequencies. In the present case, the $\mathbf{S}_j$ matrices represent the spectral response of different instrument configurations (different instruments, different probes, different pulse sequences or data over extended periods of time) that we want to transform into the target instrument. Once the data is transformed, the $\mathbf{S_1}$ model can be applied. For mean-centered spectral data ($\bar{\mathbf{S}}_j$), equation (3) becomes

$$\bar{\mathbf{S}}_\mathbf{1} = \bar{\mathbf{S}}_j\mathbf{F_b} \tag{5.4}$$

For the DS method the transfer matrix is calculated using

$$\mathbf{F_b} = \bar{\mathbf{S}}_j^{+}\bar{\mathbf{S}}_\mathbf{1} \tag{5.5}$$

where $\bar{\mathbf{S}}_j^{+}$ is the pseudoinverse of $\bar{\mathbf{S}}_j$. Calculation of the pseudoinverse employs singular value decomposition (SVD) where the response matrix is decomposed into three matrices **U**, **Σ**, and **V** using

$$\bar{\mathbf{S}}_j = \mathbf{U}\boldsymbol{\Sigma}\mathbf{V}^{\mathbf{T}} \tag{5.6}$$

The pseudoinverse is then given by

$$\bar{\mathbf{S}}_j^{+} = \mathbf{V}\boldsymbol{\Sigma}^{-1}\mathbf{U}^{\mathbf{T}} \tag{5.7}$$

The additive background term is then estimated as

$$\mathbf{b}_{j\mathbf{s}} = \mathbf{s}_{\mathbf{1m}} - \mathbf{F}_{\mathbf{b}}^{\mathbf{T}}\mathbf{s}_{j\mathbf{m}} \tag{5.8}$$

where $\mathbf{s}_{j\mathbf{m}}$ are the mean vectors of the response matrices $\mathbf{S}_j$. For NMR, the spectral baselines are commonly corrected during preprocessing such that the background $\mathbf{b}_{j\mathbf{s}}$ should be vanishingly small and will have no impact on analysis employing mean-centered data. If the baseline is highly structured (i.e. baseline roll) and not corrected during routine preprocessing prior to instrumental transfer, then the additive background term will need to be determined.

5.2.4. Piece-Wise Direct Standardization

For the DS method described above, the entire spectrum of the secondary instrument is used for the calculation of the transfer matrix $\mathbf{F}_{\mathbf{b}}$ at each frequency. For NMR data sets (as well as other type of spectroscopies), the spectral changes observed between instruments will only involve small frequency changes such that determination of $\mathbf{F}_{\mathbf{b}}$ can be restricted to nearby frequencies within the spectrum. Using piece-wise direct standardization (PDS),[91-93, 96] the spectral response on the primary instrument at the υth frequency ($\mathbf{r}_{1,\upsilon}$) can be related to the spectral response on the jth instrumental configuration at nearby wavelengths with a window width of $2k+1$ ($\mathbf{r}_{j,\upsilon-k}, \mathbf{r}_{j,\upsilon-k+1}, \cdots, \mathbf{r}_{j,\upsilon+k-1}, \mathbf{r}_{j,\upsilon+k}$). These measurements for the υth frequency can be placed into a matrix to form

$$\mathbf{X}_{\upsilon} = \left[\mathbf{r}_{j,\upsilon-k}, \mathbf{r}_{j,\upsilon-k+1}, \cdots, \mathbf{r}_{j,\upsilon+k-1}, \mathbf{r}_{j,\upsilon+k} \right] \tag{5.9}$$

A regression vector at each frequency can then be calculated using

$$\mathbf{b}_{\upsilon} = \mathbf{X}_{\upsilon}^{+} \mathbf{s}_{1,\upsilon} \tag{5.10}$$

The transformation $\mathbf{F}_{\mathrm{b}}$ is then a banded diagonal matrix given by

$$\mathbf{F}_{\mathrm{b}} = \mathrm{diag}\ \left[\mathbf{b}_1^{\mathrm{T}}, \mathbf{b}_2^{\mathrm{T}}, \mathbf{b}_3^{\mathrm{T}}, \ldots, \mathbf{b}_{\nu}^{\mathrm{T}} \right] \tag{5.11}$$

where most of the off-diagonal elements in the transformation matrix are zero.

5.2.5. Double Window Piece-Wise Standardization

The PDS method can be extended through the use of a double window (DW) PDS, where the first window length is defined by $2k+1$ frequencies and a second window of width $2m+1$ samples are used in the calculation of $\mathbf{F_b}$. This method is detailed extensively in the PLS 4.1 Toolbox software (Eigenvector Research Inc.) and will not be reproduced here.

5.2.6. *Selection of Standardization Subset*

The subset of standard samples used for the instrumental transfer must contain enough spectral information to fully describe the differences between the two instrumental configurations and span the model of interest. In this study, the transfer calibration samples were identified by calculation of the hat matrix $\mathbf{H}$ using[91]

$$\mathbf{H} = \bar{\mathbf{S}}_1 \bar{\mathbf{S}}_1^{+} \tag{5.12}$$

The diagonal elements of this matrix contain the leverage of the samples with respect to their influence on the calibration model and were used to identify the ranking of the calibration standard samples. The calculation of $\mathbf{H}$ used the combined PLS model for all three metabolites

in the mixture (glucose, glycine, and citrate). Selection of the transfer calibration samples based on the $\mathbf{H}$ leverage determined using only the glucose calibration gave similar ordering.

5.3. Results and Discussion

Figure 5.1 shows the high-resolution solution ^{1}H NMR spectra for the 15 different mixtures obtained using the broadband probe on a Bruker Avance 600 instrument. Similar spectra were collected for the other instrument, probe and pulse sequence configurations. These NMR spectra are composed of signals from glycine, glucose and citrate. The data at 0.001 ppm resolution and following 0.04 ppm binning are also shown in Figure 5.1. Only the portion of the NMR spectra between ~ +4 ppm and +2.2 ppm was used in the model development described below. This spectral range does not contain the water region (~4.8 ppm), eliminating the interference of exchangeable protons and the large dominant residual water resonance. Previous studies have shown spectral variations result from the use of different water saturation sequences including the optimization of these sequences.[73] The ability of instrumental transfer methods to correct spectral differences resulting from water presaturation was not pursued in the current study and will be the focus of future analysis. The metabolites chosen did provide examples where the NMR spectral features were isolated and well resolved (i.e. the citrate multiplet at δ ~ +2.55 ppm), while other signals contain significant overlap (i.e. the complex set of glucose multiplets and the glycine singlet at ~ +3.5 ppm).

To address the performance of the instrumental transfer methods the ^{1}H NMR spectra obtained using the eight different instrumental configurations (see Methods section) were used for the prediction of the relative glucose, glycine and citrate concentration within the mixtures.. For our analyses, the data set obtained on the Bruker Avance 600 instrument using a 5 mm broad band probe with a simple single pulse 1D excitation (1D BB Bruker) was chosen as the master (target or primary) instrument to which the other instrumental data sets were transferred using different protocols.

5.3.1. Predictions Without Instrumental Transfer

On the master NMR instrument the root-mean squared error of calibration (RMSEC) values of 0.0099, 0.0058 and 0.0075 were obtained for the relative glucose, glycine, and citrate concentrations, respectively (see Table 5.1). Figure 5.2 shows the glucose predictions for the

remaining seven instrumental configurations, with the glycine and citrate predictions displayed in Figure 5.S1 and 5.S2 (supplemental material). Using the PLS model developed for the target instrument (1D BB Bruker), the corresponding root mean squared error of prediction (RMSEP) for the other instrumental configurations are given in Table 5.1 (row 1, analysis method). It is clear that the predictive performance of the relative concentration model does not transfer well to different instrumental configurations. The exception to this trend was the NOESY data set for the BB probe (NOESY BB Bruker) that are spectra obtained on the same instrument and probe used to develop the calibration model, but with a different pulse sequence. Closer inspection of Figure 5.2 shows that the predictions from the single pulse experiments (1D) and the NOESY experiments always cluster together for a particular instrument and probe. This demonstrates that the impact of using a 1D Bloch decay experiment versus a 100 ms NOESY experiment is small and does not greatly influence the predictive model transfer between these configurations. PLS models were also developed for each instrument configuration individually and then use to predict the relative concentrations on the remaining instruments. These results are summarized in Table 5.S1.

Inspection of Figure 5.2 reveals that glucose concentrations are over-predicted (~ 20%) for low relative concentrations on all of the secondary instrumental configurations, including the data sets obtained from the same instrument console (Bruker) but with an inverse probe. This suggests that the issues in the spectral response were not simply vendor console related. At high glucose concentrations the PLS predictions under-estimate the concentration (up to 10%) with the Varian data sets showing the largest deviation from the developed model. These observed RMSEP errors result from a combination of line width changes and reduced resolution of the glycine singlet from the glucose multiplets. Note that relative concentrations were used for the PLS model development, with an error in the measurement of any single component impacting the other calculated concentrations. This is also reflected in the largest error occurring at high glycine and citrate relative concentrations (Figure 5S.1 and 5S.2) mirroring the glucose results in Figure 5.2. The consistently larger citrate RMSEP (in comparison to glycine) may also reflect the limited number of samples containing citrate in the PLS calibration samples. There are several spectral variations that could impact these concentration predictions including changes in resolution (binning), line shape and line width changes between the different instrumental configurations, variations in spectral pre-processing including baseline and phase corrections,

along with differences in pulse excitation efficiency. In the next section the impacts of these different variations are addressed, followed by the assessment of methods for improving the performance of model transfer between different NMR instrument configurations.

5.3.2. Impact of Phasing

Differences in the quality of spectral phasing are one of the simplest variations that might be encountered when comparing NMR data between different instrumental configurations. The data may be processed by automated phasing routines or manually by different operators prior to data set combination. To address the magnitude of changes in RMSEP (in the current data set) as a function of phasing, a single NMR data set was manually phased by two different operators, and automatically using two different phasing routines available in the Bruker TOPSPIN package. It was observed that the largest differences in the spectral phasing for the different operators and automatic routines involved large dominant resonances (i.e. H_2O) that in some situations may subtly impact the instrumental transfer performance. In the present study, the developed PLS models excluded the H_2O resonance, eliminating any large phasing errors associated with this major resonance. The resulting RMSEP for the glucose, glycine, and citrate concentrations as a function of the phasing protocol are included in Table 5.S2 (supplemental material). This result shows that the impact of phasing in the present example is very small, and that phasing variations do not account for the large RMSEP differences between instrumental configurations observed in Figure 5.2 (and Figures 5S.1 and 5S.2). In some cases involving large solvent peaks, phasing may play a more significant role in the instrumental variations and will need to be considered.

5.3.3. Impact of Binning

Binning is commonly utilized in the preprocessing of NMR spectral data prior to chemometric analysis to help reduce small spectral shifts and minor line shape variations. PLS models for concentration were developed as a function of binning size to address if the RMSEP between the different instrumental configurations might be improved by increasing the bin size. These results are summarized in Table 5.S3 and Figure 5.S3. For the PLS model predictions of glucose, glycine and citrate concentrations, no significant changes in RMSEC were observed with increased binning size. For the other instrumental configurations, there were modest

improvements in the RMSEP (Table 5.S3) ranging between ~5 and 30% as a function of binning size. There does not appear to be a unique binning size for optimal improvement in RMSEP between the different instrumental configurations making it difficult to select a binning size for predictive purposes. For these particular model mixtures use of 0.005 ppm binning would have produced between 6 and 28% improvement in RMSEP. The RMSEP of the different instrumental configurations still continue to be 3 to 10 times larger than that of the target instrument for which the PLS model was developed (1D BB Bruker). The exception to this is the NOESY BB Bruker configuration, again demonstrating that the pulse sequence (1D versus NOESY) has a minimal impact on the instrumental transfer.

In metabonomic studies binning helps remove small chemical shift variation due to changes in pH, concentration, temperature and ionic strength. Peak alignment or spectral registration techniques have also been employed to eliminate these chemical shift variations.[100-103] In this paper such chemical shift perturbations were expected to be small since identical standard samples were used in the analysis. It should be noted that the instrumental transfer methods that are the focus of this paper attempt to remove instrumental variations through a transfer calibration samples, and that sample-to-sample variations such as pH dependent chemical shift changes are not directly addressed by the instrumental transfer methods. These results show that while a judicious use of binning could improve the RMSEP, the small chemical shift variations addressed by binning were not responsible for the poor instrumental transfer predictions shown in Figure 5.2 (and Figures 5S.1 and 5S.2).

5.3.4. Impact of Deconvolution

The impact of line shape deconvolution on the prediction of concentration was also investigated by re-processing the data sets with the CHENOMX deconvolution algorithm. Using the TSP resonance as the internal line shape reference, the asymmetric non-Lorentzian line shapes of the other resonances were corrected. A default assessment of the line broadening based on the TSP line width for each individual spectrum was used for deconvolution and ranged from 1.0 to 5.0 Hz. By targeting the deconvolution to the observed TSP line width, the deconvolution procedure removed asymmetries present within the spectrum, but did not remove the large differences in line width observed between the different NMR instrument configurations. Figure 5.3 shows the resulting PLS predictions for the relative concentration of glucose following line

shape deconvolution of the entire data set. Comparison of this prediction to the results in Figure 5.2 shows only a minor improvement (in particular at the high glucose concentration range), but the change is still small compared to the larger deviations observed between different instrument configurations and the original PLS model. The RMSEP following spectral deconvolution are summarized in Table 5.1 (row 2, analysis method) and Table 5.S4 (supplemental material). Between 7 and 15% improvement in RMSEP was observed, but for some configurations (1D INV Bruker and NOESY INV Bruker) there was actually a decrease in RMSEP performance.

Recall that for each individual sample the shimming was optimized and thereby may introduce a sample-to-sample variation within an instrumental configuration. If all of the samples in a given instrumental configuration are not shimmed exactly the same, then the relationship on which the instrumental transfer function was developed (Equation 3) no longer strictly holds. As noted above, the target line width was chosen to match the experimental TSP line width and this effectively removes the asymmetries and distortions of the line shapes due to poor shimming between different instrumental configurations, allowing the instrumental transfer method to be employed. To reduce the impact of small line shape asymmetries and distortions unbinned but line shape deconvoluted spectral data sets were used during the remainder of the instrumental transfer analysis discussed below.

By not choosing the same target line width during deconvolution for all the spectra on all the different instrumental configurations, the impact of line width changes on the predicted performance has been maintained. In addition, it is always possible to add future additional instrumental configurations such that there is no way to know the most appropriate target line width *a priori*. Analysis using spectral data that was deconvoluted to match the smallest line width observed in all of the instrumental configurations resulted in dramatically increased RMSEP values. This was particularly true for configurations (i.e. 1D HCN(b) Varian) with large experimental line widths (~ 5 Hz) where the S/N of the deconvoluted spectra dropped dramatically when the smaller target line widths were imposed. This reduction in S/N performance as a function of the target reference deconvolution line width has been noted before.[87]

5.3.5. DS Method

The use of the direct standardization (DS) method to transfer NMR spectra between different instrumental configurations was explored first. This method has been used for NIR and IR data, with only limited application to NMR data.[99] The calculation of the transfer function $\mathbf{F_b}$ (see details in the Methods) is based on using a subset of standards, and is therefore a function of the number of transfer calibration samples utilized. The DS method is considered to have converged when the RMSEP reaches a minimum with increasing number of transfer calibration samples. One of the goals of this study was to address how many transfer samples are needed to obtain convergence in high-resolution NMR data sets. The RMSEPs for metabolite concentrations based on the PLS model developed using the target configuration (1D BB Bruker) were evaluated for increasing number of calibration samples (on unbinned, but deconvoluted data sets). As an example, Figure 5.4 shows the variation in the RMSEP of the glucose, glycine, and citrate concentrations as a function of the number of calibration samples used for instrumental transfer of the secondary 1D INV Bruker configuration. The ranking (Eqn. 12) of the transfer calibration samples chosen was based on the highest leverage for the entire PLS calibration. There is an initial large increase in RMSEP for DS when only a single sample is used for the estimation of $\mathbf{F_b}$. The RMSEP then decreases quickly and reaches a plateau or intermediate minimum when more than 4 transfer calibration samples were used. Table 1 shows the RMSEP observed for the other NMR instrumental configurations following DS instrumental transfer. By using five transfer calibration samples there is a decrease in the RMSEP error, producing between 50% and 75% improvement (Table 5.1). This improvement in the prediction error is significantly larger than that observed for simple binning (Table S3) or simple line shape deconvolution (Table 1) discussed above. Following this intermediate minimum in RMSEP there is a continued gradual decrease with increasing number of transfer calibration samples.

Similar results (Figure 5.S4, supplemental material) were observed for the RMSEP behavior in the other instrumental configurations following DS instrumental transfer. There are a few instrumental configurations where the initial intermediate minimum in RMSEP was not reached until more than 5 transfer calibration samples were utilized, specifically the 1D HCN(b) Varian and the NOESY BB Bruker instrumental configurations. This number of required transfer calibration samples (either 4 or 5) is significantly smaller than the 14 up to 56 transfer calibration samples required for instrumental transfer of the time-domain ^{1}H process NMR previously

reported,[99] and reflects the high-resolution nature of the current data set. In summary, DS instrumental transfer provided a large reduction in RMSEP for the PLS concentration models across the different instrumental configuration, with an intermediate minimum being observed for 4 or 5 transfer calibration samples. Further improvements in the model transfer can be obtained by including additional transfer calibration samples, but the improvements are very small compared to the initial RMSEP reduction observed for either 4 or 5 transfer calibration samples.

5.3.6. PDS Method

For the piece-wise direct standardization (PDS) instrumental transfer method, the RMSEP is a function of both the number of transfer calibration samples used and the number of adjacent instrumental frequencies employed in the estimation of $\mathbf{F_b}$. The variation of the RMSEP following instrumental transfer of the 1D INV Bruker instrumental configuration is shown in Figure 5.5. Similar results were obtained for the remaining NMR instrument configurations (An example for the Varian 1D HCN(b) configuration is shown in Figure 5S.5 in the supplemental material). Consistent with results obtained using the DS method, there is an initial increase in RMSEP for instrumental calibrations using only one transfer calibration sample, followed by a drop in RMSEP for additional transfer calibration samples. For PDS an intermediate minimum was observed for 2 or 3 transfer calibration samples, resulting in a 45% to 60% improvement in RMSEP (Table 1). Again this intermediate minimum was followed by a gradual decrease in RMSEP (5 to 10%) with increasing number of transfer calibration samples. Variation of RMSEP with the number of instrumental frequencies was also observed using the PDS method, but was small compared to the variation due to number of transfer calibration samples. In several of the configurations tested, there is an additional decrease in RMSEP with increasing number of instrumental frequencies (Figure 5.5). For example, the RMSEP for the prediction of glycine (Figure 5.5e) decreases noticeably for predictions increasing from 1 to 7 instrumental frequencies, but for glucose (Figure 5.5d) or for citrate (Figure 5.5f), the decrease is less pronounced. The improvement in RMSEP with increasing number of filter frequencies was more pronounced for the prediction of some metabolites, suggesting subtle chemical shift changes are occurring in these standard samples. When very large numbers of filter frequencies are employed with PDS, this method converges to the DS results (DS uses all frequencies to develop the

transfer function). The insensitivity of the RMSEP to the number of instrumental filter frequencies shows that the chemical shift variations are not the dominant source of error between these different instrumental configurations. Table 5.1 summarizes the RMSEP obtained using the PDS method for calibrations using three transfer calibration samples and one instrumental frequency, and for calibrations using four transfer calibration samples and seven instrumental frequencies. The percent improvements in RMSEP range from 45% to 75% using the PDS method, and are comparable to the results of the DS method. For example, one can compare the results for the PDS transfer results of the 1D INV Bruker configuration (Figure 5.5) to the results of the DS transfer (Figure 5.4), where the PDS method requires fewer number of transfer calibration samples (2 or 3 versus 4 or 5 in DS). This reduction in the calibration sample subset could prove beneficial for instances where a limited number of calibration samples are available for implementing the instrumental transfer.

5.3.7. DWPDS

For the double window piece-wise direct standardization (DWPDS) method, the instrumental transfer is now a function of three variables: the number of transfer calibration samples, the number of filter frequencies and the number of filter samples used in the calibration. Figure 5.6 shows an example of the RMSEP variation as a function of the number of transfer calibration samples, and the number of filter frequencies (5.6a) and the number of filter samples (5.6b). These responses are reminiscent to those observed for the PDS method (Figure 5.5). Even with the additional parameter used in the development of the transfer function the percent improvement is almost the same as in the PDS method (see Table 5.1). The calculation of the DWPDS transfer functions also took considerably longer than the PDS method. Based on these results, there is no clear reason to utilize the DWPDS method over the PDS method in the instrumental transfer of high-resolution NMR spectral data.

5.3.8. Transfer Calibration Sample Subset

The power and capability of transferring data between different NMR instrument configurations is shown in Figure 5.7. The spectral data from the target or primary instrument (1D BB Bruker, Figure 5.7a) is composed of sharp, well-resolved spectral lines. In contrast, Figure 5.7b shows the spectral data for the exact same sample set on a secondary instrumental

configuration (1D HNC(b) Varian). For this configuration there is significant broadening of the resonances. Following instrumental transfer using the DS method, the spectral data set from his secondary configuration is now also composed of sharp well-resolved resonances (Figure 5.7c), and is almost identical to the spectral data set of the target instrument.

The performance of these instrumental transfer methods (DS, PDS, DWPDS) ultimately depend on the number and information content of the transfer samples used for calibration. In particular, does the transfer calibration sample subset span the spectral space of the data set that instrumental transfer is being employed on? For the model mixtures investigated here with a limited number of components, it is simple for a limited number of transfer calibration samples to fully represent the spectral response of the entire data set. This assumption will not necessarily hold for more complex mixtures (biofluids or metabonomics) where hundreds of different compounds may be present. Two questions immediately arise: (1) Are the chosen transfer calibration samples sufficient to model all of the resonances of interest for the entire set of compounds present? (2) What happens if the transfer calibration sample subset does not contain a specific compound?" These questions are partly addressed in Figure 5.7d, where the transfer calibration samples selected were chosen such that the metabolite citrate was not present in this subset. It should be noted that this was a totally artificial selection process. The leverage matrix (Equation 5.12) used for transfer sample selection ranks the citrate containing samples very high, but in this case the ranking was ignored with the forced selection provided as an example. This "poor" selection of transfer calibration samples results in transformations in which no citrate resonances (at ~ 2.5 ppm) are present during the calculation of $\mathbf{F_b}$, such that the DS transfer method (or PDS/DWPDS) attempts to suppress signals in this spectral region in the remainder of the data set. This example shows the importance of the transfer calibration sample subset providing a complete spectral representation of the entire data set using the existing DS, PDS and DWPDS instrumental transfer methods, and shows a possible limitation of instrumental transfer methods as applied to complex mixtures. We are currently developing filtering techniques for these instrumental transfer methods to overcome this limitation (Alam, unpublished)..

5.4. Conclusions

It has been demonstrated that the DS, PDS, and DWPDS instrumental transfer methods can be used on high-resolution NMR spectral data sets. All of these transfer methods provided

significant improvement for the PLS prediction of metabolite concentrations in model mixtures between different instrumental configurations. In addition, all of these instrumental transfer methods improved the RMSEP in comparison to simple binning or line shape deconvolution techniques. The DS instrumental transfer method gave the largest percent improvement in the concentration predictions, but also required a larger number of transfer calibration samples than the PDS method. The PDS and DWPDS methods gave similar improvement in the prediction of concentrations, but required fewer transfer calibration samples. For simple mixtures and other limited examples, the instrumental transfer methods perform well and allow the transfer of calibration models between different NMR instruments. It was demonstrated that there are limitations imposed on the selection and number of transfer calibration standards. This limitation is a major issue for complex mixtures and currently precludes the direct application of instrumental transfer methods to biofluid/metabonomic studies.

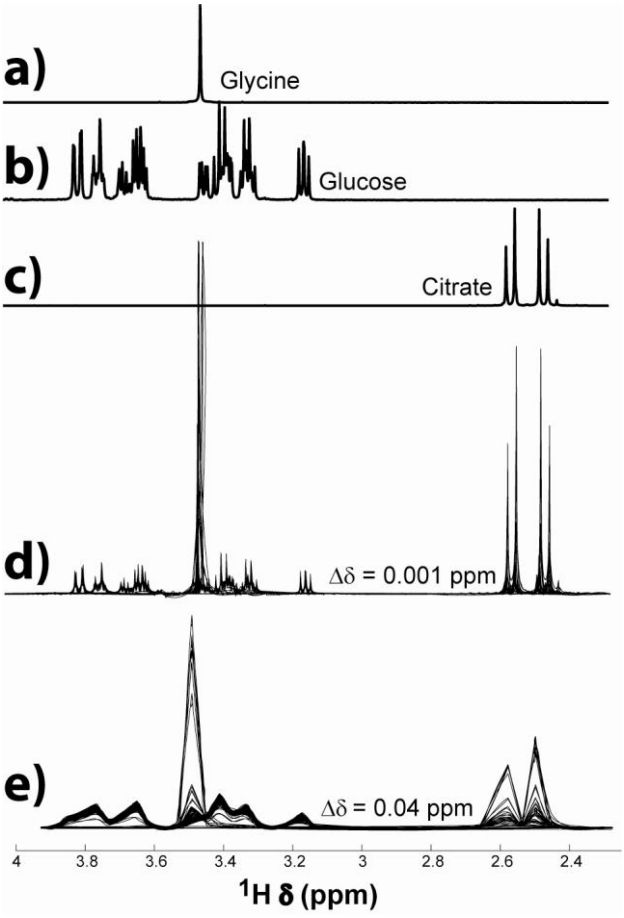

Figure 5.1. High-resolution ^{1}H NMR spectra of the individual components used to prepare the transfer calibration standard samples: a) glycine. b) glucose and c) citrate. The overlapping NMR data set of the 15 different standard mixtures with d) a spectral resolution of $\Delta\delta$ = 0.001 ppm and e) following a $\Delta\delta$ = 0.04 ppm binning.

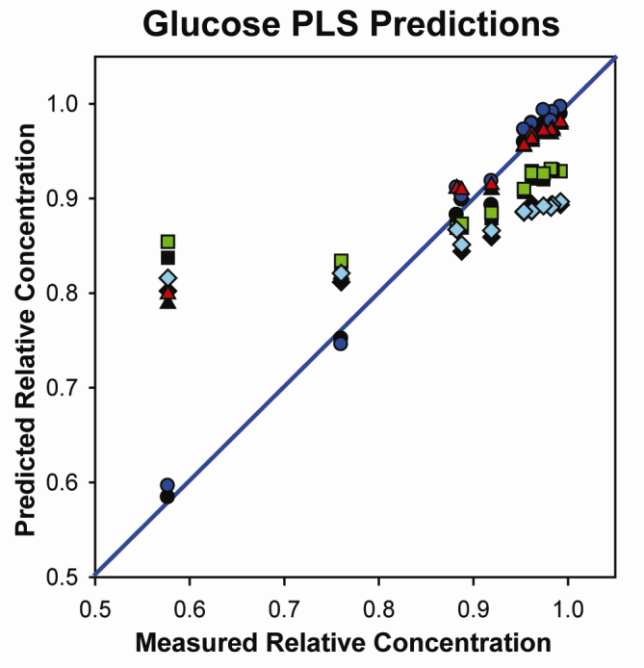

Figure 5.2. The correlation between the ^{1}H NMR PLS predicted relative concentration of glucose and the measured relative concentration of glucose, for the standard mixtures using eight different instrumental configurations. The PLS model was developed for the relative concentration of glucose, glycine and citrate simultaneously using the unbinned 1D ^{1}H NMR spectra data set from the Bruker instrument with a broadband probe, 1D BB Bruker (●). This model was subsequently used for the prediction of metabolite concentrations on the remaining configurations prior to any instrumental transfer modification, NOESY BB Bruker (●), 1D INV Bruker (▲), NOESY INV Bruker (▲), 1D HCN(a) Varian (■), NOESY HCN(a) Varian (■), 1D HCN(b) Varian (♦) and NOESY HCN(b) Varian (♦). The results for a given NMR probe utilize the same symbols, with the NOESY results being colored.

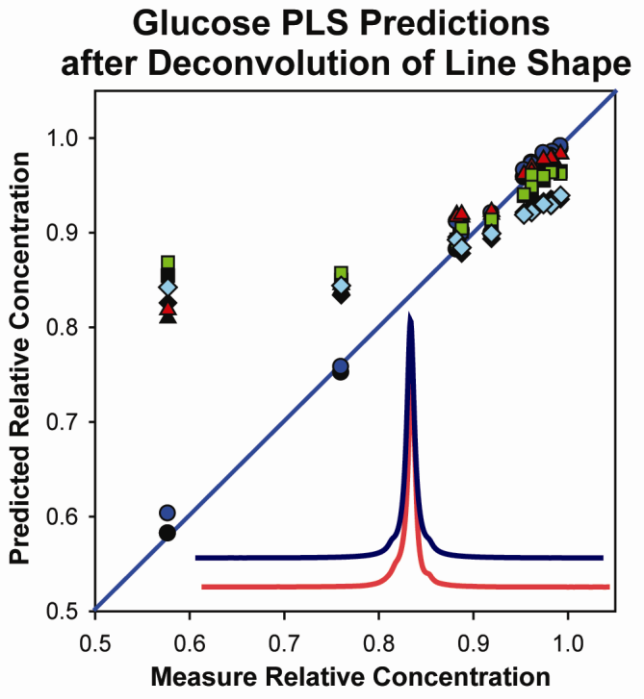

Figure 5.3. The correlation between the ^{1}H NMR PLS predicted relative concentration of glucose and the measured relative concentration of glucose, for the standard mixtures using eight different instrumental configurations following line shape deconvolution. The PLS model was developed for the relative concentration of glucose, glycine and citrate simultaneously using the unbinned 1D ^{1}H NMR spectra data set from the Bruker instrument with a broadband probe, 1D BB Bruker (●). This model was subsequently used for the prediction of metabolite concentrations in the remaining data sets, NOESY BB Bruker (●), 1D INV Bruker (▲), NOESY INV Bruker (▲), 1D HCN(a) Varian (■), NOESY HCN(a) Varian (■), 1D HCN(b) Varian (♦) and NOESYHCN(b) Varian (♦). The inset shows an example of the slight asymmetric line shape observed in the TSP resonance (red) that has undergone line shape deconvolution (dark blue).

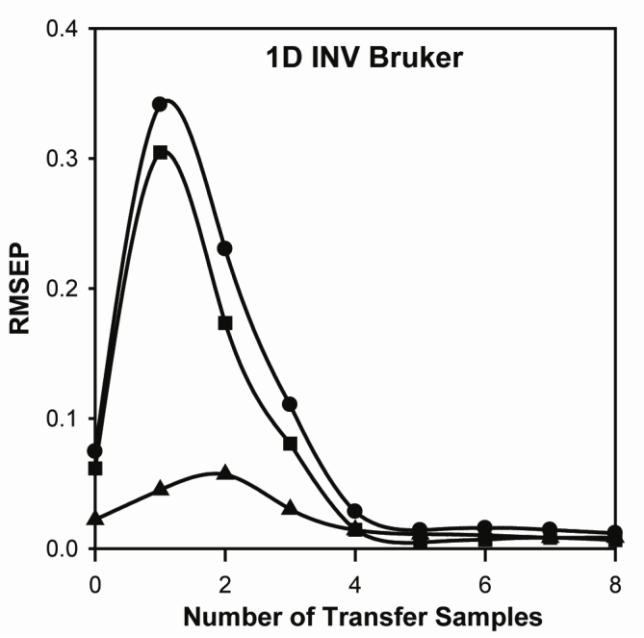

Figure 5.4. The variation of RMSEP for the relative concentration of glucose (●), glycine (■) and citrate (▲) using direct standardization (DS) instrumental transfer on the 1D INV Bruker instrument configuration as a function of number of transfer calibration samples.

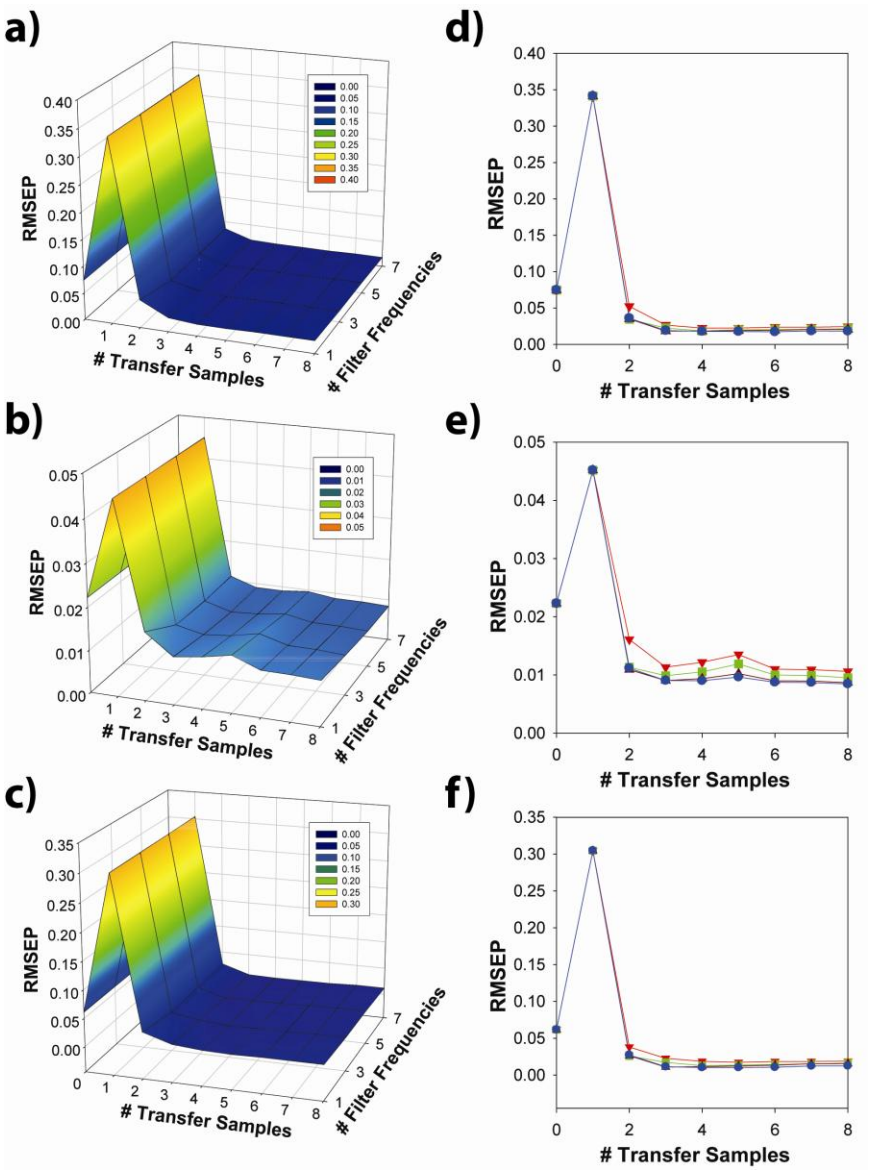

Figure 5.5. The variation of RMSEP as a function of the number of transfer calibration samples and number of instrumental frequencies used in the piece-wise direct standardization (PDS) instrumental transfer on the 1D INV Bruker configuration for the relative concentrations of a) glucose, b) glycine and c) citrate. In d)-f) the RMSEPs for different number of instrumental frequencies are shown for (▼) 1 , (■) 3, (▲) 5 and (●) 7 instrumental frequencies. These results can be compared to the RMSEP variation obtained using the DS method shown in Figure 5.4.

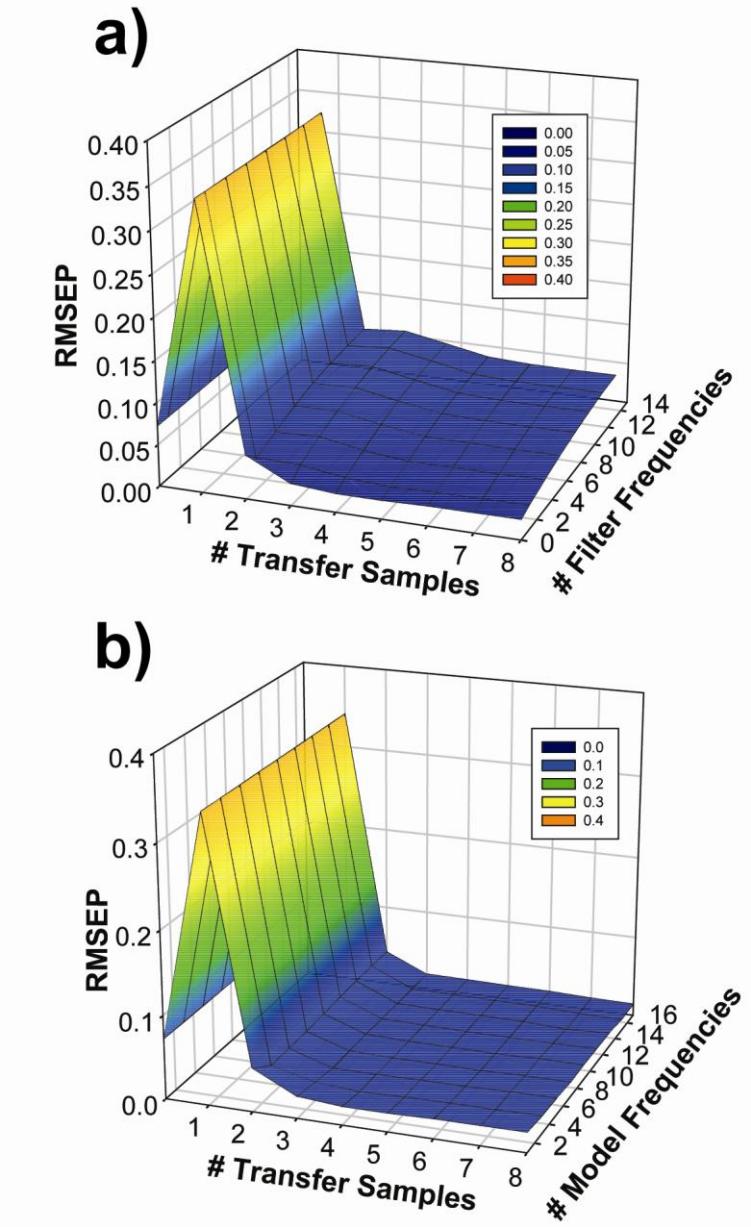

Figure 5.6. The variation of RMSEP for the prediction of glucose concentration for the 1D INV Bruker configuration following double window piece-wise direct standardization (DWPDS) method as a function of transfer calibration sample number along with a) the number of filter frequencies and b) the number of model frequencies.

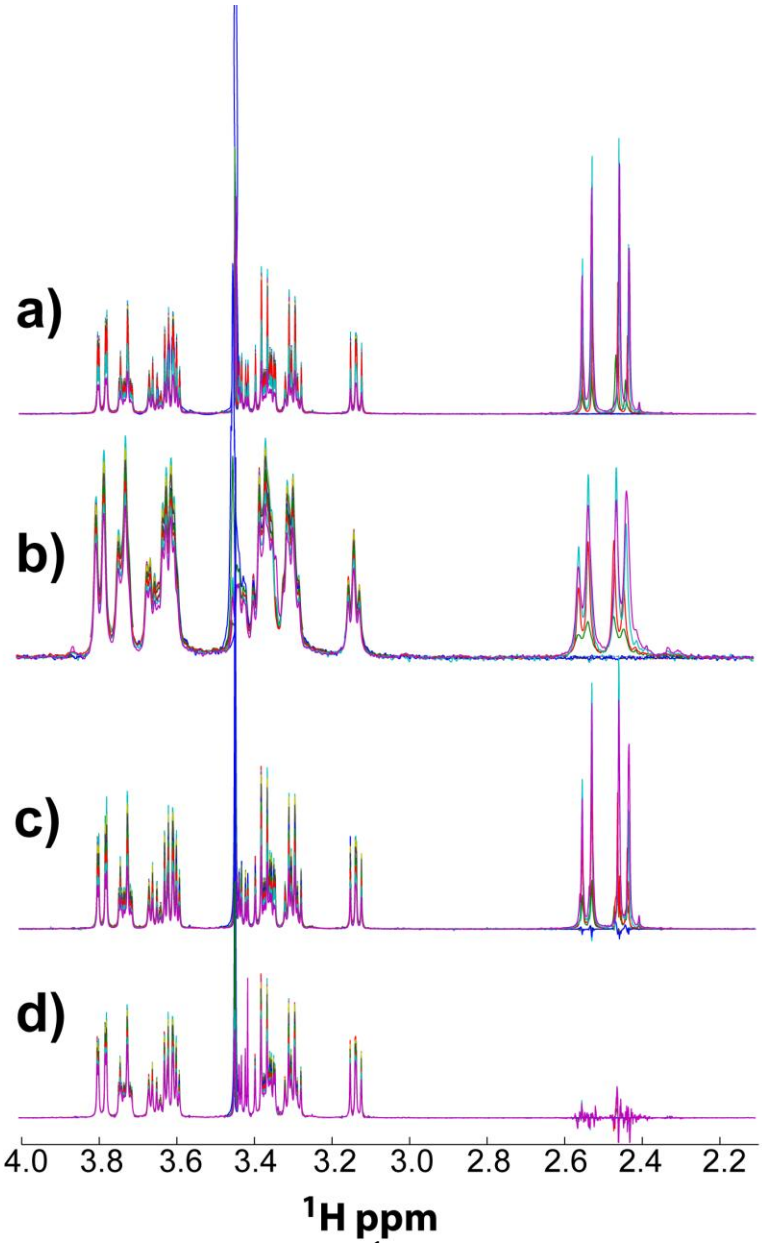

Figure 5.7. Representative ^{1}H NMR spectral data sets for different instrumental configurations: a) 1D BB Bruker and b) 1D HCN(b) Varian prior to instrumental transfer. The c) corrected spectral data set for the Varian 1D HCN(b) configuration following direct standardization (DS) instrumental transfer using 4 transfer calibration samples and d) following DS using a subset of transfer calibration standard samples in which the citrate metabolite was not present. The Bruker data set (a) was used to develop the PLS model and was the target configuration. Note the improved spectral resolution of the corrected spectra in c) in comparison to the original in b) and the close similarity to the spectral data set in a). The loss of the citrate signal for instrumental transfers using a limited subset of standard samples is clearly seen in d).

Table 5.1: RMSEP values for prediction of glucose, glycine and citrate concentration, and percent improvement for the different NMR instrumental configurations as a function of transfer method employed.

Analysis Method	RMSEP Data Set Prediction[a]							
	#1 1D BB Bruker[b]	**#2 1D INV Bruker**	**#3 1D HCN(a) Varian**	**#4 1D HCN(b) Varian**	**#5 NOESY BB Bruker**	**#6 NOESY INV Bruker**	**#7 NOESY HCN(a) Varian**	**#8 NOESY HCN(b) Varian**
Full Data No Transfer	0.0099 0.0058 0.0075	0.0647 0.0244 0.0556	0.0876 0.0227 0.0791	0.0941 0.0264 0.0894	0.0162 0.0135 0.0090	0.0678 0.0241 0.0583	0.0912 0.0228 0.0818	0.0971 0.0264 0.0920
Spectral Decovolution No Transfer	0.0090 0.0050 0.0064	0.0725 0.0219 0.0609	0.0855 0.0196 0.0726	0.0819 0.0252 0.0727	0.0137 0.0104 0.0084	0.0753 0.0212 0.0638	0.0899 0.0196 0.0766	0.0879 0.0253 0.0788
% Improvement	+12.5%	-3.8%	+8.1%	+12.1%	+15.0%	-2.8%	+7.3%	+9.3%
Spectral Deconvolution + (DS)[c]	N/A	0.0141 0.0111 0.0046	0.0142 0.0090 0.0097	0.0110 0.0125 0.0065	0.0080 0.0054 0.0055	0.0134 0.0106 0.0047	0.0184 0.0095 0.0150	0.0262 0.0129 0.0199
% Improvement	--[b]	+74.8%	+77.3%	+77.9%	+49.8%	+76.1%	+73.3%	67.5%
Spectral Deconvolution + PDS[d]	N/A	0.0225 (0.0175) 0.0135 (0.0094) 0.0174 (0.0103)	0.0450 (0.0333) 0.0151 (0.0120) 0.0327 (0.0249)	0.0421 (0.0400) 0.0138 (0.0130) 0.0303 (0.0289)	0.0134 (0.0080) 0.0124 (0.0067) 0.0078 (0.0058)	0.0225 (0.0190) 0.0128 (0.0098) 0.0176 (0.0112)	0.0484 (0.0354) 0.0159 (0.0121) 0.0355 (0.0275)	0.0436 (0.0394) 0.0129 (0.0122) 0.0343 (0.0303)
% Improvement	--[b]	59.5% (72.0%)	46.9% (59.2%)	56.4% (58.6%)	12.9% (45.5%)	61.2% (70.7%)	44.6% (58.2%)	56.3% (60.1%)
Spectral Deconvolution + DWPDS[e]	N/A	0.0180 0.0090 0.0104	0.0403 0.0132 0.0317	0.0402 0.0136 0.0317	0.0073 0.0073 0.0059	0.0190 0.0092 0.0115	0.0448 0.0140 0.0348	0.0436 0.0137 0.0330
% Improvement	--[b]	72.2%	52.0%	56.8%	45.1%	71.4%	49.0%	55.8%

[a] RMSEP = root-mean-square error of prediction. The three vertically listed errors in a group correspond to the error for glucose, glycine and citrate, respectively.

[b] RMSEC = root-mean-square error of calibration. The PLS model was developed for this target instrument (green) using 12 calibration samples. No % improvement is calculated for this sample using DS, PDS and DWPDS since this is the target instrumental configuration. The NOESY related configuration is denoted by the grey column.

[c] DS = direct standardization. Instrumental calibration RMSEP calculated using 5 transfer calibration samples.

[d] PDS = Piece-Wise Direct Standardization. Instrumental calibration RMSEP calculated using 4 transfer calibration samples and 1 calibration frequency or (7 calibration frequencies).

[e] DWPDS = Double Window Piece-Wise Direct Standardization. Instrumental calibration RMSEP calculated using 4 transfer calibration samples and window sizes of 7 and 1.

5.5. Supplemental for Chapter 5

Table 5.S0 Concentrations and Relative Concentrations of Model Mixtures

Sample ID	Concentration (mM)			Relative Concentration		
	Glucose	Glycine	Citrate	Glucose	Glycine	Citrate
1	50	0.40	0	0.992	0.008	0.000000
2	40	0.67	0	0.984	0.016	0.000000
3	30	0.55	0	0.982	0.018	0.000000
4	20	0.80	0	0.962	0.038	0.000000
5	50	2.00	0	0.962	0.038	0.000000
6	40	1.07	0	0.974	0.026	0.000000
7	30	1.47	0	0.953	0.047	0.000000
8	20	2.67	0	0.882	0.118	0.000000
9	50	2.00	2.4	0.919	0.037	0.044
10	40	1.07	4.0	0.888	0.024	0.088
11	30	1.47	8.0	0.760	0.037	0.203
12	20	2.67	12.0	0.577	0.077	0.346
13	20	0	0	1	0	0
14	0	0	8.00	0	0	1
15	0	4.0	0	0	1	0

* Samples #13, #14, and #15 were not used in the concentration development.

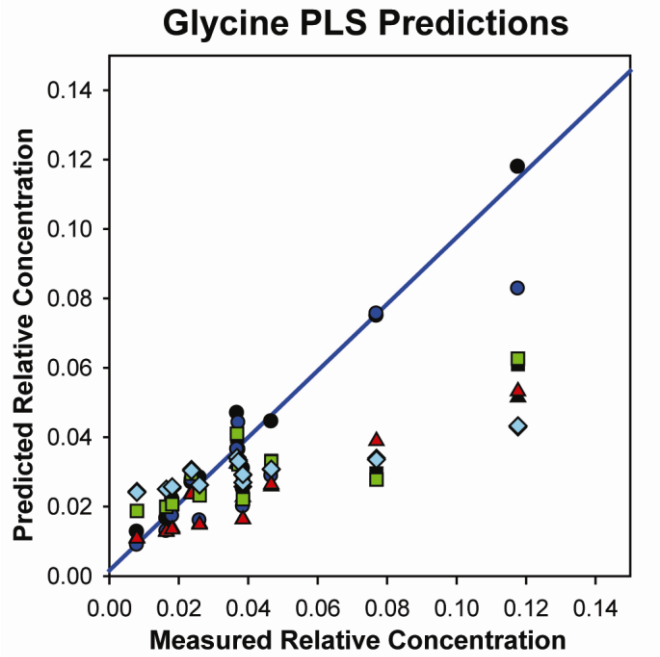

Figure 5S.1. The correlation between the ^{1}H NMR PLS predicted relative concentration of glycine and the measured relative concentration of glycine for the standard mixtures using eight different instrumental configurations. The PLS model was developed for the relative concentration of glucose, glycine and citrate simultaneously using the unbinned 1D ^{1}H NMR spectra data set from the Bruker instrument with a broadband probe, 1D BB Bruker (●). This model was subsequently used for the prediction of metabolite concentrations in the remaining instrumental configurations, NOESY BB Bruker (●), 1D INV Bruker (▲), NOESY INV Bruker (▲), 1D HCN(a) Varian (■), NOESY HCN(a) Varian (■), 1D HCN(b) Varian (♦) and NOESYHCN(b) Varian (♦). The results for a given probe utilize the same symbols, with the NOESY results being colored. Note that in general the 1D and NOESY predictions fall in pairs showing that the pulse sequence has minimal impact on the observed variations.

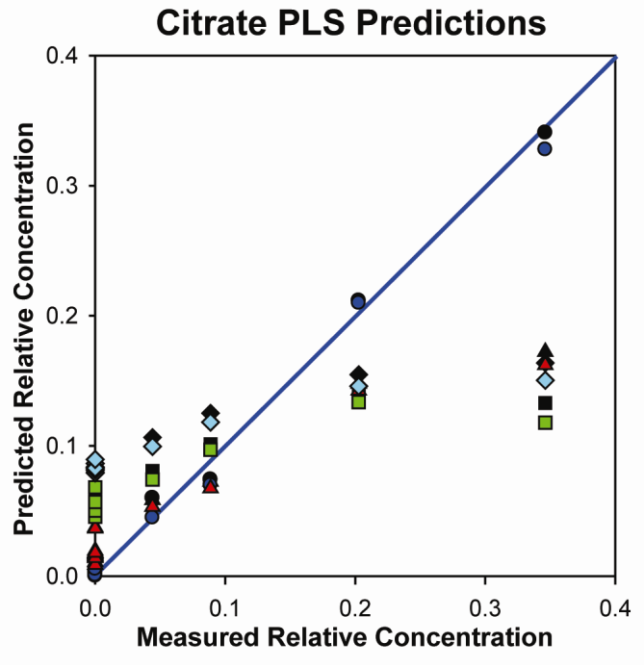

Figure 5S.2. The correlation between the ^{1}H NMR PLS predicted relative concentration of citrate and the measured relative concentration of citrate for the standard mixtures using eight different instrumental configurations. The PLS model was developed for the relative concentration of glucose, glycine and citrate simultaneously using the unbinned 1D ^{1}H NMR spectra data set from the Bruker instrument with a broadband probe, 1D BB Bruker (●). This model was subsequently used for the prediction of metabolite concentrations in the remaining instrumental configurations, NOESY BB Bruker (●), 1D INV Bruker (▲), NOESY INV Bruker (▲), 1D HCN(a) Varian (■), NOESY HCN(a) Varian (■), 1D HCN(b) Varian (♦) and NOESYHCN(b) Varian (♦).The results for a given NMR probe utilize the same symbols, with the NOESY results being colored. Note that in general the 1D and NOESY predictions fall in pairs showing that the pulse sequence has minimal impact on the observed variations.

Table 5S.1: The RMSEC and RMSEP[a] for the measurement of glucose, glycine and citrate relative concentrations in the twelve sample calibration set for eight different NMR configurations. The colored cells designate the RMSEC obtained for model calibration using all twelve samples from the data set for that particular instrument. The light gray cell note the RMSEP for the 1D/NOESY pair within an instrument configuration.

		RMSEP Data Set Prediction							
Data Set Modeled		**#1 1D BB Bruker**	**#2 1D INV Bruker**	**#3 1D HCN(a) Varian**	**#4 1D HCN(b) Varian**	**#5 NOESY BB Bruker**	**#6 NOESY INV Bruker**	**#7 NOESY HCN(a) Varian**	**#8 NOESY HCN(b) Varian**
	#1	0.0099 0.0058 0.0075	0.0647 0.0244 0.0556	0.0876 0.0227 0.0791	0.0941 0.0264 0.0894	0.0162 0.0135 0.0090	0.0678 0.0241 0.0583	0.0912 0.0228 0.0818	0.0971 0.0264 0.0920
	#2	0.1198 0.0225 0.1020	0.0089 0.0070 0.0059	0.0709 0.0136 0.0637	0.1108 0.0215 0.1044	0.1110 0.0217 0.0940	0.0115 0.0073 0.0100	0.0737 0.0144 0.0650	0.1082 0.0212 0.1018
	#3	0.2412 0.0655 0.1827	0.0976 0.0335 0.0667	0.0076 0.0066 0.0046	0.0859 0.0374 0.0524	0.2453 0.0765 0.1776	0.1045 0.0381 0.0687	0.0136 0.0078 0.0115	0.1029 0.0382 0.0694
	#4	0.1452 0.0425 0.1371	0.1302 0.0411 0.1117	0.0501 0.0283 0.0498	0.0145 0.0076 0.0079	0.1183 0.0511 0.1183	0.1300 0.0437 0.1142	0.0499 0.0297 0.0530	0.0348 0.0089 0.0298
	#5	0.0228 0.0134 0.0285	0.0624 0.0164 0.0578	0.0938 0.0199 0.0874	0.1064 0.0250 0.1035	0.0063 0.0070 0.0039	0.0648 0.0154 0.0598	0.0970 0.0201 0.0896	0.1083 0.0248 0.1049
	#6	0.1335 0.0223 0.1164	0.0121 0.0074 0.0097	0.0798 0.0144 0.0728	0.1273 0.0222 0.1198	0.1227 0.0202 0.1059	0.0088 0.0072 0.0057	0.0806 0.0151 0.0722	0.1232 0.0218 0.1158
	#7	0.2419 0.0619 0.1885	0.1354 0.0389 0.0993	0.0137 0.0076 0.0109	0.0890 0.0420 0.0505	0.2659 0.0780 0.1979	0.1440 0.0442 0.1024	0.0128 0.0076 0.0090	0.0988 0.0411 0.0624
	#8	0.2722 0.0407 0.0140	0.2961 0.0643 0.2400	0.1440 0.0333 0.1209	0.0311 0.0091 0.0258	0.2832 0.0462 0.2531	0.3015 0.0642 0.2473	0.1661 0.0369 0.1395	0.0173 0.0070 0.0140

[a] RMSEC = root-mean-square error of calibration. RMSEP = root-mean-square error of prediction.

$$\text{RMSEC (or RMSEP)} = \sqrt{\frac{\sum_{i=1}^{n} \hat{y}_i - y_i^{\,2}}{n}}$$

Where n is the number of calibration samples and $\hat{y}_i$ are the predicted value for the ith sample in the calibration set, while for RMSEP $\hat{y}_i$ corresponds to samples in a prediction set not used in the model development. The three vertically listed errors in a group correspond to the error for glucose, glycine and citrate, respectively.

Table 5S.2: The RMSEC[a] and RMSEP[a] for the measurement of glucose, glycine and citrate relative concentrations in the twelve sample calibration set following phasing using 4 different methods (see experimental for additional details). Green shaded cell designates data set used for prediction.

		RMSEP Data Set Prediction			
Data Set Modeled		**#1 User_1 Manual**	**#2 User_2 Manual**	**#3 APK Automated**	**#4 APKS Automated**
	#1	0.0099	0.0099	0.0099	0.0101
		0.0058	0.0058	0.0058	0.0059
		0.0075	0.0075	0.0075	0.0073

[a] See Table 5.S1 for definition of RMSEC and RMSEP. The three vertically listed errors in a group correspond to the error for glucose, glycine and citrate, respectively.

Table 5S.3: The RMSEC[a] and RMSEP[a] for the measurement of glucose, glycine and citrate relative concentrations in the twelve sample calibration set for eight different NMR configurations as a function of binning size with configuration #1 being used as the target instrumental configuration.

		RMSEP Data Set Prediction							
Bin Size (ppm)		**#1 1D BB Bruker**	**#2 1D INV Bruker**	**#3 1D HCN(a) Varian**	**#4 1D HCN(b) Varian**	**#5 NOESY BB Bruker**	**#6 NOESY INV Bruker**	**#7 NOESY HCN(a) Varian**	**#8 NOESY HCN(b) Varian**
	0.001	0.0099	0.0647	0.0876	0.0941	0.0162	0.0678	0.0912	0.0971
		0.0058	0.0244	0.0227	0.0264	0.0135	0.0241	0.0228	0.0264
		0.0075	0.0556	0.0791	0.0894	0.0090	0.0583	0.0818	0.0920
	0.005	0.0113	0.0489	0.0783	0.0851	0.0130	0.0527	0.0825	0.0890
		0.0064	0.0158	0.0198	0.0253	0.0074	0.0149	0.0198	0.0250
		0.0057	0.0410	0.0698	0.0843	0.0089	0.0448	0.0728	0.0871
	PI[b]	-0.2%	+28.6%	+11.7%	+6.5%	+22.0%	+27.9%	+11.2%	+6.3%
	0.01	0.0086	0.0629	0.0758	0.0762	0.0121	0.0662	0.0816	0.0819
		0.0047	0.0138	0.0153	0.0195	0.0058	0.0131	0.0159	0.0190
		0.0069	0.0534	0.0652	0.0704	0.0114	0.0572	0.0703	0.0753
	PI[b]	+13.4%	+16.7%	+21.2%	+22.1%	+18.6%	+16.6%	+18.3%	+20.6%
	0.02	0.0143	0.0667	0.0834	0.0812	0.0172	0.0694	0.0887	0.0866
		0.0038	0.0170	0.0174	0.0220	0.0044	0.0157	0.0178	0.0204
		0.0108	0.0524	0.0683	0.0668	0.0137	0.0562	0.0735	0.0729
	PI[b]	-18.0%	+11.0	+13.9%	+18.6%	+3.0%	+12.0%	+11.6%	+18.1%
	0.04	0.0145	0.0628	0.0790	0.0832	0.0169	0.0654	0.0852	0.0902
		0.0040	0.0164	0.0167	0.0254	0.0046	0.0149	0.0170	0.0239
		0.0108	0.0497	0.0648	0.0656	0.0134	0.0533	0.0709	0.0734
	PI[b]	-19.8%	+15.4	+18.1%	+14.0%	+4.2%	+16.8%	+15.1%	+12.3%
	0.06	0.0138	0.0589	0.0788	0.0910	0.0166	0.0612	0.0845	0.0978
		0.0040	0.0156	0.0174	0.0278	0.0048	0.0140	0.0176	0.0270
		0.0101	0.0467	0.0639	0.0687	0.0129	0.0501	0.0697	0.0773
	PI[b]	-14.3%	+20.3%	+17.5%	+7.0%	+6.2%	+21.9%	+15.0%	+4.3%
	0.08	0.0106	0.0525	0.0687	0.0867	0.0147	0.0548	0.0790	0.0694
		0.0034	0.0155	0.0180	0.0235	0.0048	0.0130	0.0219	0.0183
		0.0076	0.0408	0.0537	0.0677	0.0115	0.0452	0.0608	0.0573
	PI[b]	+11.0%	+27.3%	+24.8%	+14.4%	+15.3%	+29.2%	+14.3%	+32.3%

[a] RMSEC = root-mean-square error of calibration. RMSEP = root-mean-square error of prediction.

$$\text{RMSEC (or RMSEP)} = \sqrt{\frac{\sum_{i=1}^{n} \hat{y}_i - y_i^{\,2}}{n}}$$

Where *n* is the number of calibration samples and $\hat{y}_i$ are the predicted value for the *i*th sample in the calibration set, while for RMSEP $\hat{y}_i$ corresponds to samples in a prediction set not used in the model development. The three vertically listed errors in a group correspond to the error for glucose, glycine and citrate, respectively.

[b] PI = percent improvement

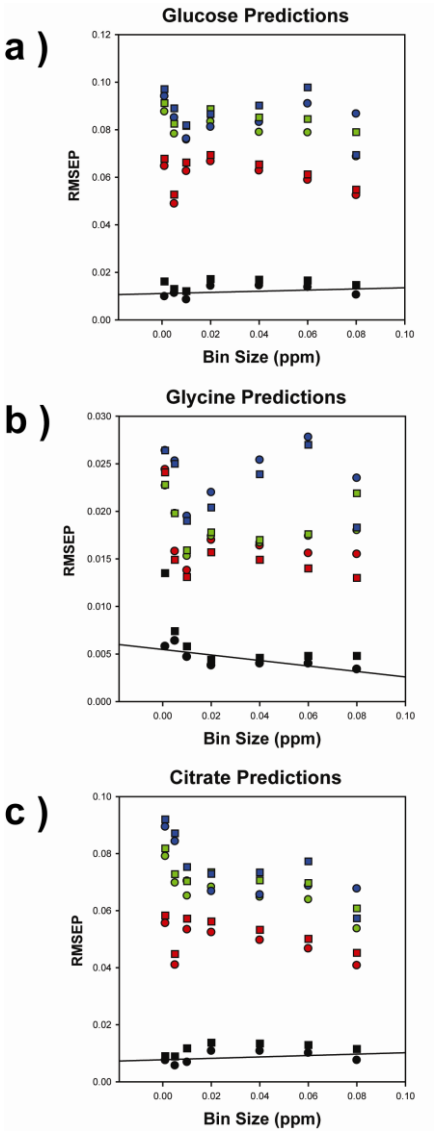

Figure 5S.3. The variation of RMSEP for the prediction of the relative concentration of a) glucose, b) glycine and c) citrate as a function of binning size. The PLS model was developed for the relative concentration of glucose, glycine and citrate simultaneously using the 1D ^{1}H NMR spectra data set from the Bruker instrument with a broadband probe, 1D BB Bruker (●). This model was subsequently used for the prediction of metabolite concentrations in the remaining instrumental configurations, NOESY BB Bruker (■), 1D INV Bruker (●), NOESY INV Bruker (■), 1D HCN(a) Varian (●), NOESY HCN(a) Varian (■), 1D HCN(b) Varian (●) and NOESYHCN(b) Varian (■). Note that in general the 1D and NOESY predictions fall in associated pairs.

Table 5S.4: The RMSEC[a] and RMSEP[a] for the measurement of glucose, glycine and citrate relative concentrations in the twelve sample calibration set for eight different NMR configurations following line shape deconvolution. The colored cells designate the RMSEC obtained for model calibration using all twelve samples from the data set for that particular instrument. The light gray cell note the RMSEP for the 1D/NOESY pair within an instrument configuration.

		RMSEP Data Set Prediction							
Data Set Modeled		**#1 1D BB Bruker**	**#2 1D INV Bruker**	**#3 1D HCN(a) Varian**	**#4 1D HCN(b) Varian**	**#5 NOESY BB Bruker**	**#6 NOESY INV Bruker**	**#7 NOESY HCN(a) Varian**	**#8 NOESY HCN(b) Varian**
	#1	0.0090 0.0050 0.0064	0.0725 0.0219 0.0609	0.0855 0.0196 0.0726	0.0819 0.0252 0.0727	0.0137 0.0104 0.0084	0.0753 0.0212 0.0638	0.0899 0.0196 0.0766	0.0879 0.0253 0.0788
	#2	0.1088 0.0185 0.0944	0.0107 0.0070 0.0061	0.4276 0.0112 0.0350	0.0684 0.0183 0.0653	0.0999 0.0182 0.0864	0.0123 0.0073 0.0090	0.0490 0.0120 0.0402	0.0765 0.0188 0.0731
	#3	0.1766 0.0376 0.1436	0.0361 0.0119 0.0267	0.0150 0.0087 0.0097	0.0263 0.0256 0.0184	0.1646 0.0394 0.1311	0.0332 0.0131 0.0222	0.0189 0.0090 0.0147	0.0331 0.0273 0.0245
	#4	0.1136 0.0355 0.0984	0.0492 0.0219 0.0430	0.0334 0.0251 0.0320	0.0149 0.0079 0.0088	0.1025 0.0384 0.0865	0.0499 0.0241 0.0447	0.0374 0.0272 0.0371	0.0239 0.0083 0.0206
	#5	0.0177 0.0111 0.0219	0.0660 0.0151 0.0596	0.0820 0.0173 0.0723	0.0833 0.0237 0.0793	0.0054 0.0072 0.0039	0.0688 0.0143 0.0624	0.0862 0.0174 0.0758	0.0893 0.0240 0.0849
	#6	0.1237 0.0190 0.1085	0.0138 0.0073 0.0100	0.0438 0.0112 0.0367	0.0833 0.0184 0.0796	0.1142 0.1767 0.1001	0.0108 0.0072 0.0061	0.0481 0.0121 0.0395	0.0905 0.0189 0.0865
	#7	0.2122 0.0432 0.1731	0.0624 0.0151 0.0492	0.0204 0.0091 0.0156	0.0372 0.0311 0.0184	0.2006 0.0452 0.1605	0.0605 0.0165 0.0456	0.0130 0.0090 0.0067	0.0434 0.0338 0.0195
	#8	0.1612 0.0240 0.1484	0.1625 0.0380 0.1298	0.1172 0.0274 0.1003	0.0273 0.0104 0.0198	0.1641 0.0261 0.1486	0.1629 0.0369 0.1322	0.1237 0.0286 0.1069	0.0150 0.0066 0.0138

[a] RMSEC = root-mean-square error of calibration. RMSEP = root-mean-square error of prediction.

$$\text{RMSEC}\,(\text{or RMSEP}) = \sqrt{\frac{\sum_{i=1}^{n} \hat{y}_i - y_i^{\,2}}{n}}$$

Where n is the number of calibration samples and $\hat{y}_i$ are the predicted value for the ith sample in the calibration set, while for RMSEP $\hat{y}_i$ corresponds to samples in a prediction set not used in the model development. The three vertically listed errors in a group correspond to the error for glucose, glycine and citrate, respectively.

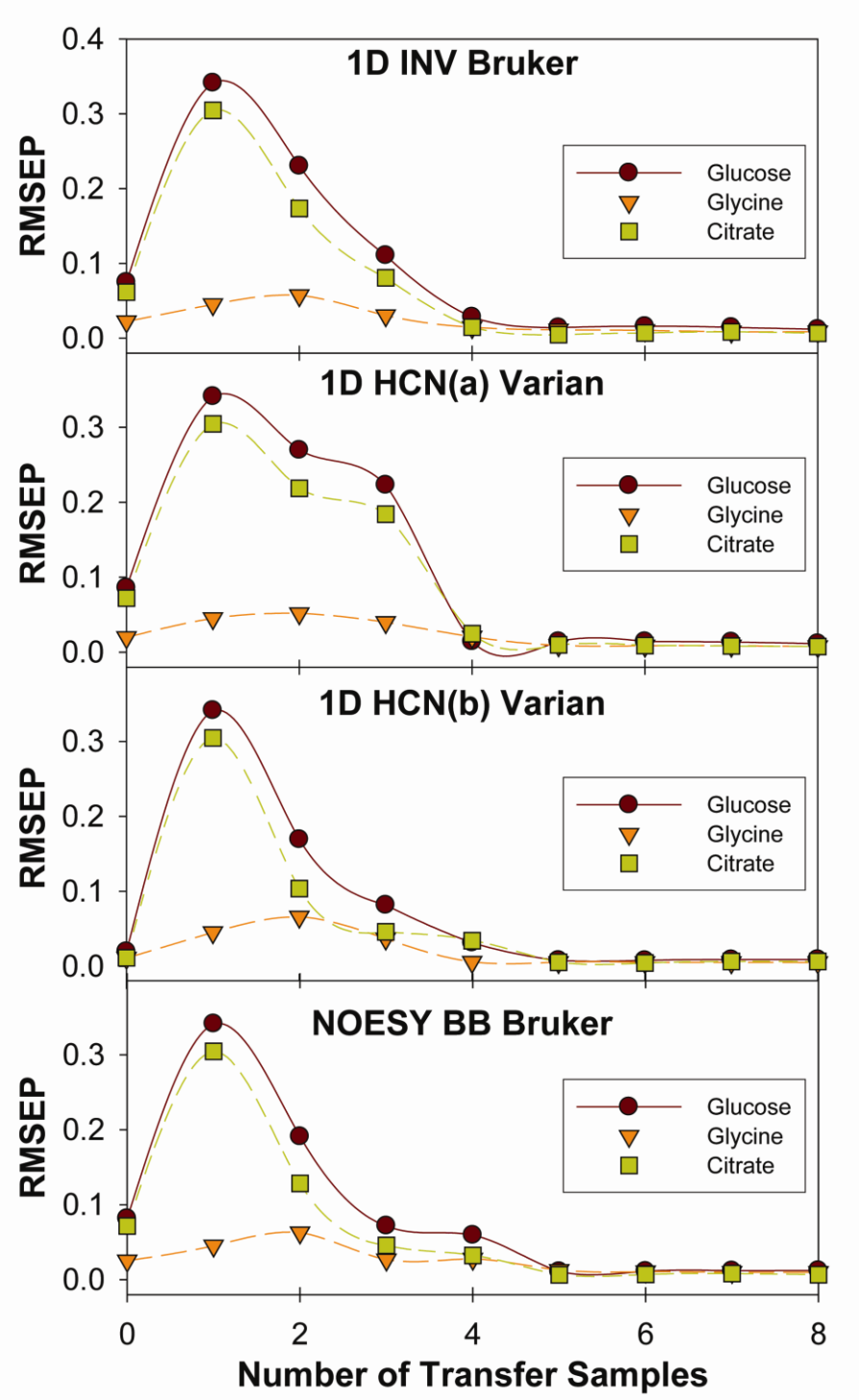

Figure 5.S4-A and S4-B. Variation of the RMSEP as a function of the number of transfer samples following direct standardization (DS) instrumental transfer. The PLS model was developed using the 1D BB Bruker configuration, with the predictive error for the different instrumental configurations shown in Figure S4-A and S4-B.

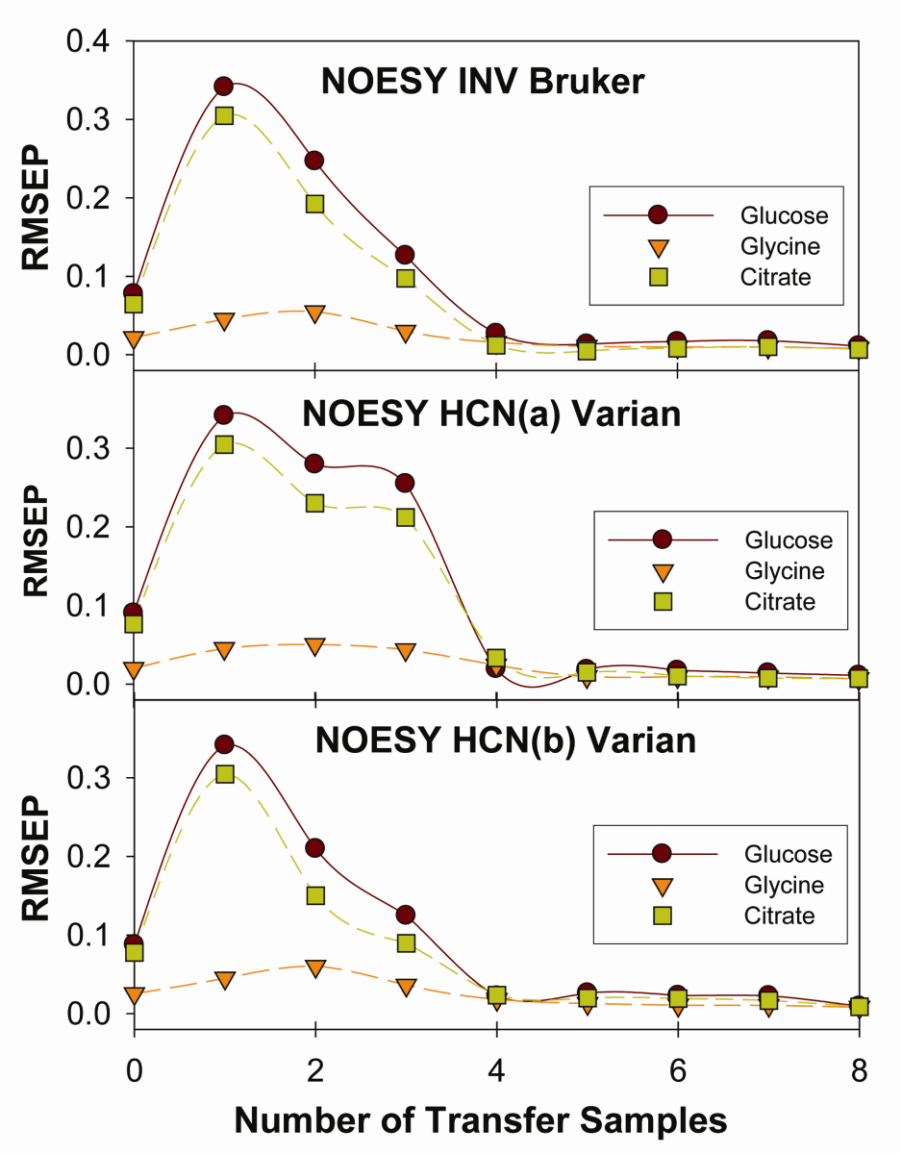

Figure 5S.4-A and S.4-B. Variation of the RMSEP as a function of the number of transfer samples following direct standardization (DS) instrumental transfer. The PLS model was developed using the 1D BB Bruker configuration, with the predictive error for the different instrumental configurations shown in Figure S4-A and S4-B.

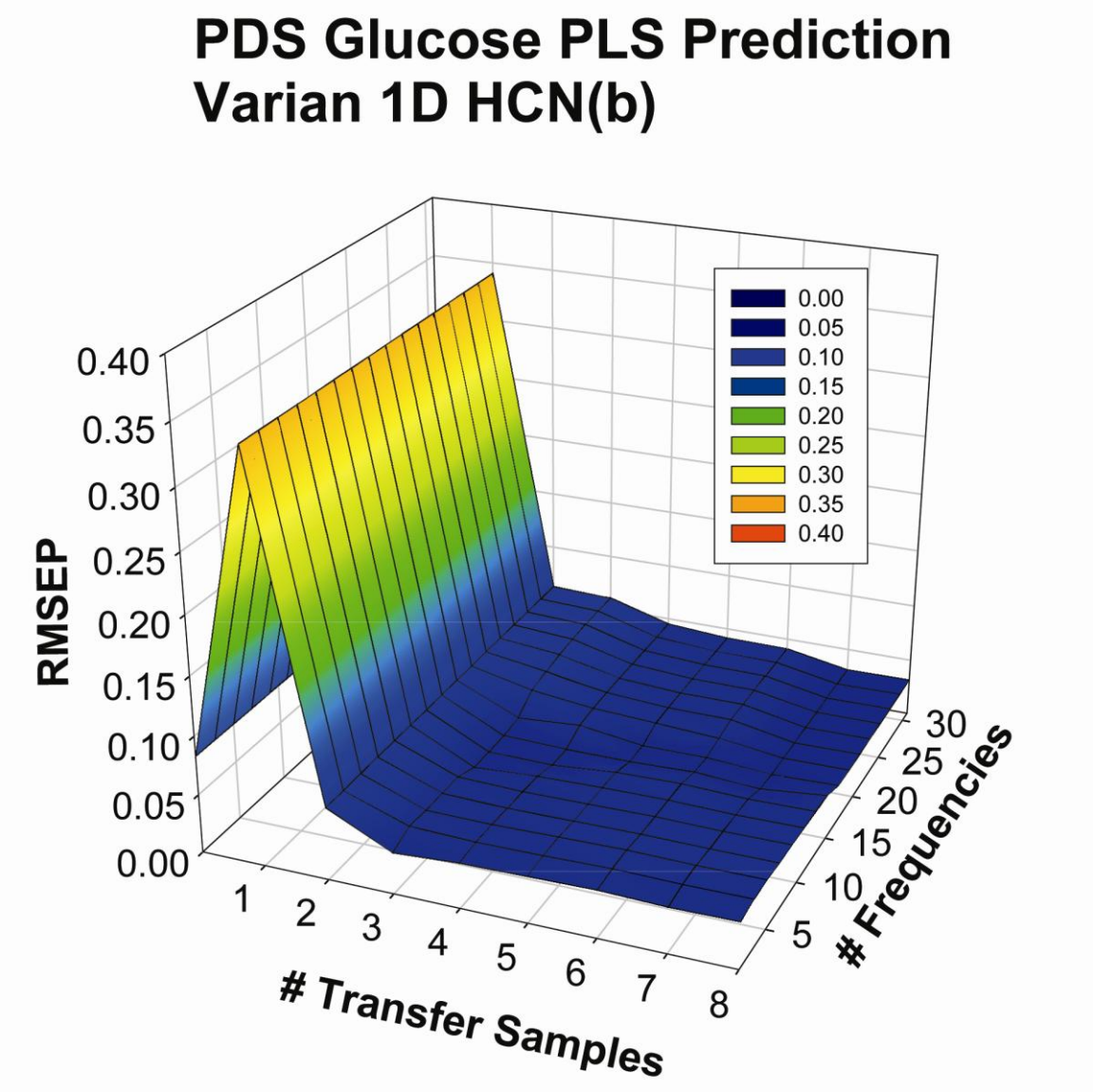

Figure 5S.5. Variation of the RMSEP for the prediction of glucose concentration for the Varian 1D HCN(b) instrumental configuration. The error was evaluated as a function of number of transfer samples and number of frequencies used in calculating transfer function during Piece-Wise Direct Standardization (PDS) instrumental transfer. The PLS model was developed using the 1D BB Bruker configuration. The number of frequencies used showed very little impact on the RMSEP showing that instrumental drift and line broadening were the dominant factor controlling the performance of prediction between the different instrumental configurations.

Chapter 6

Development of Variance-Filtered Instrumental Transfer Methods for High-Resolution NMR Spectroscopy

6.1. Introduction to Variance Filtered Instrumental Transfer

High-resolution NMR spectroscopy continues to be a powerful tool for the investigation of complex mixtures including quantitative analysis. In many fields and applications it is becoming common to utilize very large NMR data sets, and in particular, those resulting from the combination of numerous smaller spectral data sets. Analysis of combined data sets presents a unique challenge, as they often contain variances not related to the chemistry present in the samples. Instead, these combined data sets may present large variances resulting from using multiple NMR instruments in different laboratories, variance within a single NMR instrument over extended periods of time, and changes in NMR data related to the use of different pulse sequences and solvent saturation techniques. The influence of instrumental identity has been previously noted during the multivariate analysis of NMR data sets and was attributed to differences in the pulse sequences employed, spin-relaxation effects, hardware implementation and base line distortions related to different solvent suppression techniques [32, 73-77].

This group recently demonstrated the implementation of instrumental transfer methods for high-resolution ^{1}H NMR that allowed spectral data from multiple instrumental configurations to be evaluated [104]. In that study it was demonstrated that for simple model mixtures, NMR instrument variations could be corrected using either the direct standardization (DS) or piece-wise direct standardization (PDS) instrumental transfer methods [91-94, 96, 97] using a limited number of transfer calibration standard samples. A significant improvement in the prediction of relative metabolite concentrations following instrumental transfer was realized [104]. In the same study it was noted that if the transfer calibration samples did not contain signals for an "unrepresented" compound it was possible for spectral information about this compound to be removed or corrupted during the DS and PDS instrumental transfer process.

In this chapter, we introduce a variance-filtered modified DS and PDS instrumental transfer method as applied to high-resolution NMR to address the issue of incomplete spectral representation by the limited number of transfer calibration standard samples. Examples and specific issues related to the use of the variance-filtered instrumental transfer methods are presented.

6.2. NMR Experimental

Details concerning the preparation and acquisition of the multiple NMR data sets for different instrumental configurations have been previously described [104]. In summary, a set of standard samples for a model mixture containing the metabolites citrate, glucose and glycine in D_2O (pH = 7.0, 10 mM phosphate buffer) with 5 mM 3-trimethylsilylpropionate (TSP) as an internal chemical shift reference were analyzed on 8 different instrumental configurations. These configurations included two different NMR instruments, a Bruker Avance 600 and a Varian Unity Plus 600, the use of either a single pulse 1D or a 1D NOESY (100 ms) pulse sequence, acquired on a 5 mm broadband (BB) X(^{1}H) probe (Bruker), a ^{1}H(X) inverse (INV) probe (Bruker) or two different vintages of an HCN probe (Varian). In this paper these 8 instrumental configurations will designated as 1D BB Bruker, NOESY BB Bruker, 1D INV Bruker, NOESY INV Bruker, 1D HCN(a) Varian, NOESY HCN(a) Varian, 1D HCN(b) Varian and NOESY HCN(b) Varian. The multiple NMR data sets were all transformed, phased, referenced and baseline corrected in CHENOMX NMR Suite 5.0 (Edmonton, Canada) prior to analysis and instrumental transfer using the MATLAB 2007b software (The Mathworks, Inc.) and the PLS Toolbox 4.1 (Eigenvector Research, Inc). The spectral region between +4 and +2.2 ppm was used for the analysis as this region did not contain the dominant H_2O signal. The data sets were integral normalized to the total signal intensity and mean-centered prior to instrumental transfer and analysis.

6.3. Methods

6.3.1. Direct Standardization (DS) Instrumental Transfer

Using the DS instrumental transfer method the spectra (or FIDs) between different NMR instruments (or configurations) can be related to each other by modeling the responses using [91, 92, 96]

$$\mathbf{S_1} = \mathbf{S}_j\mathbf{F_b^{DS}} + \mathbf{1b_{js}^T} = \mathbf{S}_j\mathbf{F_b^{DS}} + \mathbf{B}_{js} \qquad (6.1)$$

where $\mathbf{S_1}$ is the matrix containing the spectra of a target (primary or standard) NMR instrument to which data is being transferred. The matrix $\mathbf{S}_j$ contains the spectra obtained on the *j*th NMR instrumental configuration (e.g. different instruments, different probes, different pulse sequences or the same instrument at a later time), $\mathbf{F_b^{DS}}$ is the DS transformation matrix and $\mathbf{b_{js}^T}$ is the transpose of the additive background correction vector for the *j*th configuration. It is possible to replace the $\mathbf{1b_{js}^T}$ term with the background matrix $\mathbf{B}_{js}$. For high-resolution NMR, baseline correction is a common processing step prior to multivariate analysis, and should result in a vanishingly small background $\mathbf{B}_{js}$ component. In addition, $\mathbf{B}_{js}$ has no impact during transfer of mean-centered data (see Equation 2, below). Highly structured baselines resulting from receiver/probe distortions, filter edge effects, or presaturation issues that are not removed during preprocessing may be reflected in $\mathbf{B}_{js}$, and in those cases should be evaluated during the instrumental transfer procedure.

The data set matrices $\mathbf{S}_j$ are composed of n samples and ν frequencies ($n \times \nu$), and for simplicity is assumed to have the same dimensions for all instrumental configurations. Mean-centering the data matrices ($\bar{\mathbf{S}}_j$) allows Equation (1) to be rewritten as

$$\bar{\mathbf{S}}_\mathbf{1} = \bar{\mathbf{S}}_j\mathbf{F_b^{DS}} \qquad (6.2)$$

The DS transfer function $\mathbf{F_b^{DS}}$ is a $\nu \mathbf{x} \nu$ matrix and is defined using

$$\mathbf{F_b^{DS}} = \bar{\mathbf{S}}_j^{+}\bar{\mathbf{S}}_\mathbf{1} \qquad (6.3)$$

with $\bar{\mathbf{S}}_j^{+}$ being the pseudoinverse of $\bar{\mathbf{S}}_j$ and was determined using singular value decomposition (SVD). It should be noted that during the calibration of the transfer function the DS method

correlates the entire spectrum of the secondary instrument to each individual spectral frequency such that $\mathbf{F_b}^{DS}$ is a dense (ν x ν) matrix.

6.3.2. The Piece-Wise Direct Standardization (PDS) Method

For NMR spectroscopy, the spectral variations between different instrumental configurations typically involve only very small frequency shifts and intensity differences, allowing the instrumental transfer function to be evaluated over a limited range of nearby spectral frequencies. The spectral response on the primary instrument at the *k*th frequency ($\mathbf{s}_{1,k}$) can be related to the spectral response on the *j*th instrumental configuration at nearby freqencies with a window width of $2n+1$ ($\mathbf{s}_{j,k-n}, \mathbf{s}_{j,k-n+1}, \cdots, \mathbf{s}_{j,k+n-1}, \mathbf{s}_{j,k+n}$). These measurements for the *k*th frequency are placed into a matrix to form

$$\mathbf{X}_k = \left[\mathbf{s}_{j,k-n}, \mathbf{s}_{j,k-n+1}, \cdots, \mathbf{s}_{j,k+n-1}, \mathbf{s}_{j,k+n} \right] \tag{6.4}$$

A regression vector at each frequency is then calculated using

$$\boldsymbol{\beta}_k = \mathbf{X}_k^{+} \mathbf{s}_{1,k} \tag{6.5}$$

Under the PDS method the transformation $\mathbf{F_b}^{PDS}$ is a banded diagonal (ν x ν) matrix containing the regression vectors, with the majority of the off-diagonal elements being zero, as defined by

$$\mathbf{F_b}^{PDS} = \text{diag} \left[\boldsymbol{\beta}_1^{\mathbf{T}}, \boldsymbol{\beta}_2^{\mathbf{T}}, \boldsymbol{\beta}_3^{\mathbf{T}}, \ldots \boldsymbol{\beta}_\nu^{\mathbf{T}} \right] \tag{6.6}$$

For both the DS and PDS methods, the spectra on secondary instrumental configurations are corrected to match the spectra obtained on the primary instrument, while the calibration model (developed on the primary instrument) remains unchanged. It should be emphasized that the type of calibration model is not important since the results of the calibration are not directly utilized

during the calculation of the transfer functions ($\mathbf{F}_\mathbf{b}^{\mathrm{DS}}$ and $\mathbf{F}_\mathbf{b}^{\mathrm{PDS}}$). For example, no concentrations or other measurables are utilized in evaluating Equations (3) and (6).

6.3.3. Variance-Filter Transfer Function

In this paper, we introduce a filter into the DS and PDS instrumental transfer methods to select only those spectral regions in the NMR spectra that are adequately described by the limited N_T transfer calibration samples. This filter is based on comparison between the standard deviation present at each frequency, $\sigma(\nu)$, for the N spectra of the combined primary and secondary datasets to the standard deviation within the transfer calibration samples subset, $\sigma'(\nu)$. The standard deviations are given by the square root of the intensity variance from the intensity mean $\bar{s}(\nu)$ at each frequency and are defined by

$$\sigma(\nu) = \left(\frac{1}{N-1} \sum_{i=1}^{N} s_i(\nu) - \bar{s}(\nu)^{\,2} \right)^{\frac{1}{2}}$$
$$\bar{s}(\nu) = \frac{1}{N} \sum_{i=1}^{N} s_i(\nu) \tag{6.7}$$

where in this equation N represents the total number of spectra present in the combined data set ($\mathbf{S}_1 + \sum \mathbf{S}_j$). Similarly, $\sigma'(\nu)$ is restricted to the N_T transfer calibration samples over the j different instrumental configurations and is defined by

$$\sigma'(\nu) = \left(\frac{1}{j \cdot N_T - 1} \sum_{i=1}^{j \cdot N_T} s_i(\nu) - \bar{s}(\nu)^{\,2} \right)^{\frac{1}{2}} \tag{6.8}$$

Using these standard deviations, a variance-filtered instrumental transfer function can be defined

$$\mathbf{F}_\mathbf{b}^{\mathrm{Filter}} = \begin{cases} \bar{\mathbf{S}}_\mathbf{i}^{+} \bar{\mathbf{S}}_\mathbf{1} & \text{(DS)}, \quad \text{if } \sigma'_\nu > s \cdot \sigma \\ \mathrm{diag}\left(\boldsymbol{\beta}_1^{\mathrm{T}}, \boldsymbol{\beta}_2^{\mathrm{T}}, \boldsymbol{\beta}_3^{\mathrm{T}}, \ldots, \boldsymbol{\beta}_\nu^{\mathrm{T}} \right) & \text{(PDS)}, \quad \text{if } \sigma'_\nu > s \cdot \sigma \\ c \bullet \mathbf{I} & \text{(Filter)}, \quad \text{if } \sigma'_\nu \le s \cdot \sigma \end{cases} \tag{6.9}$$

For regions of the NMR spectra where there is significant spectral information or variance present in the limited N_T calibration transfer samples (as defined by the user controlled tolerance level $s \cdot \sigma$), the transfer function $\mathbf{F_b}^{\text{Filter}}$ is given by the original DS or PDS transfer function described in section 3.1 and 3.2. For those frequencies where there is not significant information in the transfer calibration samples, the transfer function $\mathbf{F_b}^{\text{Filter}}$ is modified by inserting a scaled identity matrix ($c \bullet \mathbf{I}$). In practice, the scale factor was necessary to maintain total intensity relationships of the transferred spectra used during subsequent analysis.

6.3.4. Using of Transfer Calibration Samples to Estimate $\mathbf{F_b}$

For the DS, PDS and variance-filtered instrumental transfer methods, Equations (6.1-6.9) are used to correct spectral data on secondary NMR instrumental configurations to match the spectra obtained on the primary NMR instrument. To calculate the transfer function $\mathbf{F_b}$, a limited number of transfer calibration samples (N_T) which is less than the total number of samples in the data set (N_s) are selected and measured on both the primary (or target) instrument ($\mathbf{T_1}$) and on the secondary instrumental configurations ($\mathbf{T}_j$). The number of distinct transfer calibration samples should be at least equal to the rank of $\mathbf{S_1}$ in order to correctly estimate the transfer function $\mathbf{F_b}$. There are different methods employed for this subset selection and include using the sample leverage based on the Hat matrix [91], the Euclidean distance via the Kennard and Stone algorithm [105], or determination through the maximization of smallest inter-point distance (MSID) between samples [97]. In general, the transfer calibration samples are chosen from the data set of the primary instrument, but an equivalent argument can be made for selection of the transfer sample subset from any instrumental sample set. The $\mathbf{T_1}$ and $\mathbf{T}_j$ data sets are then used to evaluate transfer matrices $\mathbf{F_b}^{\text{DS}}$ (DS), $\mathbf{F_b}^{\text{PDS}}$ (PDS), or $\mathbf{F_b}^{\text{Filter}}$ (variance-filtered) via Equation (6.3), (6.6) or (6.9), respectively.

3.5 Combining Data Sets Using Instrumental Transfer

As noted above, the calculation of the transfer functions does not require the use of a specific calibration model. It is true that the selection of the limited transfer samples may be determined with respect to the impact on a model (i.e. sample leverage in a PLS model), but this

is not a strict requirement. It is possible to utilize these instrumental transfer methods to modify spectral data sets obtained on different NMR instrumental configurations to match the spectral response of a target (primary) NMR instrument prior to data set combination and subsequent analysis. This transfer (or modification) of the secondary data sets can be accomplished, in analogy to Equation (6.2), using

$$^{\mathrm{Tr}}\mathbf{S}_j = \mathbf{S}_j\mathbf{F}_\mathbf{b} \tag{6.10}$$

where $^{\mathrm{Tr}}\mathbf{S}_j$ is the transferred data set from the *j*th instrumental configuration.

6.4. Results and Discussion

6.4.1. Combined NMR data sets

It was recently shown that for high-resolution NMR both the DS and PDS instrumental transfer methods provided a significant improvement in the predictions of partial least squares (PLS) concentration models between different NMR instrument configurations [104]. These same instrumental transfer methods can also be used to modify or correct data sets using equation (10) from different NMR instruments prior to incorporating them into a large data set for subsequent analysis. As an example, the ^{1}H NMR spectra for a set of model mixtures (12 samples) containing the metabolites glucose, glycine and citrate were obtained on four different instrumental configurations. Figure (6.1a) and (6.1b) show the NMR spectra for two of these instrumental configurations prior to instrumental transfer, along with the identification of the different metabolite spectral contributions. The unbinned NMR data sets from the four different instrumental configurations were combined and then analyzed using principal component analysis (PCA). The scores for the first two PCs using the model developed on the target (or primary) NMR instrumental configuration (1D BB Bruker, ●) are shown in Figure (6.2a). Given ideal and identical response on the different NMR instruments the PC scores for the different configurations should be coincident. This is clearly not the case in Figure (6.2a), where subtle clustering based on the identity of the NMR instrumental configuration is observed. Of particular interest are the PC scores for the four samples in the model mixtures containing the citrate

metabolite (samples designated C1, C2, C3, and C4) and the one sample in the data set with a relative glycine concentration that was an order of magnitude higher than the other standard samples (G8) [104]. On the primary NMR instrument 1D BB Bruker (●), the positive PC1 scores may provide a classification signature for the presence of citrate metabolite, while the large PC2 score provides a marker for high relative glycine concentrations. These results show that prior to NMR data set modification (using instrumental transfer), PCA on the combined data set from the different instrumental configurations does not allow clear identification of the unique C1-C4 and G8 samples.

Combining the NMR data sets following DS instrumental transfer (N_T = 4 transfer calibration samples), PCA reveals a marked improvement in the similarity of the PC scores between the different instrumental configurations as shown in Figure (6.2b). In particular, the scores for the C1-C4 and G8 samples are nearly identical to the PC scores observed on the primary NMR instrument, and the clustering based on instrumental identification has been removed. Similarly, Figure (6.2c) shows the PC scores of the combined data sets following PDS instrumental transfer (N_T = 4 and 1 filter frequency) revealing overall improvement. For PDS-modified data the C1-C4 and G8 samples on all the instrumental configurations can be clearly separated from the other samples in the data set based on their PC scores. The PCA results of the combined DS-modified data sets are slightly better than results of the PDS-modified data sets. This difference between DS and PDS transfer for this data set has been previously noted and discussed [104].

While the results of using instrumental transfer methods in combining NMR data sets are encouraging, there are several issues and pitfalls to implementation of these methods that need to be addressed. The most important issue is that the performance and applicability of transferring and combining different data sets strongly depends on the transfer calibration sample subset ($\mathbf{T}_1$) representing (or spanning) the complete instrumental response. As previously noted [91, 92, 96], for DS instrumental transfer method the number of transfer calibration samples (N_T) needs to be at least equal to the rank of the data set being transformed ($\mathbf{S}_j$), or at least equal to the rank of the regression matrix $\mathbf{X}_k$ defined in Equation (4). More accurately, the rank of $\mathbf{T}_1$ needs to be equal or greater than the rank of $\mathbf{S}_j$. For simple systems this can be accomplished, but for complex mixtures (such as biofluids) this requirement may be difficult to fulfill. A second issue is that while the $\mathbf{T}_1$ samples are most commonly selected from the complete data set on the

primary instrument ($\mathbf{S}_1$), this calibration subset may not necessarily describe (or fully span) the response of the *j*th instrumental $\mathbf{S}_j$

$$\mathbf{T}_1 \subseteq \mathbf{S}_1 \not\subseteq \mathbf{S}_j \tag{6.11}$$

This situation could occur when a later data set $\mathbf{S}_j$ contains a new chemical species (new metabolite) not present in the data set of the original target instrument. This requirement of fully describing the data sets also will make it difficult to create a "universal" transfer calibration set without some prior knowledge of the systems being investigated. It should be noted that it is possible to select a new calibration transfer sample subset to span the combined data sets from all the different instrumental configurations ($\mathbf{S}_1 + \sum \mathbf{S}_j$), and then obtain spectra for this new $\mathbf{T}_1$ sample set on each instrumental configuration, estimate the new transfer functions, and then perform the instrumental transfer prior to combining the data sets. Unfortunately, this would require revaluation of the $\mathbf{T}_1$ subset every time a new instrumental configuration was to be incorporated, and would prove prohibitively restrictive. Issues involving the inability to completely map the instrumental response will produce significant errors in the transferred data and are described in the next section.

6.4.2. Issues with Transfer Calibration Sample Selection

Insight into the problems of using these instrumental transfer methods can be obtained by inspection of the transferred NMR data sets. The unmodified ^{1}H NMR spectra of the glucose, citrate and glycine mixtures on the primary or target instrument (1D BB Bruker) are shown in Figure (6.1a, bottom), while Figure (6.1b) shows the NMR spectra for the same mixtures obtained on a different instrument configuration (NOESY BB Bruker). For this secondary data set the spectra were obtained using the same NMR instrument and probe as the primary instrument, but using a different pulse sequence. These two data sets were acquired sequentially to eliminate changes in sample conditions, probe tuning and variations in magnetic field homogeneity. The experimental residuals between the different instrumental configurations are given in Figure (6.3a), and reveal instrumental variations. The largest residual observed results

primarily from the differential relaxation of the glycine resonance (δ = +3.55 ppm) occurring during the 1D NOESY and single pulse 1D sequence.

Some of these spectral differences can be corrected using instrumental transfer. If the $\mathbf{T_1}$ subset contained all the metabolites of interest (glucose, glycine, and citrate) the DS and PDS transfer of the data set from the secondary instrument was successful, as shown in Figures (6.1c) and (6.1d), respectively. The experimental residuals following DS instrumental transfer are shown in Figure (6.3b), revealing an improvement of ~3 in the magnitude of the residual errors, primarily for the glycine resonance. For this model mixture the optimum number of $\mathbf{T_1}$ samples required ranged from between 3 and 5 samples depending if the DS or PDS protocol was employed (4 were used for all the examples shown in this manuscript), with the performance of the instrumental transfer as a function of calibration sample number detailed previously [104].

Now consider the example where the $\mathbf{T_1}$ subset is missing some of the compounds present within the secondary data set. The ^{1}H NMR of the reduced subset is shown as the upper inset in Figure (6.1a) and does not contain any samples containing citrate. Figures (6.1e) and (6.1f) shows the errors introduced following DS and PDS instrumental transfer with this "incomplete" transfer calibration sample set. The transferred data sets have suppressed or corrupted citrate resonances (δ ~ 2.59 ppm). This error occurs because the transfer matrix $\mathbf{F_b}$ attempts to eliminate signal in this spectral region because there is no citrate signal (just noise) present in $\mathbf{T_1}$. In this example, the suppression of the citrate sample is almost complete using the DS method, because it correlates the entire spectra for each frequency in estimation of $\mathbf{F_b^{DS}}$. This signal suppression is typically considered beneficial during instrumental transfer in that spurious noise signals present on secondary instruments would be eliminated during transfer, but in this case $\mathbf{T_1}$ subset selection produces the error during transfer.

The spectral residuals between the two data sets following DS and PDS instrumental transfer are shown in Figures (6.3c) and (6.3e), respectively, and were obtained by subtracting the target instrument data set from the transferred instrumental data set ($^{Tr}\mathbf{S}_2 - \mathbf{S}_1$). These residuals show another error introduced due to "unrepresented" compounds being present within the transferred data sets. The dominant negative residual is produced by the disappearance of the citrate signals (δ ~ + 2.59 ppm) in the transferred data set. In the residuals involving the DS modified data in

Figure (6.3c), there is also an increase in the glucose and glycine intensities for any sample containing citrate. This intensity variation results from the normalization of the total spectral integral following the instrumental transfer (i.e. total spectral intensity is set to one). In the case of DS, the complete suppression of the citrate signal biases the unit normalization. For the PDS method the normalization impact is less pronounced since there is still some citrate intensity following the data set transfer. These intensity errors introduced during re-normalization can be partially eliminated by using Probabilistic Quotient Normalization (PQN) following the transfer of the secondary data set (results not shown) [62].

Issues associated with a non-representative $\mathbf{T}_1$ subset are also reflected in the PCA analysis of the transferred data sets. Figure (6.4a) and (6.4b) show the scores of the combined data from four different instrumental configurations following DS and PDS instrumental transfer, respectively. These results show a reduction in the scattering due to instrumental identity (compared to Figure (6.2a)). For this combined data set the G8 sample has almost the same score for every instrumental configuration, and is a dramatic improvement over the PCA results of the original untransferred data sets (Figure (6.2a)). Unfortunately the PC scores for samples containing the citrate metabolite (C1-C4) vary greatly for the different NMR instrumental configurations.

These results clearly show that attempts to apply existing DS and PDS instrumental transfer methods to combine data sets involving complex mixtures will introduce errors if $\mathbf{T}_1$ does not include all the compounds present in the combined data sets. For biofluid and metabolite studies this restriction would be extremely detrimental, as entire spectral regions might be eliminated or corrupted during the transfer and data set combination process.

6.4.3. The Use of Variance-Filtering for Combined Data Sets

It is possible to circumvent some of the issues of data loss and spectral corruption by introduction of the variance-filtered DS and PDS transfer function described by Equation (6.9). Figures (6.1g) and (6.1h) show the data sets of the secondary instrument (NOESY BB Varian) following variance-filtered DS and PDS instrumental transfer, respectively. The tolerance cut-off level was chosen at 10%, but this is a user controlled variable. Using this variance-filter the resonance for the “missing” compound (citrate) is retained (compare to Figures (6.1e) and (6.1f)), while correction of the instrumental variations for the other spectral regions are realized

under the DS and PDS transfer. The resulting spectral residuals following variance-filtered DS and PDS transfer are shown in Figure (6.3d) and (6.3f), and reveal a reduction in the residuals compared to the standard instrumental transfer method shown in Figures (6.3c) and (6.3e). This variance-filtering allows subsequent analysis of combined data sets, including data sets with "new" compounds, while matching the instrumental response for as many portions of the NMR spectra as possible.

The improvement provided by variance-filtering can also be seen in the PCA analysis of the DS and PDS transferred data sets as shown in Figures (6.4c) and (6.4d), respectively. In this example, the $\mathbf{T}_1$ subset still does not contain any samples with the citrate metabolite. For this combined variance-filtered data, the similarity of the scores of the C1-C4 samples are improved in comparison to the unfiltered DS (Figure 6.4(a)) and PDS transferred data (Figure (6.4b)). The variance-filtered PDS transferred data sets show slightly less instrumental scatter than the DS transferred data, in particular for the C1-C4 citrate containing samples. The performance of the combined data following variance-filtered DS and PDS transfers with incomplete $\mathbf{T}_1$ sample sets will always be less optimal than combined data sets obtained using unfiltered transfers that incorporate representative $\mathbf{T}_1$ since there are spectral regions not matched between the different instrumental configurations when using the variance-filter.

A particular weakness of the variance-filtered DS and PDS instrumental transfer methods is highlighted in Figure 6.5. In this example, the NMR data set obtained on the secondary instrumental configuration 1D HCN(a) Varian is shown in Figure (6.5b). The spectra in this NMR data set have a line width that is ~ 3 times larger than on the primary instrument (Figure (6.5a)), and represents an extreme example of instrumental-to-instrument variation. The modified data sets following DS and PDS instrumental transfer (with an incomplete $\mathbf{T}_1$ sample set) are shown in Figure (6.5c) and (6.5d), respectively. Note the dramatic improvement in line width of the transferred data (compared to Figure 6.5b), approaching the line width on the target instrument (Figure 6.5a). These results again demonstrate the benefit of instrumental transfer methods during combination of spectral data sets. As in the previous section, the use of an incomplete $\mathbf{T}_1$ corrupts the citrate signal (δ = 2.59 ppm) in the reconstructed data sets. The transferred data sets for this secondary instrumental configuration following variance-filtered DS and PDS are shown in Figure (6.5e) and (6.5f). While the citrate resonances are transferred for

this secondary instrument, they retain the large line width of the original data set. Unfortunately, subsequent multivariate analysis of combined data set will then contain a PC that can classify the NMR instrument based on the line width of the citrate signal. This currently remains an issue for combining data sets obtained using the variance-filtered transfer matrix. It may be possible to bin these spectral regions (smart binning) selected by the variance-filter to eliminate line width variations during subsequent multivariate analysis, or to apply selective reference line deconvolution to this spectral region. The ability to identify data obtained on different NMR instruments during classification due to line width differences reemphasizes the need to match line shapes and line widths for different instrumental configurations as closely as possible prior to combining data sets. While the instrumental transfer method can correct line width differences, it will remain an issue for combined data sets utilizing the variance-filter. It has been suggested that correction of the line width based on reference deconvolution would provide similar results. For closely matched line widths this is true, but it should be remembered that instrumental transfer methods also correct other instrumental variations (intensity variations, filter edge, relaxation effects, etc) in addition to the line width variations. For the secondary instrumental configuration shown in Figure (6.5b), reference deconvolution to the smaller line width of the primary NMR instrument was not a viable option, since the deconvolution introduces large, unacceptable amounts of noise.

6.5. Conclusions and Outlook

This chapter introduces the variance-filtered direct standardization (DS) and piece-wise direct standardization (PDS) instrumental transfer methods as applied to high-resolution ^{1}H NMR spectra. Using these instrumental transfer methods, data sets from different instruments can be modified and then combined. It was shown that the selection of the transfer calibration samples is crucial in determining the performance of the instrumental transfer process. These results also demonstrated that many of the errors associated with "new" resonances in the transferred data set can be eliminated by utilizing the variance-filtered transfer function. This variance-filter maintains all the spectral signatures originally present in the secondary instrument data sets, while correcting for instrumental variations in spectral regions that are adequately described (spanned) by the transfer calibration samples. In limited situations, the introduction of the variance-filtered instrumental transfer does allow for matching and combining of spectral data sets from different NMR instruments, even without a complete transfer calibration sample set. For NMR studies involving mixtures with a limited number of compounds, it will be possible to correctly apply instrumental transfer methods prior to combining NMR data sets. The application of combining data sets following instrumental transfer for very complex mixtures (biofluids and metabonomics) appears to be difficult, but has yet to be fully experimentally explored and is an area of ongoing effort. The variance-filtered DS and PDS methods presented here represent the initial steps in an attempt to resolve these difficulties.

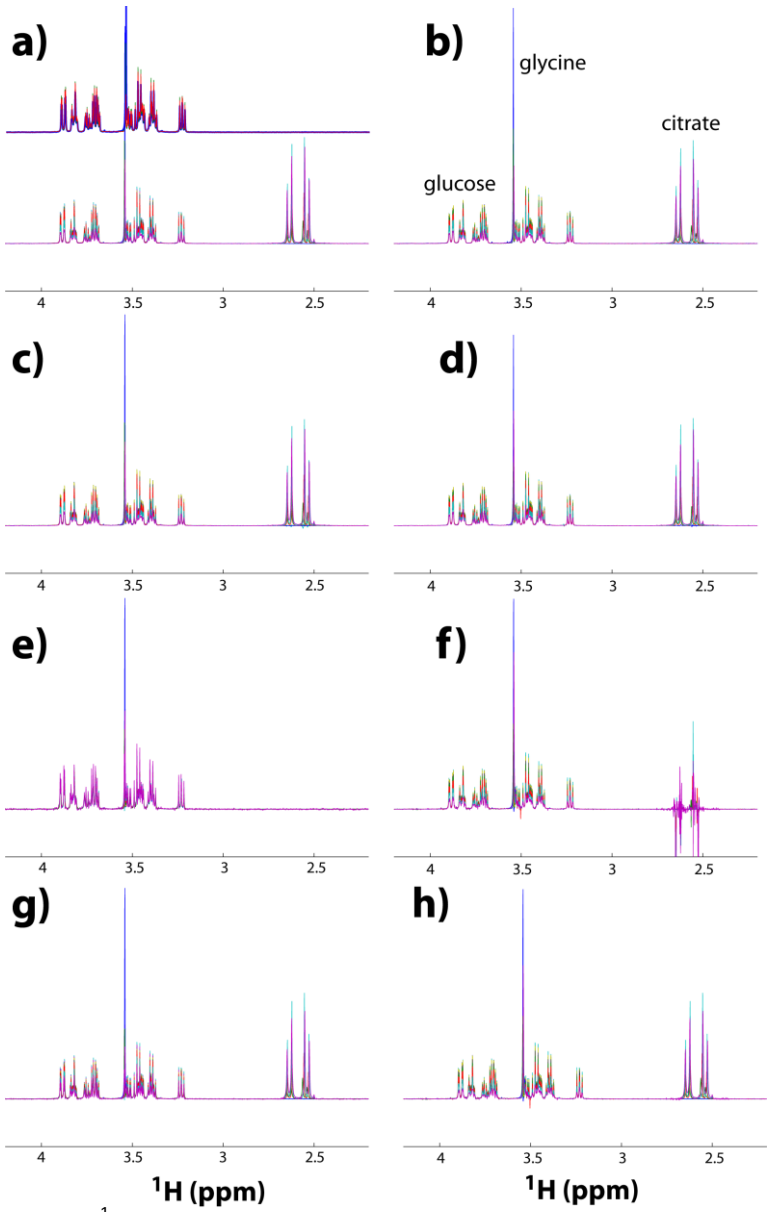

Figure 6.1. High-resolution ^{1}H NMR spectra of model mixtures containing glucose, glycine, and citrate acquired on a) a Bruker Avance 600 instrument, using a single pulse 1D pulse sequence and a 5 mm broad band probe (target instrumental configuration, 1D BB Bruker), and b) using a NOESY 1D (100 ms) pulse sequence (secondary instrumental configuration, NOESY BB Bruker). The modified NMR spectra of the secondary configuration following c) direct standardization (DS) and d) piece-wise direct standardization (PDS) instrumental transfer method. In these examples the samples use for transfer calibrations contained all three metabolites. The modified NOESY BB Bruker data set obtained using transfer calibration samples not containing citrate (spectral subset shown as inset in 2a) using both the e) DS and f) PDS instrumental transfer method. Modified data sets obtained using the variance filter for the g) DS and h) PDS instrumental transfer method. Note that the citrate signal is retained for the variance-filtered methods even though this metabolite is missing from the transfer calibration.

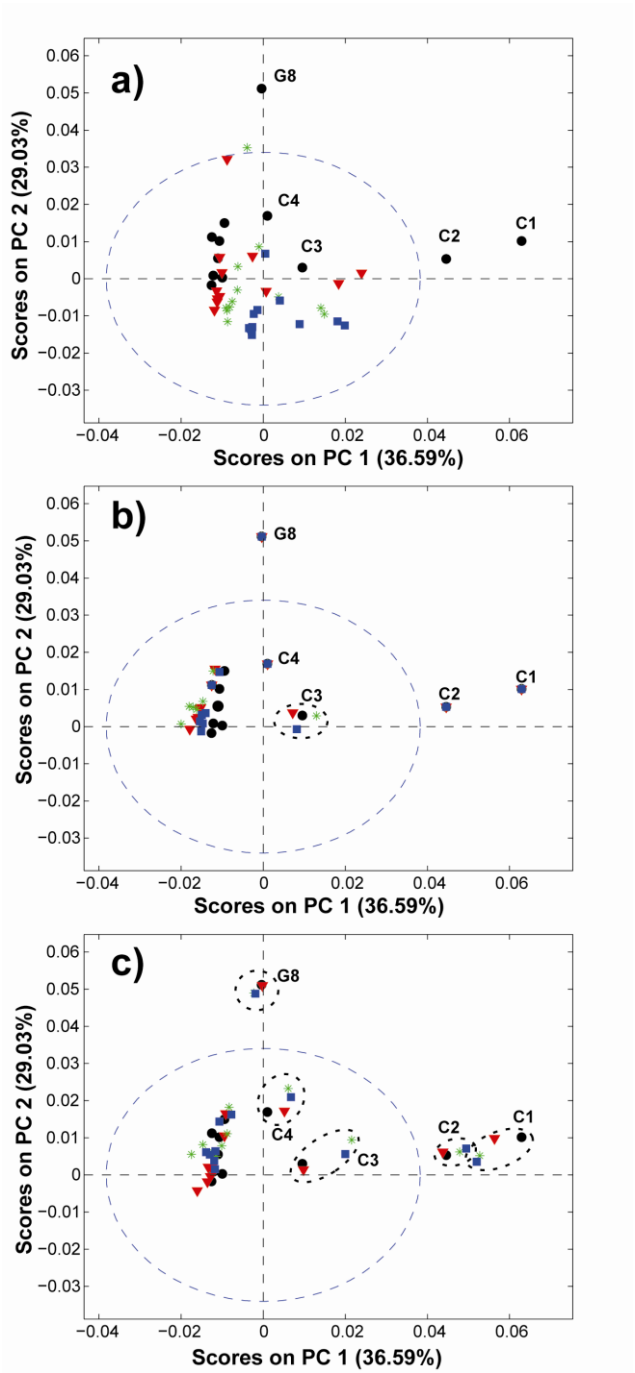

Figure 6.2. PCA of the ^{1}H NMR for a model mixtures of glucose, glycine, and citrate on four different instrumental configurations using the unbinned data sets (a) prior to instrumental transfer, (b) following DS instrument transfer, and (c) following PDS instrumental transfer, Results are shown for the primary instrumental configuration 1D BB Bruker (●), and the secondary instrumental configurations 1D INV Bruker (▼), 1D HCN(a) Varian (■), and 1D HCN(b) Varian (*). Samples designated as C1-C4 contain the metabolite citrate, while sample G8 has a glycine concentration significantly higher than the remaining samples. Note that in (b) the C1-C4 and G8 scores closely overlap and are not distinguishable in the figure.

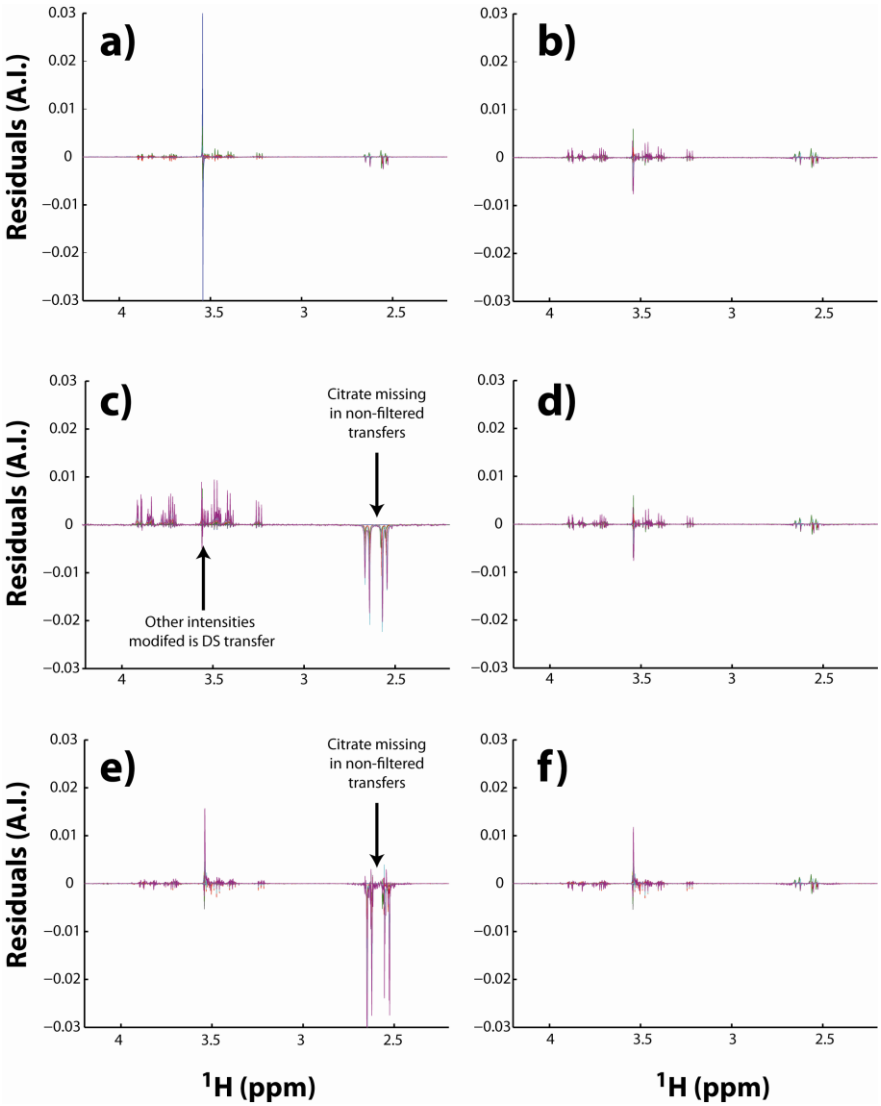

Figure 6.3. Experimental residuals between the ^{1}H NMR spectra for a set of model mixtures obtained using a 1D or a 1D NOESY (100 ms) pulse sequence on the same Bruker Avance 600 instrument. The residuals were calculated for a) original data sets ($\mathbf{S}_2 - \mathbf{S}_1$), b) following DS instrumental transfer, c) DS with a limited calibration subset, d) variance-filtered DS instrumental transfer, e) PDS instrumental transfer with a limited calibration subset, and f) variance-filtered PDS instrumental transfer ($^{Tr}\mathbf{S}_2 - \mathbf{S}_1$). See text for additional details.

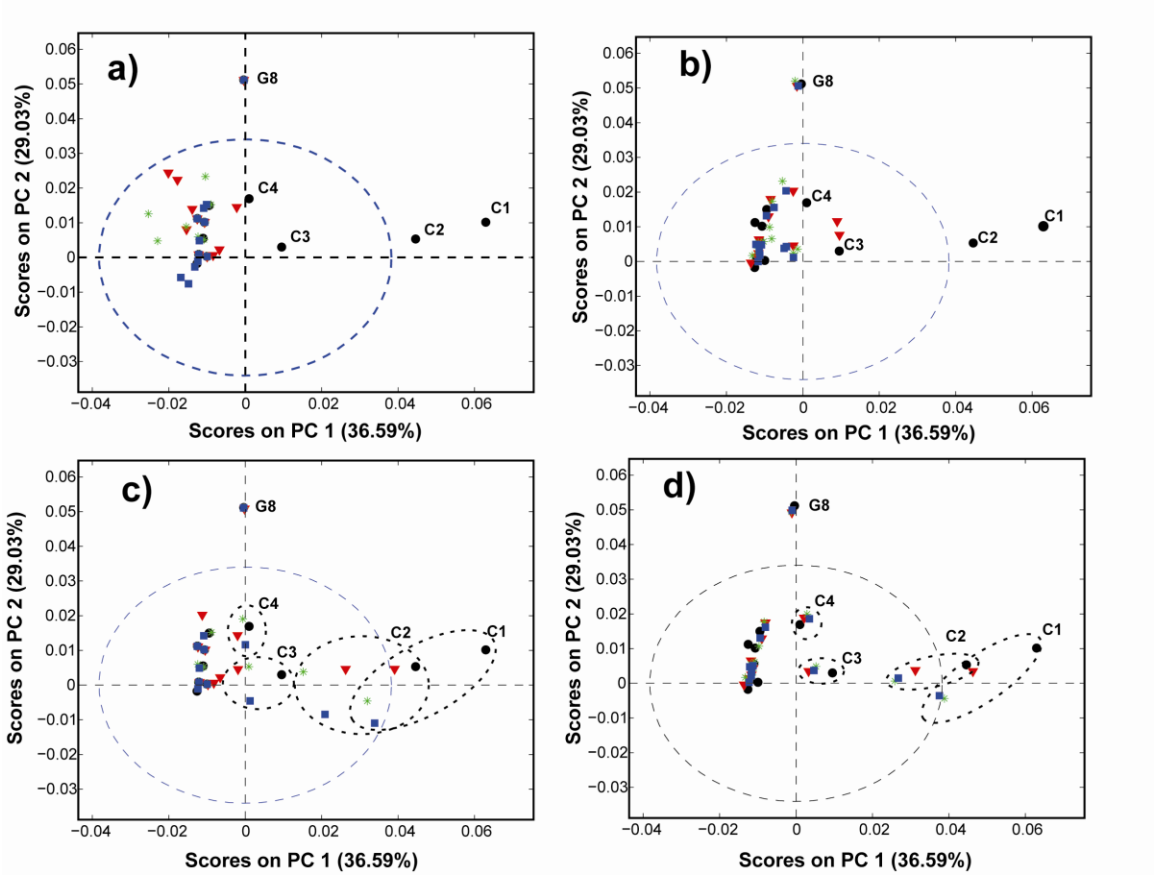

Figure 6.4. PCA of the ^{1}H NMR spectra for a set of model mixtures containing glucose, glycine and citrate obtained on four different NMR instrumental configurations using an incomplete transfer calibration sample set. The PCA results following (a) DS, (b) PDS, (c) variance-filtered DS, and (d) variance-filtered PDS instrumental transfer. Results are shown for the primary instrumental configuration 1D BB Bruker (●), and the secondary instrumental configurations 1D INV Bruker (▼), 1D HCN(a) Varian (■), and 1D HCN(b) Varian (*).

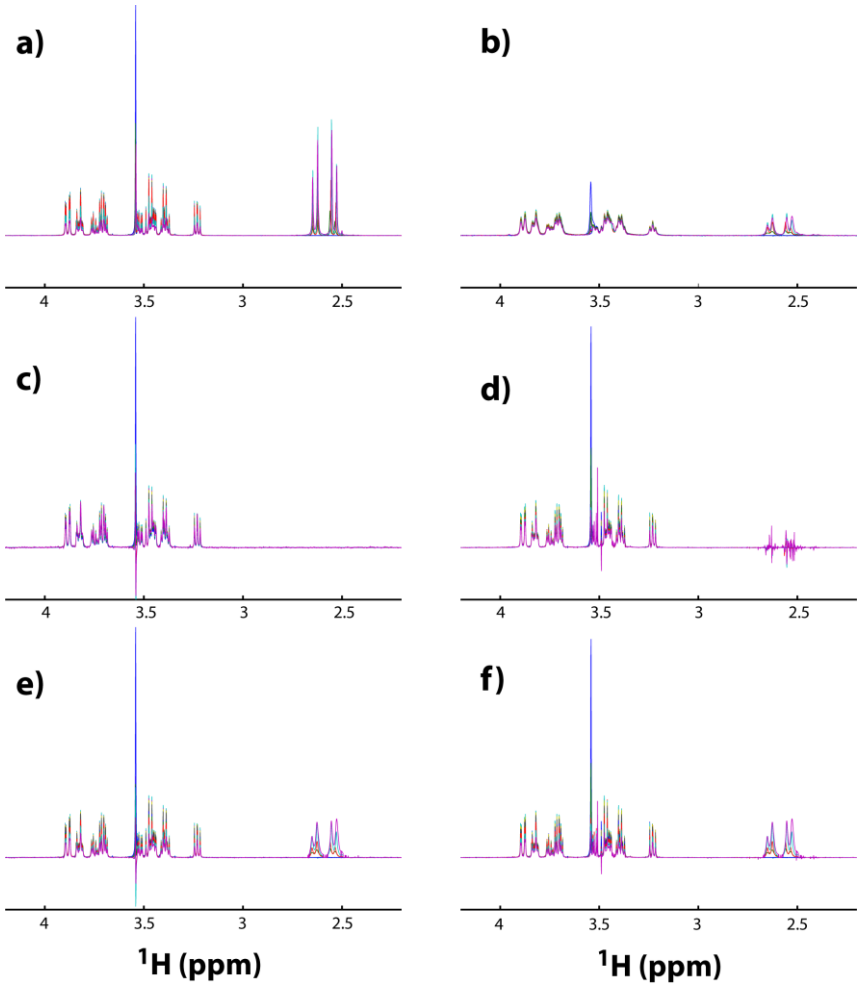

Figure 6.5. High-resolution ^{1}H NMR spectra of model mixtures containing glucose, glycine and citrate acquired on a) the primary target NMR instrument, 1D BB Bruker and on b) the secondary instrumental configuration 1D HCN(a) Varian. The modified NMR spectra of the secondary configuration following instrumental transfer with a limited transfer calibration sample subset using the c) direct standardization (DS), d) piece-wise direct standardization (PDS), e) variance-filtered DS, and f) variance-filtered PDS method. Note that the citrate signal is maintained in the variance-filtered methods, but variations in the line width for these resonances are not corrected during the instrumental transfer step. See text for additional details.

References

1. *Environmental Monitoring for Nuclear Safeguards*, U.S.G.P. Office, Editor. 1995, U.S. Congress, Office of Technology Assessment: Washington, D.C.
2. Wisconsin, U.o. *Metabolomics/Metabonomics*. 2009 [cited; Available from: http://www.bmrb.wisc.edu/metabolomics/.
3. Weissman, K., *Deciphering Plants*, in *Chemistry World*. 2004, Royal Chemical Society.
4. Griffiths, W.J. and Y. Wang, *Mass Spectrometry: from proteomics to metabolomics and lipidomics.* Chemical Society Reviews, 2009. **38**: p. 1882-1896.
5. Sompson, M.J. and J.R. McKelvie, *Environmental Metabolomics: New Insights Into Earthworm Ecotoxicity and Contaminant Bioavailability in Soil.* Analytial Bioanalytical Chemistry, 2009. **394**: p. 137-149.
6. Griffin, J.L., et al., *Metabolic Profiling of Chronic Cadmium Exposure in the Rat.* Chemical Research in Toxicology, 2001. **14**(10): p. 1428-1434.
7. Ceglarek, U., et al., *Challenges and developments in tandem mass spectrometry based clinical metabolomics.* Molecular and Cellular Endocrinology, 2009. **301**(1-2): p. 266-271.
8. Miller, M.G., *Environmental Metabolomics: A SWOT Analysis (Strengths, Weaknesses, Opportunities, and Threats).* Journal of Proteome Research, 2007. **6**(2): p. 540-545.
9. Pavia, A.P. and P. Malik, *Recent Advances on the Chemistry of Solvent Extract Applied to the Reprocessing of Spent Nuclear Fuels and Radioactive Wastes.* Journal of Radioanalytical and Nuclear Chemistry, 2004. **261**(2): p. 485-496.
10. Madic, C., et al., *Recent achievements in the development of partitioning processes of minor actinides from nuclear wastes obtained in the frame of the NEWPART European programme (1996-1999).* Progress in Nuclear Energy. **40**(3-4): p. 523-526.
11. Demina, G.A., et al., *[Metabolism of a 238Pu tributyl phosphate complex on entry into the respiratory organs]*. Gig Sanit, 1990(9): p. 57-8.
12. Muller, W.U., C. Streffer, and L. Markoski, *Does tributyl phosphate influence the radiation risk of a highly proliferating system--the early mouse embryo in vitro?* Health Phys, 1987. **53**(6): p. 667-71.
13. Stradling, G.N., et al., *The metabolism and decorporation of Pu after inhalation of the tributyl phosphate complex by the rat.* Health Phys, 1985. **49**(3): p. 499-502.
14. Berne, C., et al., *CYP201A2, a cytochrome P450 from Rhodopseudomonas palustris, plays a key role in the biodegradation of tributyl phosphate.* Appl Microbiol Biotechnol, 2007. **77**(1): p. 135-44.
15. Raushel, F.M., *Bacterial detoxification of organophosphate nerve agents.* Curr Opin Microbiol, 2002. **5**(3): p. 288-95.
16. Abou-Donia, M.B. and A.A. Nomeir, *The role of pharmacokinetics and metabolism in species sensitivity to neurotoxic agents.* Fundam Appl Toxicol, 1986. **6**(2): p. 190-207.
17. Auletta, C.S., *A Dietary Oncogenicity Study of Tributyl Phosphate in the CD-1 Mouse.* Toxicology, 1998. **128**: p. 135-141.
18. Hernandez, O., *SIDS Initial Assessment Report, Tributyl Phosphate*, I.L.O. United Nations Environment Programme, World Health Organization, Editor. 2001, United Nations Environment Programme, International Labour Organisation, World Health Organization.
19. Michel, K., et al., *Acute toxicity investigations of ester-based lubricants by using biotests with algae and bacteria.* Environ Toxicol, 2004. **19**(4): p. 445-8.

20. Nakamura, A., *International Programme on Chemical Safety- Environmental Health Criteria 112--tri-n-Butyl Phosphate.* In: Organization WH (ed). World Health Organization, Geneva, Switzerland, 1991.
21. Nakamura, A., *Tri-n-butyl phosphate. Monograph of International Program on Chemical Safety.* EHC, 1991: p. 112.
22. Feng, J., et al., *1H NMR analysis for metabolites in serum and urine from rats administrated chronically with La(NO3)3.* Anal Biochem, 2002. **301**(1): p. 1-7.
23. Wei, L., et al., *Toxicological effects of cinnabar in rats by NMR-based metabolic profiling of urine and serum.* Toxicol Appl Pharmacol, 2008. **227**: p. 417-429.
24. Viant, M.R., E.S. Rosenblum, and R.S. Tieerdema, *NMR-based metabolomics: a powerful approach for characterizing the effects of environmental stressors on organism health.* Environ Sci Technol, 2003. **37**(21): p. 4982-9.
25. Coen, M., et al., *Integrated application of transcriptomics and metabonomics yields new insight into the toxicity due to paracetamol in the mouse.* J Pharm Biomed Anal, 2004. **35**(1): p. 93-105.
26. Jordan, K.W. and L.L. Cheng, *NMR-based metabolomics approach to target biomarkers for human prostate cancer.* Expert Rev Proteomics, 2007. **4**(3): p. 389-400.
27. Shockcor, J.P. and E. Holmes, *Metabonomic applications in toxicity screening and disease diagnosis.* Curr Top Med Chem, 2002. **2**(1): p. 35-51.
28. Torgrip, R.J.O., et al., *A note normalization of biofluid 1D 1H-NMR data.* Metabolomics, 2008. **4**: p. 114-121.
29. Suzuki, T., et al., *Metabolism of Tributyl Phosphate in Male Rats.* Journal of Agricultural Food Chemistry, 1984. **32**: p. 603-610.
30. Auletta, C.S., M.L. Weiner, and W.R. Richter, *A Dietary Toxicity/Oncogenicity Study of Tributyl Phosphate in the Rat.* Toxicology, 1998. **128**: p. 125-143.
31. Suzuki, T., et al., *Some S-Containing Metabolites of Tributyl Phosphate in the Rat.* J. Agric. Food Chem., 1984. **32**: p. 1278-1283.
32. Saude, E.J., C.M. Slupsky, and B.D. Sykes, *Optimization of NMR Analysis of Biological Fluids for Quantitative Accuracy.* Metabolomics, 2006. **2**(3): p. 113-123.
33. Holmes, E., et al., *Proton NMR monitoring of the onset and recovery of experimental renal damage.* J Pharm Biomed Anal, 1990. **8**(8-12): p. 959-62.
34. Nicholson, J.K., J.A. Timbrell, and P.J. Sadler, *Proton NMR spectra of urine as indicators of renal damage. Mercury-induced nephrotoxicity in rats.* Mol Pharmacol, 1985. **27**(6): p. 644-51.
35. Yang, B. and L. Bankir, *Urea and urine concentrating ability: new insights from studies in mice.* Am J Physiol Renal Physiol, 2005. **288**(5): p. F881-96.
36. Schimke, R.T., *Differential effects of fasting and protein-free diets on levels of urea cycle enzymes in rat liver.* J Biol Chem, 1962. **237**: p. 1921-4.
37. Lord, R.S. and J.A. Bralley, *Clinical applications of urinary organic acids. Part1: Detoxification markers.* Alternative Medicine Review, 2008. **13**: p. 205-215.
38. Merck, 2006.
39. Sood, D.D. and Patil, *Chemistry of Nuclear Processing: Current Status.* J. Radioanalytical and Nuclear Chemistry, Articles, 1996. **203**(2): p. 547-573.
40. Paiva, A.P. and P. Malik, *Recent Advances on the Chemistry of Solvent Extraction Applied to the Reprocessing of Spent Fuels and Radioactive Wastes.* J. Radioanalytical and Nuclear Chemistry, 2004. **261**(2): p. 485-496.

41. Dave, G. and U. Lidman, *Biological and Toxicological Effects of Solvent Extraction Chemicals. Range Finding Acute Toxicity in the Rainbow Trout (Salmo gaidnerii Rich.) and in the Rat (Rattus norwegicus L.).* Hydrometallurgy, 1978. **3**: p. 201-216.
42. Laham, S., G. Long, and B. Broxup, *Induction of Urinary Bladder Hyperplasia in Sprague-Dawley Rats Orally Administered Tri-n-Butyl Phosphate.* Archives Environmental Health, 1985. **40**(6): p. 301-306.
43. Laham, S., G. Long, and B. Broxup, *Subacute Oral Toxicity of Tri-n-butyl Phosphate in the Sprague-Dawley Rat.* J. Applied Toxicology, 1984. **4**(3): p. 150-154.
44. Oishi, H., S. Oishi, and K. Hiraga, *Toxicity of Tri-n-butyl Phosphate, with Special Reference to Organ Weights, Serum Components and Chilinesterase Activity in Male Rats.* Toxicology Letters, 1980. **6**: p. 81-85.
45. Oishi, H., S. Oishi, and K. Hiraga, *Toxicity of Several Phosphoric Acid Esters in Rats.* Toxicology Letters, 1982. **13**: p. 29-34.
46. Arnold, L.L., et al., *Tributyl Phosphate Effects on Urine and Bladder Epithelium in Male Sprague-Dawley Rats.* Fundamental and Applied Toxicology, 1997. **40**: p. 247-255.
47. Suzuki, Y., et al., *Effect of Alkyl Phosphates on B-Glucuronidase in rats: Release of B-Glucuonidase from Liver Microsomes Into Serum.* Biochemical Pharmacology, 1977. **26**: p. 881-885.
48. Laham, S., J. Szabo, and G. Long, *Effects of Tri-n-Butyl Phosphate on the Peripheral Nervous System of the Sprague-Dawley Rat.* Drug and Chemical Toxicology, 1983. **6**(4): p. 363-377.
49. Noda, T., et al., *Effects of Tri-n-butyl Phosphate on Pregnancy in Rats.* Fund. Chem. Toxic., 1994. **32**(11): p. 1031-1036.
50. Hinton, D.M., et al., *Evaluation of Immunotoxicity in a Subchronic Feeding Study of Triphenyl Phosphate.* Toxicology and Industrial Health, 1987. **3**(71-89).
51. Hinton, D.M., et al., *Evaluation of Immunotoxicity in a Subchronic Feeding Study of Triphenyl Phosphate.* Intl. J. Occupational Medicine, Immunology and Toxicology, 1996. **5**(1): p. 43-60.
52. Welsh, J.J., et al., *Teratogenic Potential of Triphenyl Phosphate in Sprague-Dawly (Spartan) Rats.* Toxicology and Industrial Health, 1987. **3**(3): p. 357-369.
53. Burka, L.T., et al., *Metabolism of Tris(2-choloethyl) Phosphate in Rats and Mice.* Drug Metabolism and Disposition, 1991. **19**(2): p. 443-447.
54. Neerathilingam, M., et al., *^{1}H NMR-Based Metabonomic Investigation of Tributyl Phosphate Exposure in Rats.* Bioanalytical Chemistry, 2009: p. submitted.
55. Lindon, J.C., J.K. Nicholson, and E. Holmes, eds. *The Handbook of Metabonomics and Metabolomics*. 2007, Elsevier. 561.
56. Clarke, C.J. and J.N. Haselden, *Metabolic Profiling as a Tool for Understanding Mechanisms of Toxicity.* Toxicologic Pathology, 2008. **36**: p. 140-147.
57. Coen, M., et al., *NMR-Based Metabolic Profiling and Metabonomic Approaches to Problems in Molecular Toxicology.* Chem. Res. Toxicol., 2008. **21**: p. 9-27.
58. Lindon, J.C. and J.K. Nicholson, *Spectroscopic and Statistical Techniques for Information Recovery in Metabonomics and Metabolomics.* Annu. Rev. Anal. Chem., 2008. **1**: p. 45-69.
59. Lindon, J.C. and J.K. Nicholson, *Analytical Technologies for Metabonomics and Metabolomics, and Multi-Omic Information Recovery.* Trends Analytical Chemistry, 2008. **27**(3): p. 194-204.

60. Wishart, D.S., *Quantitative Metabolomics Using NMR.* Trends Analytical Chemistry, 2008. **27**(3): p. 228-237.
61. Vitols, C. and P. Mercier. *Correcting Lineshapes in NMR Spectra*. 2006 [cited; Available from: http://www.chenomx.com/publications/applicationNotes/HTML/ar04.html.
62. Dieterle, F., et al., *Probalistic Quotient Normalization as Robust Method to Account for Dilution of Complex Biological Mixtures. Application in ^{1}H NMR Metabonomics.* Analytical Chemistry, 2006. **78**: p. 4281-4290.
63. Craig, A., et al., *Scaling and Normalization Effects in NMR Spectroscopic Metabonomic Data Sets.* Analytical Chemistry, 2006. **78**: p. 2262-2267.
64. Cavaghan, C.L., I.D. Wilson, and J.K. Nicholson, *Physiological Variation in Metabolic Phenotyping and Functional Genomic Studies: Use of Orthogonal Signal Correction and PLS-DA.* FEBS Letters, 2002. **530**: p. 191-196.
65. Trygg, J., E. Holmes, and T. Lundstedt, *Chemometrics in Metabonomics.* Journal Proteome Research, 2007. **6**: p. 469-479.
66. Trygg, J. and S. Wold, *Orthogonal Projections to Latent Structures (O-PLS).* J. Chemometrics, 2002. **16**: p. 119-128.
67. Cloarec, O., et al., *Evaluation of the Orthogonal Projection on Latent Structure Model Limitations Caused by Chemical Shift Variability and Improved Visualization of the Biomarker Changes in ^{1}H NMR Spectroscopic Metabonomic Studies.* Analytical Chemistry, 2005. **77**: p. 517-526.
68. Westerhuis, J.A., et al., *Assessment of PLSDA Cross Validation.* Metabolomics, 2008. **4**: p. 81-89.
69. Chong, I.-G. and C.-H. Jun, *Performance of Some Variable Selection methods When Multicollinearity is Present.* Chemometrics and Intelligent Laboratory Systems, 2005. **78**: p. 103-112.
70. Lindon, J.C., E. Holmes, and J.K. Nicholson, *Pattern Recognition Methods and Application in Biomedical Magnetic Resonance.* Prog. NMR Spectroscopy, 2001. **39**: p. 1-40.
71. Alam, T.M. and M.K. Alam, *Chemometric Analysis of NMR Spectroscopy Data: A Review.* Annual Reports NMR Spectroscopy, 2005. **54**: p. 41-80.
72. Lindon, J.C. and J.K. Nicholson, *Spectroscopic and Statistical Techniques for Information Recovery in Metabonomics and Metabolomics.* Annual Review Analytical Chemistry, 2008. **1**: p. 45-69.
73. Potts, B.C.M., et al., *NMR of Biofluids and Pattern Recognition: Assessing the Impact of NMR Parameters on the Principal Component Analysis of Urine from Rat and Mouse.* J. Pharmaceutical and Biomedical Analysis, 2001. **26**: p. 463-476.
74. Beckwith-Hall, B.M., et al., *Application of Orthognal Signal Correction to Minimize the Effects of Physical and Biological Variation in High Resolution ^{1}H NMR Spectra of Biofluids.* Analyst, 2002. **127**: p. 1283-1288.
75. Van, Q.N., G.N. Chmurny, and T.D. Veenstra, *The Depletion of Protein Signals in Metabonomics Analysis with the WET-CPMG Pulse Sequence.* Biochemical Biophysical Research Communications, 2003. **301**: p. 952-959.
76. Keun, H.C., et al., *Analytical Reproducibility in ^{1}H NMR-Based Metabonomic Urinalysis.* Chem. Res. Toxicol., 2002. **15**: p. 1380-1386.
77. Antti, H., et al., *Batch Statistical Processing of ^{1}H NMR-Derived Urinary Spectral Data.* J. Chemometrics, 2002. **16**: p. 461-468.

78. Wouters, J.M. and G.A. Peterson, *Reference Lineshape Adjusted Difference Spectroscopy. I. Theory.* J. Magnetic Resonance, 1977. **28**: p. 81-91.
79. Wouters, J.M., et al., *Reference Lineshape Adjusted Difference NMR Spectroscopy. II. Experimental Verification.* J. Magnetic Resonance, 1977. **28**: p. 93-104.
80. Taquin, J., *Line-Shape and resolution Enhancment of High-Resolution FT-NMR in an Inhomogenous Magnetic Field.* Revue de Physique Appliquée, 1979. **14**: p. 669-681.
81. Morris, G.A. and D. Cowburn, *Suppresion of Artifacts in Nuclear Overhauser Effect Difference Spectroscopy by Reference Deconvolution.* Magnetic Resonance Chemistry, 1989. **27**: p. 1085-1089.
82. Morris, G.A., *Compensation of Instrumental Imperfections by Deconvolution using an Internal Reference Signal.* J. Magnetic Resonance, 1988. **80**: p. 547-552.
83. Green, D.V.S., et al., *Determination of the Barrier to C-N Bond Rotation in Captopril: Application of Reference Deconvolution to Line-Shape Analysis.* Magnetic Resonance Chemistry, 1990. **28**: p. 820-823.
84. Bothner-By, A.A. and J. Dadok, *Useful Manipulations of the Free Induction Decay.* J. Magnetic Resonance, 1987. **72**: p. 540-543.
85. Gibbs, A. and G.A. Morris, *Reference Deconvolution. Elimination of Distortions Arising from Reference Line Truncations.* J. Magnetic Resonance, 1991. **91**: p. 77-83.
86. Morris, G.A., H. Barjat, and T.J. Horne, *Reference Deconvolution Methods.* J. Progress Nuclear Magnetic Resonance Spectroscopy, 1997. **31**: p. 197-257.
87. Metz, K.R., M.M. Lam, and A.G. Webb, *Reference Deconvolution A Simple and Effective Method for resolution Enhancement in Nuclear Magnetic Resonance Spectroscopy.* Concepts in Magnetic Resonance, 2000. **12**(1): p. 21-42.
88. Ozdemir, D., M. Mosley, and R. Williams, *Hybrid Calibration Models: An Alternative to Calibration Transfer.* Applied Spectroscopy, 1998. **52**(4): p. 599-603.
89. Sjöblom, J., et al., *An Evaluation of Orthogonal Signal Correction Applied to Calibration Transfer of near Infrared Spectra.* Chemometrics and Intelligent Laboratory Systems, 1998. **44**: p. 229-244.
90. Blank, T.B., S.T. Sum, and S.D. Brown, *Transfer of Near-Infrared Multivariate Calibrations Without Standards.* Analytical Chemistry, 1996. **68**: p. 2987-2995.
91. Wang, Y., D.J. Veltkamp, and B.R. Kowalski, *Multivariate Instrument Standardization.* Analytical Chemistry, 1991. **63**: p. 2750-2756.
92. Wang, Z., T. Dean, and B.R. Kowalski, *Additive Background Correction in Multivariate Instrument Standardization.* Analytical Chemistry, 1995. **67**: p. 2379-2385.
93. Wang, Y., M.J. Lysaght, and B.R. Kowalski, *Improvement of Multivariate Calibration Through Instrument Standardization.* Analytical Chemistry, 1992. **64**: p. 562-564.
94. Gemperline, P.J., et al., *Appearance of Discontinuities in Spectra Transformed by the Piecewise Direct Instrument Standardization Procedure.* Analytical Chemistry, 1996. **68**: p. 2913-2915.
95. Anderson, C.E. and J.H. Kalivas, *Fundamentals of Calibrations Transfer through Procrutes Analysis.* Applied Spectroscopy, 1999. **53**(10): p. 1268-1276.
96. Wang, Y. and B.R. Kowalski, *Calibration Transfer and Measurement Stability of Near-Infrared Spectrometers.* Applied Spectroscopy, 1992. **46**(5): p. 764-771.
97. Bouveresse, E., et al., *Standardization of Near-Infrared Spectrometric Instruments.* Analytical Chemistry, 1996. **68**: p. 982-990.
98. Wise, B.M., et al., *PLS_Toolbox* 2006, Eigenvector Research, Inc.: Wenatchee, WA.

99. Gislason, J., H. Chan, and M. Sardahti, *Calibration Transfer of Chemometric Models Based on Process Nuclear Magnetic Resonance Spectroscopy.* Applied Spectroscopy, 2001. **55**(11): p. 1553-1560.
100. Ammann, L.P., et al., *Peak-Finding Partial Least Squares for the Analysis of ^{1}H NMR Spectra.* J. Chemometrics, 2006. **20**: p. 231-238.
101. Bylund, D., et al., *Chromatographic Alignment by Warping and Dynamic Programming as a Pre-Processing Tool for PARAFAC Modelling of Liquid Chromatography-Mass Spectrometry Data.* J. Chromatography A, 2002. **961**: p. 237-244.
102. Vogels, J.T.W.E., et al., *Partial Linear Fit: A New NMR Spectroscopy Preprocessing Tool for Pattern Recognition Applications.* J. Chemometrics, 1996. **10**: p. 425-438.
103. Torgrip, R.J.O., et al., *Peak Alignment Using Reduced Set Mapping.* J. Chemometrics, 2003. **17**: p. 573-582.
104. Alam, T.M., et al., *Investigation of Chemometric Instrumental Transfer Methods for High-Resolution NMR.* Analytical Chemistry, 2009. **81**(11): p. 4433-4443.
105. Stone, L.A. and R.W. Kennard, *Computer Aided Design of Experiments.* Technometrics, 1969. **11**(1): p. 137-148.

Distribution

1	MS0886	Todd M. Alam	1816 (electronic)
1	MS0886	Sarah K. McIntyre	1816 (electronic)
1	MS1455	M. Kathy Alam	2555 (electronic)
1	MS1378	Nancy Jackson	6726 (electronic)
2	MS9018	Central Technical Files	8944 (electronic)
1	MS0899	Technical Library	4536 (electronic)
1	MS0123	D. Chavez, LDRD Office	1011 (electronic)


Sandia National Laboratories